UNIVERSITY OF OKLAHOMA

GRADUATE COLLEGE

EXPERIMENTAL INVESTIGATION OF MOLECULAR HYDROGEN EFFECT ON CEMENT RELATED TO WELL INTEGRITY FOR UNDERGROUND HYDROGEN STORAGE

A THESIS

SUBMITTED TO THE GRADUATE FACULTY

In partial fulfillment of the requirements for the

Degree of

MASTER OF SCIENCE

By

ESTEBAN UGARTE
Norman, Oklahoma

2022

EXPERIMENTAL INVESTIGATION OF MOLECULAR HYDROGEN EFFECT ON CEMENT RELATED TO WELL INTEGRITY FOR UNDERGROUND HYDROGEN STORAGE

A THESIS APPROVED FOR THE

MEWBOURNE SCHOOL OF PETROLEUM AND GEOLOGICAL ENGINEERING

BY THE COMMITTEE CONSISTING OF

Dr. Saeed Salehi, Chair

Dr. Runar Nygaard

Dr. Ruzbeh Moghanhloo

Acknowledgments

I want to thank and express my deepest gratitude to my advisor and mentor, Dr. Saeed Salehi. Who took me from day one, and you gave me all the support, time, and guidance during the pursue of my master's degree. You received me under your mentorship during one of the worst moments of my life. There are no words to express how grateful I am to you. In my academic development for the completion of this research and the other projects, papers, and competitions I have been involved. Your insightful feedback motivates me to learn more and to keep challenging myself in whatever the future holds for me. Thank you for your patience, dedication, and unconditional support. I am sincerely thankful and will forever be in your debt.

I want to express my deepest appreciation and special thanks to my committee members, Dr. Runar Nygaard and Dr. Ruzbeh Moghanloo. Dr. Nygaard it has been a privilege to be a student at The University of Oklahoma during your time as director of Mewbourne School of Petroleum and Geological Engineering. The school is in great hands with you. Dr. Moghanloo, I am happy to have the great opportunity and privilege of being your student and learning from you. For both of you, I want to thank you both for agreeing to serve on my thesis committee and for taking the time to review my work providing me your valuable feedback.

Thanks to The University of Oklahoma and the Mewbourne School of Petroleum and Geological department for building in my strong desire to learn and grow as a professional and human being. In this outstanding school I have had the opportunity to meet and work with great people with professional qualities. I want to thank all the people who I meet and work during my time at The University of Oklahoma. I am particularly grateful for the assistance given by Gary Stowe and Jeff

McCaskill for the laboratory support, teachings, and guidance during my experimental research. I would not have been able to achieve anything without your unwavering support and time.

I would also like to extend my thanks to my teammates and friends, Cesar, Daniel, Chinedum, Nabe, Raymos, Abdelmjeed, Son, Michael, Juan Camilo, Aly, Eduardo, Mohammed, and Mayra; thank you for giving me your friendship, support, and motivation.

Lastly, I would like to thank my family, parents and my little brother. My parents Jaime and Sofia for their continual love, support, and prayers during this journey. I owe you everything to both of you. My little brother Joaquin who is my greatest motivation to keep pushing myself to be better as a professional and as a human being.

Table of Contents

List of Figures

List of Tables

Abstract

Underground Hydrogen Storage (UHS) in the subsurface is an alternative to overcome limitations associated with a fluctuating production of renewable energy sources. The excess energy produced can be converted to hydrogen and stored in porous media. Hydrogen is injected and produced from geological formations via wells. There are several concerns regarding the interactions of hydrogen with the different well components responsible for maintaining proper well integrity, such as cement. This experimental study investigates the interaction between molecular hydrogen and cement Class H. The methodology provides a comparison of experimental tests to highlight the effects hydrogen can have on cement during aging. Samples were cured in two different environments were then characterized using different physical and chemical tests such as Unconfined Compressive Strength (UCS), Fourier Transform Infrared Spectroscopy (FTIR), Porosity and Permeability (PP), Nuclear Magnetic Resonance (NMR), Scanning Electron Microscopy (SEM) and Energy Dispersive X-Ray Spectroscopy (EDS). Samples exposed to molecular hydrogen exhibited a greater compressive strength in both the short and long terms. Porosity was found to be lower in samples exposed to hydrogen. Similarly, permeability was lower in samples exposed to hydrogen. NMR distributions showed a reduction of larger pores and an increase of smaller pore spaces. The compositional analysis demonstrated that hydrogen presence increases the amount of hydrated product (portlandite and ettringite) formed. The crystalline needle-shaped structure observed in the SEM confirmed the presence of portlandite and ettringite within some of the larger pores. Acoustic velocities showed hydrogen-exposed samples to be stiffer and less flexible. This could be detrimental because, during UHS, cement is exposed to multiple cycles of injection and production. This experimental study showed that molecular hydrogen present could generate the formation of hydrated products, causing a shift in the porosity distribution affecting the mechanical strength of the cement.

1. INTRODUCTION

1.1 Research Motivation

To combat climate change, energy generated from renewable sources has gained interest in replacing fossil fuel energy such as coal, oil, and natural gas, which are considered adverse for the environment by reducing greenhouse gas emissions. Renewable energies are set to keep increasing their share in the market. In the last two decades and at the same time, our energy demand has grown year to year. For example, in 2000, energy consumption from renewable sources was 6.2% of the total energy consumption share in the U.S., and in 2019, it reached an all-time high of 11.45% (EIA, 2020). The projections from the U.S. Department of Energy's Energy Information Administration (EIA) expect an increase in renewable energies overcoming other electricity generation sources, as shown in **Figure 1**. Based on projections, by the year 2300, approximately 1400 quads will be supplied by renewable energies worldwide, which is a 3780% increase from 462 quads reported in 2005 (Fronk et al., 2010). Renewable energy share is set to keep rising; nevertheless, there are still limitations regarding renewable energy production.

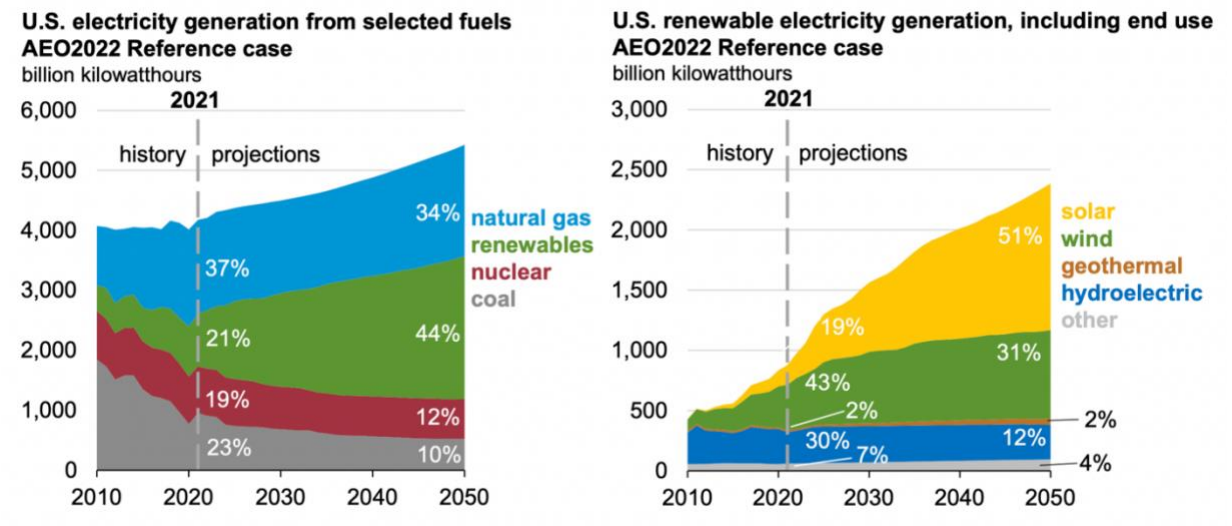

Figure 1. U.S. Department of Energy's Energy Information Administration (EIA) electricity mix projection over the next 30 years. Annual Energy Outlook 2022 (EIA, 2022).

The main limitation associated with the highest producing renewable source, such as solar and wind, is that these are weather dependent. The intermittency of these energies is a disadvantage that creates a gap between supply and demand, making these clean energies unreliable. The lack of flexibility to match the fluctuations makes them unable to keep a steady supply (Benato and Stoppato, 2017; Shang et al., 2020; Camara et al., 2019; Sharan et al., 2020). Energy storage is indispensable to overcome the gap by storing surplus energy generated during surplus and producing it during peak consumption periods. It is a practical response to the intermittency and baseload issues to avoid wasting generated energy daily and seasonal (Camara et al., 2019). An underground storage facility is an artificially created accumulation of fluid in a natural environment in the subsurface at a certain depth that must fulfill certain characteristics in order to contain the desired fluid. Storage in the subsurface has multiple advantages: reliability, safety, available space, wide availability of geological formations, and low economic costs. Hydrogen is an attractive alternative as it is a clean energy source and an economically feasible energy carrier that can be implemented in storage applications.

Hydrogen can be generated by different thermochemical, biological, electrolysis, or water-splitting processes (Das and Veziroğlu, 2001; Wang et al., 2012). It is produced from different sources, such as oil, natural gas, coal, and water. The production of hydrogen from oil, natural gas, and coal generates pollutants, and hydrogen production from water only accounts for a small percentage; as technologies develop, this can become a tipping point for broader implementation. A comparison and description of the different methods for hydrogen production from water can be found in Shahid et al. (2012). Hydrogen can be stored by several methods, such as gas cylinders, cryogenic tanks, ammonia, absorbed on metals, chemically bound to covalent and ionic compounds, or through oxidation of reactive metals (McPherson et al., 2018; Reuß et al., 2017). Nevertheless, these methods are expensive and are space limited. Therefore, it is possible to store the hydrogen in porous media of underground geological formations such as depleted oil

and gas reservoirs, aquifers, and salt caverns to meet the huge demand. According to Taylor et al. (Taylor et al., 1986), underground storage is the cheapest method to store hydrogen.

Underground hydrogen storage (UHS) has gained attention worldwide in recent years as project and research publication numbers have been increasing. It is still in an early stage of development compared to more mature analogs subsurface storage options such as underground gas storage (UGS) or carbon capture and storage (CCS) (Ugarte and Salehi, 2021). UHS still lacks implementation and experience. There are only a limited number of projects that have successfully used subsurface geological structures to store hydrogen. **Table 1** shows all UHS projects worldwide. Teeside, Clemens, and Moss Bluff are the only known successful pure hydrogen (95%) projects in the U.S. and U.K.; all implemented in salt formations (Tarkowski, 2019). Ketzin, Beynes, and Lobodice are successful UHS aquifers storing amounts between 50% and 62% of hydrogen in Europe. Numerous research projects have started in the last decade, such as ANGUS+ (Kabuth et al., 2013), H2STORE (Pudlo et al., 2012), HyINTEGER (Pudlo and Henkel, 2016), HyUnder (Simon et al., 2012), HyStorPor (Mouli-Castillo et al., 2021) and Underground Sun Storage (RAG, 2016). These studies aim to investigate the feasibility of hydrogen production, storage, and utilization.

Table 1. Worldwide operating hydrogen storage sites (Zivar et al., 2020)

Field/project name	Storage type	H_2 (%)	Working condition	Depth (m)	Volume (m^3)	Status
Teesside (UK)	Bedded salt	95	45 bar	365[a]	210,000	Operating
Clemens (USA)	Salt dome	95	70–137 bar	1,000[a]	580,000	Operating
Moss Bluff (USA)	Salt dome		55–152 bar	1,200[a]	566,000	Operating
Spindletop (USA)	Salt dome	95	68–202 bar	1,340[a]	906,000	Operating
Kiel (Germany)	Salt cavern	60	80–100 bar		32,000	Closed
Ketzin (Germany)	Aquifer	62	Not reported	200–250	Not reported	Operating with natural gas
Beynes (France)	Aquifer	50	Not reported	430	3.3×10^8	Operating with natural gas
Lobodice (Czech Republic)	Aquifer	50	90 bar/34 °C	430	Not reported	Operating
Diadema (Argentina)	Depleted gas reservoir	10	10 bar/50 °C	600	Not reported	Not reported
Underground Sun Storage (Austria)	Depleted gas reservoir	10	78 bar/40 °C	1000	Not reported	Operating

Wells involved in this process have to meet specific criteria for successful long-term containment during injection/withdrawal and storage phases. The objective is to have a wellbore with the least potential for exposure to fluid migration, longevity, and reliable hydraulic and mechanical barriers (Kiran et al., 2017). UHS is associated with multiple potential risks that can affect downhole components such as casing, tubing, and connections fabricated of steel, plus elastomer sealants like packers typically made of rubber or polymers. It can also permeate elements of wellbore completion, such as cement which is a silica-based material. Failure of any component can lead to a loss of wellbore integrity, generating a negative environmental impact, accidents, and costs associated with damage repair.

Figure 2 depicts the assessment methodology and model framework. Energy is produced from renewable sources, and the surplus not destined for electricity can be used to generate hydrogen from electrolyzers. Hydrogen generated by the electrolysis process can be further injected into different types of geological formations that can be selected depending on multiple characteristics (e.g., location, availability, capacity, and costs). Then the stored hydrogen can be produced in periods of high demand to be used in gas combustion, electricity, or other possible uses. The framework addresses potential problems that can compromise the storage model by developing a case study of multiple reactions that can occur under subsurface conditions due to microorganisms living under these conditions that can affect the storage.

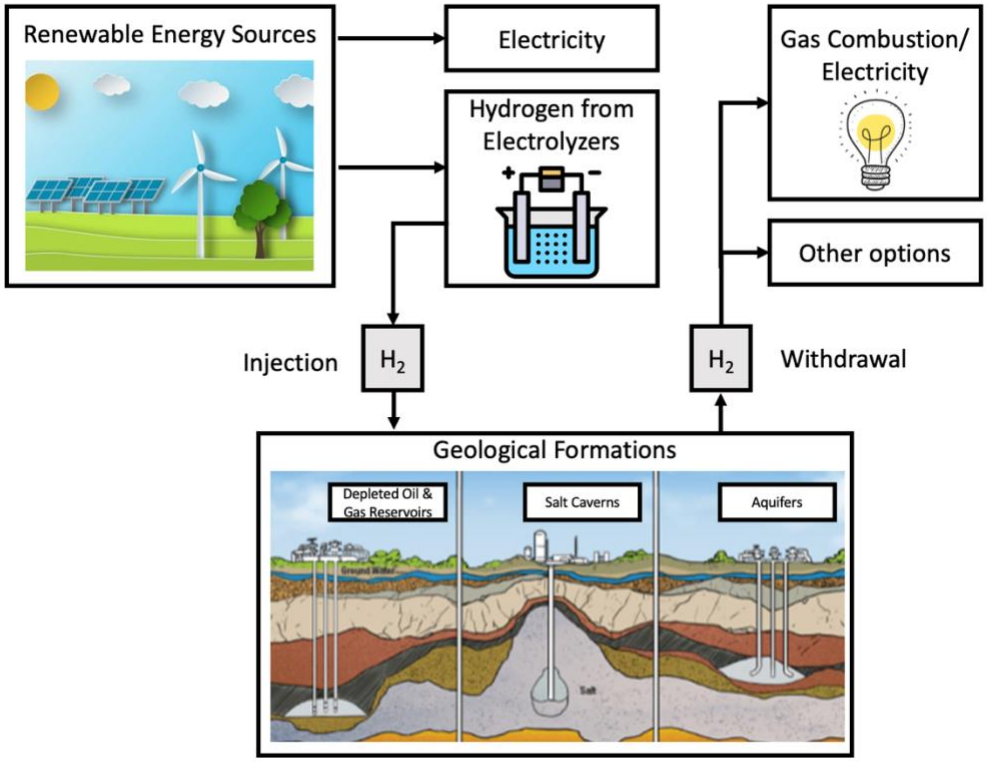

Figure 2. Assessment Methodology of Undeground Hydrogen Storage.

1.2 Research Statement

Well integrity is defined by ISO 16530-1 (2017) as the capacity of the drilled open hole to maintain its shape and remain intact after drilled. NORSOK D-010 (2013) standard defines it as the application of technical, operational, and organizational solutions to reduce the risk of uncontrolled release of formation fluids to the surface throughout the well's life cycle. NORSOK D-010 (2013) details the different well integrity issues that are part of any well design and operation in order to prevent or mitigate formation fluid invasion throughout the life of the well (NORSOK, 2004a). Failure of wellbore integrity is the result of the time-dependent formation of fluid leakage due to the creation of leakage pathways along the well (Kiran et al., 2017; Vrålstad et al., 2018). This could happen at any stage of the life cycle of the well: initial construction, completion, production, or abandonment. For UHS, well integrity is vital as the well is subjected to multiple injection and withdrawal phases depending on the design.

Well integrity is a challenging problem due to the complicated loads surrounding the wellbore (Ahmed et al., 2019). In UHS, the multiple injection/withdrawal phases create changing loads that can affect the well integrity components such as cement. Potential problems are associated with induced dynamic loading, therefore geomechanical analysis, should be considered to prevent the development of leakages in the barriers. Possible leakage pathways assuming the cement is elastic or brittle (Thiercelin et al., 1998) include casing/cement interface, permeate through the barrier, leak in the casing, leak in cement, and cement/rock interface (Gasda et al., 2004). The creation of these leakage pathways could be attributed to different factors: casing corrosion, debonding, micro-annuli, incomplete annular cement, and induced fractures in cement (Gasda et al., 2004; Nygaard et al., 2014; Kiran et al., 2017). In addition, well integrity issues can generate financial costs to solve problems and environmental effects from the fluid leakage to the atmosphere and safety concerns due to life-threatening situations.

During hydrogen storage in the subsurface, multiple mechanisms can affect wellbore integrity. These include fluid migration through existing leakage pathways, hydrogen blistering and hydrogen embrittlement, casing microbial corrosion, cement degradation, elastomer failure, and caprock sealing failure, as shown in **Figure 3**. Hydrogen is an electron donor more active in chemical or microbial reactions. In subsurface conditions, Microorganisms' survival depends on the characteristics of the environment. The effect of the conditions generated by hydrogen storage in the subsurface inhibits microorganisms' growth. These are the catalysts for multiple reactions that can compromise well integrity. Several biotic reactions known to consume hydrogen can generate reactions that directly or indirectly affect well integrity. The following bacteria cause these processes: methanogens, acetogens, sulfate-reducing bacteria (SRB), and iron-reducing bacteria (IRB).

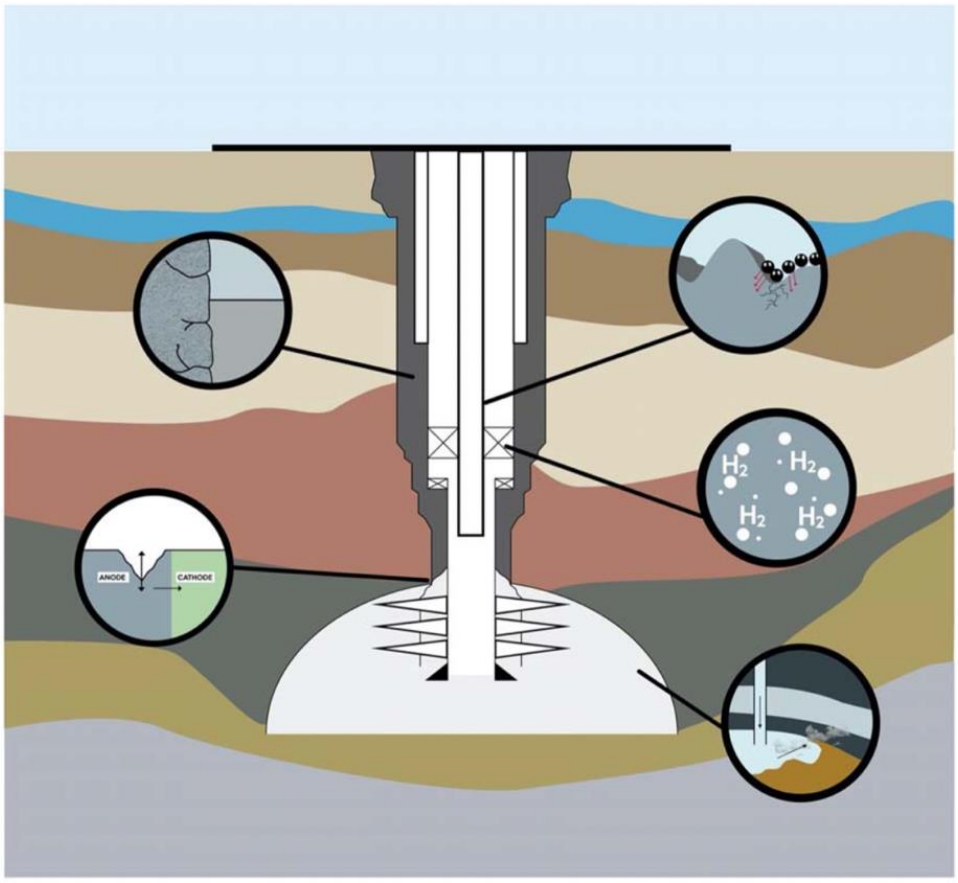

Figure 3. Mechanisms causing well integrity failure in UHS in the subsurface (Ugarte and Salehi 2021).

Failure in Well Integrity during storage operations can be financially costly and generate safety concerns. There have been multiple incidents that occurred in storage facilities in the US. Some reported incidents include Yaggy facility in Kansas, Magnolia facility in Louisiana, Leyden facility in Colorado, Moss Bluff in Texas, and Montebello in Los Angeles. All these incidents failed to properly contain the storage fluid that leaked in different ways generating incidents that ended in explosions, high costs, the release of gases through the atmosphere, contamination, and consequences on the health of the people in the vicinity of the facility (Miyazaki, 2009). Some of these incidents ended up in multiple deaths. In contrast, financial liabilities resulted from evacuations, compensation, fines, lawsuits, and damaged structures (Miyazaki, 2009). Common causes of these incidents were casing leaks caused by corrosion, casing damages, rusted steel,

casing shoe leaks, gas channeling in the annular, deteriorated annular seals, and poor cement bonding (Miyazaki, 2009). Well integrity barriers can be compromised during UHS ensuring proper containment all components must be carefully selected during the design and constantly monitored throughout the life of the well.

1.3 Research Objectives

This research study aims to understand the interaction between cement and molecular hydrogen in an aqueous environment by performing a mechanical and chemical analysis. Hydrogen was introduced to the curing environment during cement setting. This is meant to simulate conditions during cement settling in new wells. New wells are important as hydrogen can affect the cement before it fully hydrates and sets affecting its properties throughout the life of the storage. Mechanical, Petrophysical, Composition, and Imaging experiments were run on Class H cement without any additives at constant pressure and temperature over multiple extended periods. The main objectives of this work include:

- Provide a complete literature review of well integrity related to UHS.
- Compare with more advanced storage alternative such as UGS and CCS.
- Understand the interaction between cement and hydrogen during prolonged curing exposure times by comparing with the base case.
- Investigate the effect of hydrogen on the mechanical properties of the cement sheath.
- Evaluate any change in the petrophysical properties of cement exposed to hydrogen.
- Investigate any compositional change the cement might suffer over the different time frames.
- Observe the microstructural changes in samples exposed to hydrogen.

2. LITERATURE REVIEW

This section provides a complete literature review regarding issues associated with well integrity in underground hydrogen storage. Gas storage is a widely implemented technology, yet pure hydrogen has only been implemented in salt caverns. Currently, only one project is studying behavior in a depleted oil & gas field. This review will discuss possible geological formations for hydrogen storage to highlight the advantages of depleted oil and gas reservoirs. It will discuss hydrogen properties and compare them to other gases used in storage operations. Then discuss all potential well integrity issues discussed in literature regarding UHS. Analogously hydrogen storage will be compared to other storage technologies to provide criteria, recommendations, and design for UHS. The focus will be shifted to cement, including classification, hydration process, stresses subjected, and microstructure.

2.1 Underground Hydrogen Storage

The concept of storing fluids in underground geological formations was first successfully accomplished with natural gas in 1915 in a partially depleted gas field in Ontario, Canada (Zivar, 2020). There are only a few number of UHS projects worldwide (**Table 1**). However, there are similarities with more developed storage technologies such as Underground Gas Storage (UGS). Several underground gas storage facilities are operating worldwide, with the US holding the highest count. Currently, there are three major types of underground storage options, which include depleted oil and gas reservoirs, aquifers, and salt caverns. Other storage options such as coal mines, lined hard rock caverns, and refrigerated mined caverns can be implemented in the near future if costs associated with them reduce and storage increases (Lord et al., 2014). Each option has unique characteristics and specific requirements.

Salt caverns are artificially created by a process called solution mining, which consists of leaching out large cavities by injecting water in a controlled manner. Salt domes are structurally

stable thick homogenous bodies that can operate up to a depth of 6000 ft. Above this depth, salt deformation occurs, affecting stability due to the high temperature and pressure (Michaski et al., 2017). The main concern in the construction of salt caverns would be salt intrusion. Salt caverns are the only formation that has proven capable of storing pure hydrogen. The salt surrounding the cavern is impermeable and leak-proof, creating a sealed containment with good mechanical stability. Additionally, high saline conditions of the storage environment affect the microorganism that can live under these conditions (Sainz-Garcia et al., 2017). These factors provide a suitable environment to safely contain hydrogen underground.

Aquifers are geological structures that contain a trap capped with an impermeable layer called caprock. The porous rock in the formation is filled with water that would need to be displaced to store the hydrogen. A major advantage of aquifers is that this type of formation is commonly available worldwide and can be set close to major energy-consuming locations. In this case, aquifers and salt caverns wells would have to be drilled and constructed. Therefore, new wells design and construction are required. An advantage is that components can be designed to fit UHS applications, although this can be quite costly.

Depleted oil and gas reservoirs are similar to aquifers; these have effectively contained hydrocarbons over time. Most storage applications are implemented in depleted oil and gas reservoirs since they have a number of advantages compared to the other types of geological formations. They are known geological formations that have been studied before development, meaning there is existent available information on the geological setting. These formations have proven ability to store hydrocarbons, although hydrogen has different properties compared to these. **Figure 4** shows the share of these types of geological gas storage. There are multiple UGS projects developed in depleted oil and gas reservoirs but non-UHS projects. Further research on the matter is needed to ensure that depleted oil and gas reservoirs could trap the stored hydrogen gas. This type has certain advantages, such as costs, information on the geological setting, and

existing components. Surface and subsurface installations are already available, reducing the cost of these types of storage. Additionally, some natural gas residuals in the reservoir could act as cushion gas to maintain the storage pressure, further reducing the cost. A complete well integrity evaluation of the condition of these old wells is required to ensure their components are suitable for conversion to storage applications. A negative aspect would be that residual oil in the reservoir might generate possible reactions, reduce the purity of the hydrogen gas, and dissolution, causing losses.

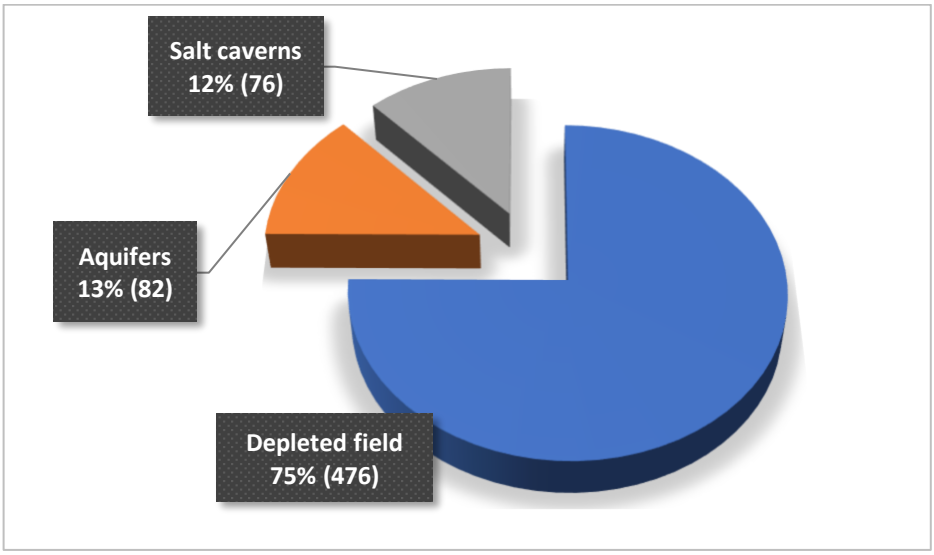

Figure 4. Share of worldwide UGS by 2010 (modified from Tarkowski, 2019).

2.2 Hydrogen Properties

Hydrogen is the smallest chemical particle in existence; it has the highest energy content per unit mass. Combustion of one cubic meter of hydrogen produces 12.7 MJ (Megajoules) of energy. Methane generates 40 MJ (Megajoules) of energy per cubic meter. Compared to methane, its energy content is three times higher by weight. However, hydrogen can easily be converted into electricity or heat, making hydrogen an efficient energy carrier because of its transporting, or storing capabilities (Zivar, 2020). **Table 2** compares the properties of hydrogen (H), methane (CH4), and carbon dioxide (CO2). It can be observed that compared to methane, hydrogen is

eight times less dense. Then storing the same mass amounts requires more space and pressure. It is less viscous than methane and has higher mobility, leading to lower residual in porous media during the withdrawal phases. Solubility is lower than methane, but diffusivity is higher. This can generate losses through diffusion and dispersion. Due to its low molecular weight and high diffusivity, it can leak through the over-burden layers (Amid et al., 2016; Heinemann et al., 2018). Carbon dioxide has higher physical properties than methane and hydrogen. Its molecular weight is 22 times higher than hydrogen, and its density is three times greater than methane. Carbon Dioxide can be stored in its supercritical state due to its critical pressure and temperature adapting properties between gas and liquid. Solubility and diffusion are considerably higher than methane and hydrogen; when dissolved in water, it forms carbonic acid, which is highly corrosive. The kinetic diameter is lower for hydrogen, while kinetic energy is the same as any gas that behaves like an ideal gas and has the same energy per mol. However, hydrogen's root mean square speed is almost 3 times methane and almost 5 times carbon dioxide.

Table 2. Physical properties of hydrogen, methane, and carbon dioxide (Ugarte and Salehi, 2021)

Properties	H2	CH4	CO2
Molecular Weight	2.016	16.043	44.009
Density @ SC	0.082 kg/m3	0.657 kg/m3	1.98 kg/m3
Viscosity @ SC	0.89 x 10^-5 Pa s	1.1 x 10^-5 Pa s	1.49 x 10^-5 Pa s
Solubility in pure water @ SC	16 x 10^(-4) g/L	22.7x 10^(-3) g/L	1.45 g/L
Normal boiling point	neg 253 C	neg 165 C	neg 78.44 C
Critical Pressure	12.8 atm	45.79 atm	72.8 atm
Critical Temperature	neg 239.95 C	neg 82.3 C	31 C
Heating Value	120-142 kJ/g	205-55.5 kJ/g	-
Diffusion in pure water @ SC	5.13 x 10^(-9) m2/s	1.85 x 10^(-9) m2/s	1.6 x 10^(-3) m2/s
Kinetic Diameter	2.89 A	3.8 A	3.3 A
Kinetic Energy	3.74 kJ/mol	3.74 kJ/mol	3.74 kJ/mol
Root mean square speed @ SC	1934 m/s	684 m/s	412 m/s

Figure 5 shows a comparison of the density and viscosity of hydrogen, methane, and carbon dioxide. Hydrogen and methane densities and viscosities are considerably lower compared to Carbon Dioxide. This allows them to have a wider variety of potential storage sites as they are not restricted by depth. Carbon Dioxide storage requires a minimum depth of 2625 ft (800 m) due to its physical behavior to ensure it remains in a supercritical state (Edlemann et al., 2016; Heinemann et al., 2018). Hydrogen and methane do not exhibit any drastic change in properties with depth. The selected geological formation will determine the depth; it requires proper containment features to trap and seal the fluid. At subsurface conditions, hydrogen density is ten times lower than methane and 100 times lower than carbon dioxide, which means that it requires more space to store the same amount of energy.

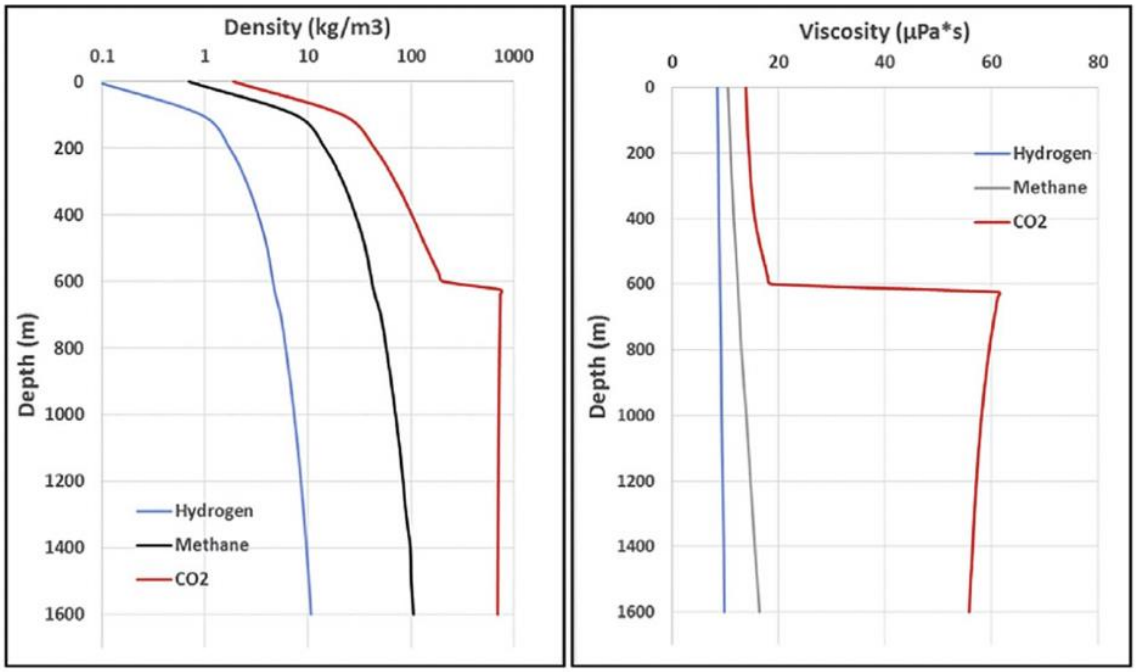

Figure 5. Density and viscosity of hydrogen, methane, and carbon dioxide calculated from data of the Midland Valley region (Heinemann et al., 2018)

2.3 Mechanisms that can affect Well Integrity in UHS

From literature there are five issues mentioned that can compromise the integrity of the storage due to hydrogen properties. Well components that can be affected are steel casing, cement barrier and rubber elastomers. The issues include but are not limited to microbial casing corrosion; hydrogen blistering, induced cracking and embrittlement; cement degradation, elastomer failure; caprock sealing failure.

2.3.1 Microbial Casing Corrosion

Microbial corrosion is generated by the activity of microorganisms that inhabit the subsurface. It is also referred to as microbial-induced corrosion, microbiological corrosion, bacterial corrosion, bio-corrosion, or microbiologically influenced corrosion. During hydrogen storage, the processes responsible for microbial corrosion are sulfate reduction, methanogenesis, and iron (III) reduction. Corrosion caused by these living organisms can compromise multiple steel downhole components affecting the well integrity.

Sulfate Reducing Bacteria (SRB) are single-celled organisms that can grow in aqueous conditions under temperatures between 40 °C and 60 °C and adapt and survive at 80 °C or more (Loto, 2017). These microorganisms are known to consume hydrogen and produce hydrogen sulfide as a product when sulfur is available. SRB can corrode the steel casing surface in two ways: chemically by producing hydrogen sulfide and electrically by withdrawal (Iverson, 1987). Most organisms do not form a continuous film, which manifests as localized corrosion. **Figure 6** shows the reaction taking place on the surface of the casing. SRB can act via cathodic depolarization as the mechanism for sulfide production (Loto, 2017).

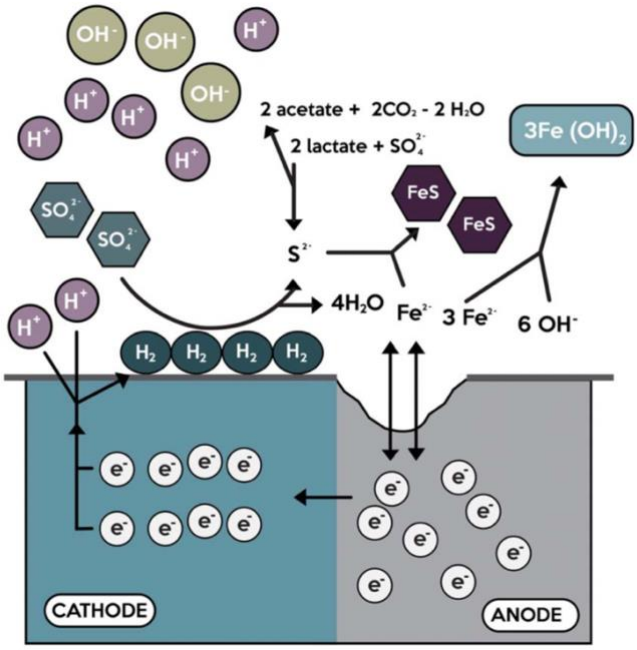

Figure 6. Reactions in the metal surface by SRB cause microbial corrosion (modified from Loto, 2017)

Other microorganisms living in the subsurface can also generate or contribute to corrosion. Methanogenic bacteria are the more likely bacteria to thrive under subsurface conditions due to hydrogen availability as an electron donator. These anaerobic can survive at high depths and temperatures. Methanogenesis is the process caused by these microorganisms that convert hydrogen and carbon dioxide into methane through the Sabatier reaction. Methanogenic bacteria are not directly responsible for microbial corrosion. Although when found in a corrosive environment, these bacteria can work with SRB to accelerate the corrosion rate (Boopathy and Daniels, 1991).

IRB is another bacterial group that can generate corrosion to the casing but a smaller degree than SRB. IRB uses the electron donator hydrogen to support metal oxidation processes and reduce iron (III) phases. They rely on the availability of iron oxides, organic carbon, and minerals such as smectite and chlorite. IRB and SRB can both survive in the same environment and work together in the corrosion process because IRB uses acetate, which is a common product of SRB

(Rickard, 2012). In environments rich in iron oxides and organic carbon, IRB can thrive over SRB due to the higher affinity for hydrogen (Lovely and Philips, 1986).

2.3.2 Hydrogen Blistering, Hydrogen-Induced Cracking, and Hydrogen Embrittlement

Hydrogen blistering, hydrogen-induced cracking (HIC), and hydrogen embrittlement occur due to the abundance of hydrogen combined with its physical properties. These phenomena can reduce steel's mechanical properties depending on the amount of hydrogen available and the nature of the environment. **Figure 7** shows the schematic of hydrogen blistering and hydrogen embrittlement on the surface of a metal in an aqueous environment.

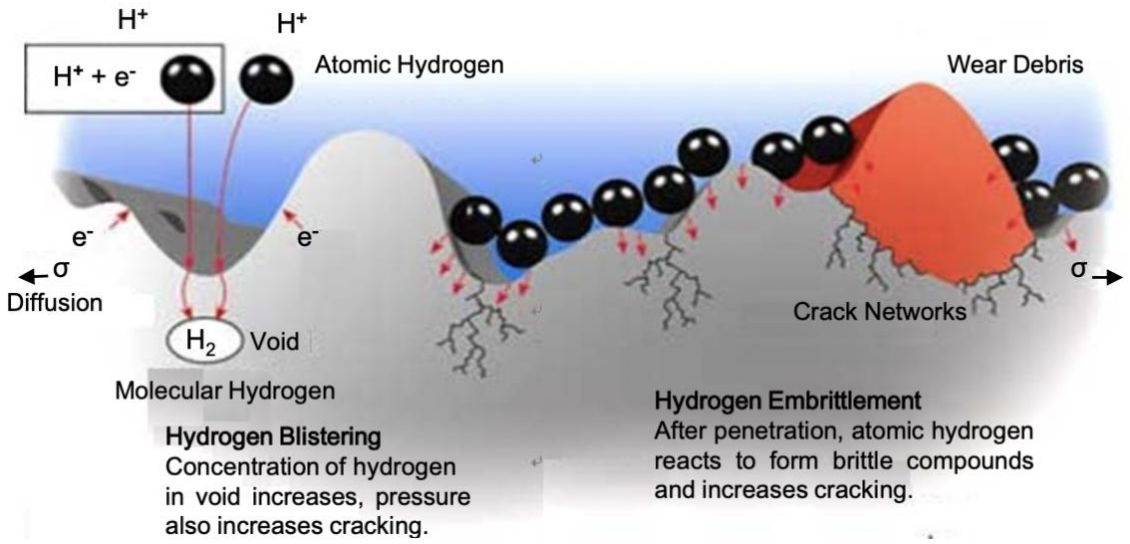

Figure 7. Schematic of hydrogen blistering and hydrogen embrittlement (Zhang, 2016)

Hydrogen blistering occurs when atomic hydrogen is formed on the metal surface by dissociative chemical sorption. In this atomic form, hydrogen can accumulate beneath the metal surface in trap locations. The accumulation causes pressure to rise, producing plastic deformation. Some hydrogen is also lost by dissolution. If the rate of supply of atomic hydrogen exceeds the dissolution rate, then a rupture will occur (Condon and Schober, 1993). Hydrogen blistering can initiate cracks leading to sudden failure at lower stresses due to hydrogen concentration and high

pressure (Reitenbach et al., 2015). Hydrogen-induced cracking is referred to as the crack that results from the entry of hydrogen into the steel surface. Hydrogen embrittlement occurs due to hydrogen molecules entering the steel microstructure; it can increase the susceptibility to cracking at lower stresses and reduce material ductility and resistance. Diffusion of hydrogen in steel is affected by microstructure phases present (grain boundaries, grain shapes, vacancies and dislocations, interfaces with nonmetallic inclusions, precipitates, and microvoids), which affect the mobility of hydrogen (Ghosh et al., 2018). These traps can be classified into reversible or irreversible depending on the hydrogen's binding energy. Usually, a small amount of hydrogen can enter the metal while the rest moves on the surface and become part of other reactions. Nevertheless, due to microorganisms in the environment, the entry of hydrogen can be enhanced. In the case of SRB, it can be done by producing sulfides, which increase hydrogen's entry into the steel by disrupting the surface film (Edyvean et al., 1997).

2.3.3 Cement Degradation

Well cementing is an essential component in well integrity. Cement in the subsurface experiences mechanical or chemical degradation over time. Mechanical degradation occurs due to exposure to extreme loading conditions due to pressure, thermal expansion, and volume change during hydration. Several chemical reactions can lead to various processes, such as corrosion, leaching, and strength reduction. The basic compounds in cement consist of combinations of lime, silica-alumina, and iron oxide. During hydration, tobermorite ($3CaO{\cdot}2SiO2{\cdot}3H2O$), also known as the CSH phase, and portlandite ($Ca(OH)2$), known as CH, are the two main binding elements responsible for the cement strength. Hydrogen permeation can be a risk as it may leak through the cement sheath due to its physical properties. In addition, microorganisms inhabiting hydrogen environments can promote chemical reactions affecting cement properties.

Chemical degradation of cement due to carbon dioxide presence in an aqueous environment is referred to as carbonation (Strazisar et al., 2009). When pH lowers due to the acidic environment, CH and CSH start dissolving. Calcium aluminate and ferrite hydrates follow the dissolution until only silica is left at a pH of 2 (Lecolier et al., 2010). This process depends on the depth of penetration which depends on the permeability of the cement sheath and the amount of calcium oxide found. These factors promote the formation of calcium carbonate (CaCO3), which precipitates and reduces porosity and permeability, increasing cement strength. Regardless, if carbonation continues, calcium carbonate is converted to bicarbonate (Ca(HCO3)2) (Santra et al., 2009), which is water-soluble and will dissolve, leading to a reduction of the cement strength (Teodoriu et al., 2010). For UHS, the carbonation process will be dependent on the amount of carbon dioxide found in the rock mineral and the formation fluids. It will also depend on the pH of the environment, which can maximize the release of carbon dioxide from carbonates. The temperature has more influence on the degradation than pH, and a value of 2.4 and a temperature of 50 °C can generate conditions for severe degradation (Kutchko et al., 2010).

Cement can also experience chemical degradation by the attack of hydrogen sulfide (**Figure 8**). This can be a problem during hydrogen storage as it is a common by-product of sulfate reduction due to microorganism reactions. Microorganisms such as SRB can generate a reduction of sulfate and generate hydrogen sulfide, which can cause cement degradation. These microorganisms can be present in the cement sheath surface or within the interstitial space. Sulphidation can lead to secondary ettringite formation. Primary ettringite is formed before the hardening of the cement, but it does not generate expansion and internal stresses in the cement sheath. However, secondary ettringite expands within the cement structure generating internal stress that can lead to cracks (Kutchko et al., 2011; Collepardi, 2003). Secondary ettringite is formed when calcium found in lime or CSH, aluminum found in hydrated ferrite, sulfate from H2S, and H2O are present in the hardened cement (Collepardi, 2003). When the aluminate supply is depleted from the cement

sheath, gypsum will be formed instead of secondary ettringite. Gypsum also tends to expand within the cement structure (Kutchko et al., 2011). Low pH values from the environment can generate instability in pyrite and become part of hydrogen sulfide-producing reactions (Truche et al., 2013).

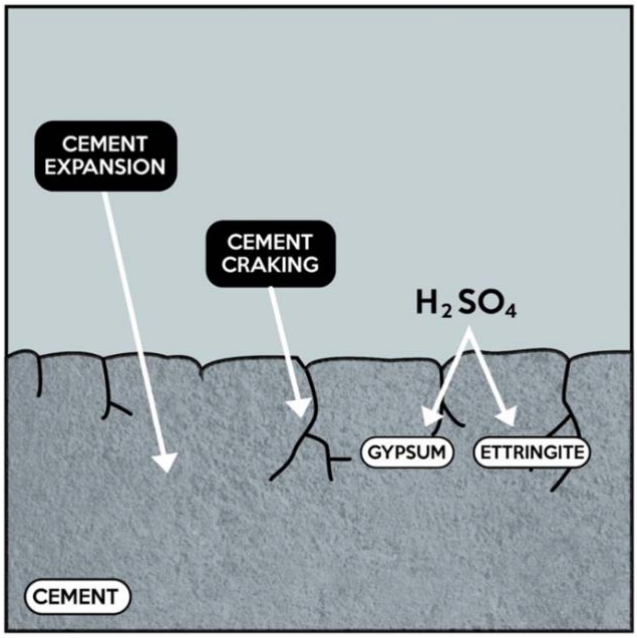

Figure 8. Cement degradation by sulfate attack in aqueous environments (Ugarte and Salehi, 2021)

2.3.4 Elastomer Failure

Packers are rubber sealing assemblies used to isolate fluids within the casing, tubing, and/or annuli. This is considered a secondary barrier in maintaining well control. Packer failure can affect well integrity, generate potential leakage, increase costs of repairing the well, compromise safety, and potential environmental hazards. Packers consist of elastomer materials made of rubber or polymers and the body of steel, making them susceptible to chemical degradation. Mainly, the steel body of the packer will be prone to corrosion. The elastomer material can be compromised during UHS operations due to rapid gas decompression (RGD). At high pressures, hydrogen can permeate inside the rubber elastomers. After RGD, the rubber material can become

oversaturated with hydrogen. This can exceed the material's yield tensile strength and generate internal blister fractures within the sealing rubber elastomer material (**Figure 9**). At high initial pressures, failure can occur within minutes; at moderate and lower pressures, it can take longer; the severity is proportional to the temperature, pressure, and decompression times (Ghosh et al., 2018).

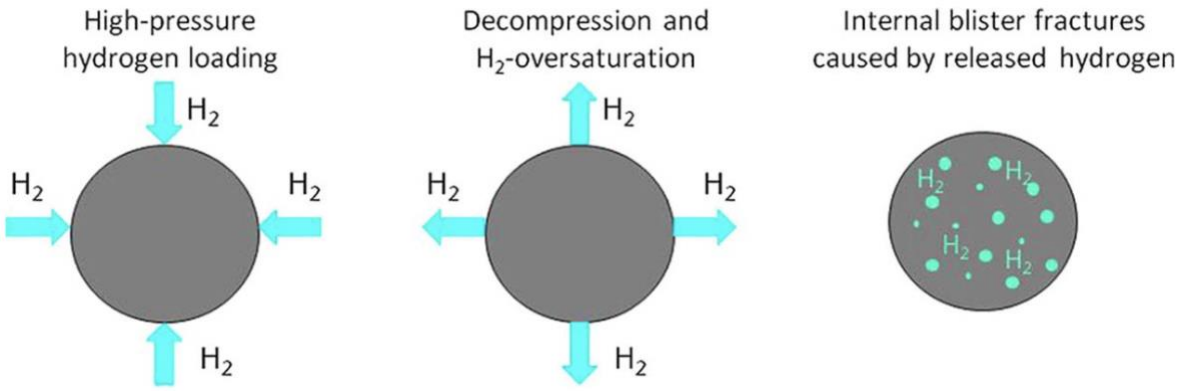

Figure 9. Mechanism of internal blister fracture damage to elastomer material caused by high-pressure hydrogen loading and fast decompression (Reitenbach et al., 2015)

Chemical degradation can occur when the elastomer material comes in contact with fluids that include drilling fluids, completion fluid, fracturing fluid, formation brine, or production fluid containing various solvents, caustics, acids, or corrosive chemicals (Patel et al., 2019). Leaching of chemicals into the elastomer can weaken its molecular structure (Campion et al., 2005). Gases such as hydrogen sulfide (H2S), carbon dioxide (CO2), and methane (CH4) can contribute to elastomer chemical degradation. When the elastomer is exposed to H2S present in the subsurface environment, its high reaction activity can lead to hemolysis and heterolysis, causing a reduction of tensile strength, ultimate elongation, and hardness (Patel et al., 2019; Salehi et al., 2019). Studies performed by Fernández and Castaño (2016) observed the development of brittle fracture surfaces on the elastomer with increased H2S concentration. CO2 is stable, inert, and not toxic. However, when carbonic acid is made in the presence of water and in large quantities, it can

become corrosive and cause a chemical reaction with the elastomer (Patel et al., 2019; Salehi et al., 2019). Fernández and Castaño (2016) observed an increase in volumetric swelling and permanent deformation with an increase in CO2 concentration. Dajiang et al. (2017) studied the mechanical effect load has on elastomers in the presence of liquid and gaseous CO2. Results showed that an increase in compression load increases swelling and damage, making CO2 degradation worse. Furthermore, the damage is more severe when CO2 is in the liquid phase than in the gaseous phase. CH4 is a very weak acid, but it does not react chemically with the elastomer, although it can permeate the material and cause other physical alterations affecting its properties (Campion et al., 2005).

2.3.5 Caprock Sealing Integrity

Caprock is an essential feature of the geological containment, as it prevents fluids from migrating upwards. Sealing integrity failure can lead to potential fluid leakage to the surface. Because of the properties, hydrogen may leak from the storage as a result of diffusion and dissolution due to its small molecules. Only small amounts, around 2%, can be lost by dissolution and diffusion (Amid et al., 2016; Carden and Paterson, 1979). Caprock sealing strength needs to be evaluated to avoid any possible losses, which are dependent on porosity, permeability, and capillary pressure. Salts and clay layers are the most common type of caprock; they provide tightness and hydraulic integrity against hydrogen. Capillary pressure is the pressure at which hydrogen gas can enter the larger pores of the caprock. Capillary pressure is controlled by interfacial tension, and contact angle are the two parameters that control. The low interfacial tension in a hydrogen water system results in low capillary pressure and a higher risk of hydrogen leakage through the caprock (Zivar, 2020). Therefore, water-saturated caprock provides an impermeable barrier for hydrogen due to the high capillary pressure. If the threshold pressure of the caprock is exceeded, gas will push water out of the caprock generating a leak (Carden and Paterson, 1979). The storage system needs to operate below the threshold pressure of the caprock to avoid losing caprock

sealing integrity. Hydrogen gas fingering (**Figure 10**) is another issue as it can generate path of faster viscous movement, leading to gas leaking points on the edges or spilling points of the sealing structure (Carden and Paterson, 1979). Depending on the trap structure. The viscosity difference between water and gas seems to be the factor dominating gas fingering.

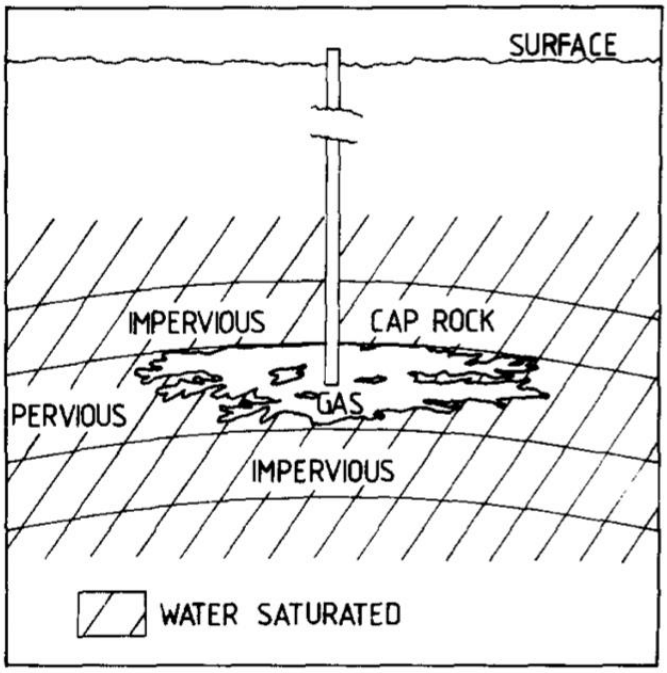

Figure 10. Gas fingering concept in Undeground Hydrogen Storage (Carden and Paterson, 1979)

Minerals precipitation and/or dissolution can also compromise the caprock sealing integrity. When the precipitation rate exceeds the dissolution rate, the caprock integrity will remain intact, though the porosity and permeability can be reduced, affecting the efficiency of injection and withdrawal operations. When the dissolution rates are greater than precipitation rates, injection and production efficiency may increase due to porosity and permeability enhancement. However, this will also lead to potential leaks due to sealing failure (Zivar, 2020). Rock mineralogy and pore size distribution can change due to rock and fluid interaction (Heinemann et al., 2018). Kaolinite, Illite, and Feldspar are common minerals in clay caprocks that can react, causing

porosity and permeability reduction (Hemme and Van Berk, 2018). Results obtained in experiments performed by Shi et al. (2020) showed that the permeability of the caprock decreased after injecting hydrogen and natural gas into the core samples. Given the results, this can be favorable for UHS operations as it would reduce the risk of caprock sealing failure.

2.4 Comparison with more implemented Technologies

The cyclic storage of hydrogen gas in the subsurface has similarities to conventional natural gas storage (UGS) and carbon capture and sequestration (CCS). Well construction and material selection for each storage type depend on the severity of the mechanisms that can compromise well integrity. **Table 8** shows a risk comparison between the different types of storage and the multiple mechanisms that can compromise storage integrity.

Table 3. Comparison between UGS, UHS and CCS with respect to the different mechanisms that can affect well integrity (Ugarte and Salehi, 2020)

	UGS	CCS	UHS
Corrosion	Depends on the selected geological formation, rock minerals, gas composition, pH, temperature, and salt concentration	Galvanic, pitting, and cervice corrosion. Carbonic acid from scale of iron carbonate as a corrosion product	High risk due to microbial organisms and hydrogen availability as an electron donor. Microorganisms' survival depends on pH, temperature, and salt concentration
Hydrogen blistering, HIC, and hydrogen embrittlement	Medium risk depending on the availability of hydrogen near the metal surfaces	Low due to lack of hydrogen presence	Due to abundance of hydrogen can increase the susceptibility to cracking at lower stresses, reduction of material ductility, and resistance
Cement carbonation	Reaction will depend on the amount of CO_2 found in the rock mineral and formation fluids	High risk due to abundance of CO_2 forming carbonic acid. Temperature and pH can aggravate degradation	Reaction will depend on the amount of CO_2 found in the rock mineral and formation fluids
Sulphidation	Depend on the amount of H_2S that can be found in the environment. Low pH can make pyrite become part of H_2S producing reactions	Low risk due to less probability of finding high amount of H_2S	Higher risk as H_2S is a by-product of microbial reactions caused by SRB
RGD	Methane can permeate and cause physical properties alteration	High risk as CO_2 in gas phase can cause degradation and permeate the elastomer element	Due to hydrogen physical properties, it can easily permeate the elastomer. Severity is proportional to temperature, pressure, and time
Elastomer degradation	Natural gas will not react chemically with the elastomer	High risk when elastomer material is in contact with carbonic acid	Moderate to high as H_2S by-product of SRB can cause a reduction of tensile strength, ultimate elongation, and hardness
Caprock integrity	Higher interfacial tension in a methane-water system results in high capillary pression and less risk of leakage	If dissolution rates are greater than precipitation rates in the caprock, efficiency may increase due to porosity and permeability enhancement leading to potential leaks	Low interfacial tension in a hydrogen-water system results in low capillary pression and high risk of diffusion

Microbial corrosion is the primary concern in UHS due to hydrogen acting as an electron donor for microorganisms living in the subsurface. This corrosion type will depend on the archaea inhabiting the formation, and it can vary from location to location. SRB is known to consume

hydrogen to produce corrosive H_2S and can inhabit any gas storage. These bacteria can be found in natural gas storage, but methane and carbohydrates such as guar gum and xanthate are not directly utilized by SRB (Kleinitz and Boehling, 2005). Salt concentration, temperature, and pH of the environment will determine if microorganisms causing corrosion can survive under subsurface storage conditions. Methane by itself is not highly corrosive for metals. The presence of CO_2 and H_2S found with natural gas are responsible for the related corrosion. In CCS, CO_2 can lead to galvanic, pitting, and crevice corrosion. In addition, chloride presence can accelerate crevice corrosion. CO_2 dissolved in water produces carbonic acid, which generates electrochemical reactions with steel. A scale of iron carbonate is formed as a product. All these corrosion types damage the material by removal, making the metal thinner leading to material failure.

Hydrogen blistering, HIC, and hydrogen embrittlement are dependent on the amount of hydrogen found in contact with the surface under certain conditions. Hydrogen embrittlement severely affects high-strength steels, which limits their application to UHS. Common severe corrosion alloys used in the oil and gas industry exhibit martensitic structure and provide better resistance against H_2S or CO_2 but will be susceptible to H_2 (Reitnebach et al., 2015). For CCS, corrosion rates are high (5–15 mm/year); under severe corrosive conditions, duplex steel and super austenitic steel can achieve smaller corrosion rates (Crotogino, 1995).

Cement carbonation is the biggest challenge associated with CCS. The attack of CO_2 reduces compressive strength and increases porosity and permeability. The alteration process is more efficient in the wet supercritical phase than in CO_2 dissolved in water (Barlet-Gouedard et al., 2006). For UHS and UGS, carbonation can be considered a problem depending on the amount of CO_2 found in the stored gas, cushion gas, or formation. Cement class H and class G, commonly used in oil and gas applications, have proven suitable for UGS. For CCS, Portland cement can be modified with additives to slow the reactions with CO_2; pozzolanic blended materials can

minimize the chemical attack of CO_2. No field test proves class G and class H cements will be suitable for UHS. Furthermore, hydrogen's physical properties could make it able to permeate to cement sheath. Therefore, low water-to-cement ratios are desired. Cement deterioration by sulphidation can occur in UHS due to H_2S producing reactions. Secondary ettringite formation leads to expansion crack within the cement sheath. It can be minimized by using latex additives. Sulphidation risk in CCS and UGS will be dependent on the amounts of H_2S present in the formation.

The packer elastomer element, hydrogen can permeate the rubber body more easily than methane. Chemical degradation of the elastomer can happen in the presence of CO_2, H_2S, and CH_4. In UGS, methane gas does not react chemically with the elastomer, although it can still permeate the material and cause other physical alterations (Patel et al., 2019). For CCS, CO_2 in the gas phase is inert and not toxic, but if carbonic acid is formed, it can corrode the rubber material and the steel body. The sealing performance of elastomers can be compromised after CO_2 chemical degradation, resulting in a decline in their sealing capabilities (Salehi et al., 2019; Ahmed et al., 2019). Fluorocarbon elastomers can exhibited more resistance to CO_2 degradation.

Caprock integrity failure is dependent on interfacial tension, capillary pressure, porosity, and permeability. Leakage risk is greater in UHS due to hydrogen's physical properties. In hydrogen-water systems, the low interfacial tension generates low capillary pressure and increases the risk of hydrogen gas diffusion through the sealing caprock. The opposite happens with methane-water systems from UGS. The high interfacial tension will generate high capillary pressure minimizing the risk of leakage through the caprock. Therefore, it is not a problem in UGS. For CCS, the dissolution of minerals due to the corrosive environment can lead to an increase in the porosity and permeability of the caprock, enhancing the risk of leakage through the caprock.

2.5 Cement

The focus of this study was to observe any variation in cement samples exposed to hydrogen. To understand this, it is important to understand cement manufacturing, classification, components, hydration process, structure, and pore size distribution.

2.5.1 Manufacturing and Classification

Portland cement is the most common cement type used in the oil and gas. It is composed of argillaceous (source of silica- SiO_2) and calcareous (source of lime- $CaCO_3$) ground materials that are mixed with other materials, such as gypsum. Mixing then occurs in temperatures above 1500 ^oC (2700 ^oF) to create Portland cement (**Figure 11**).

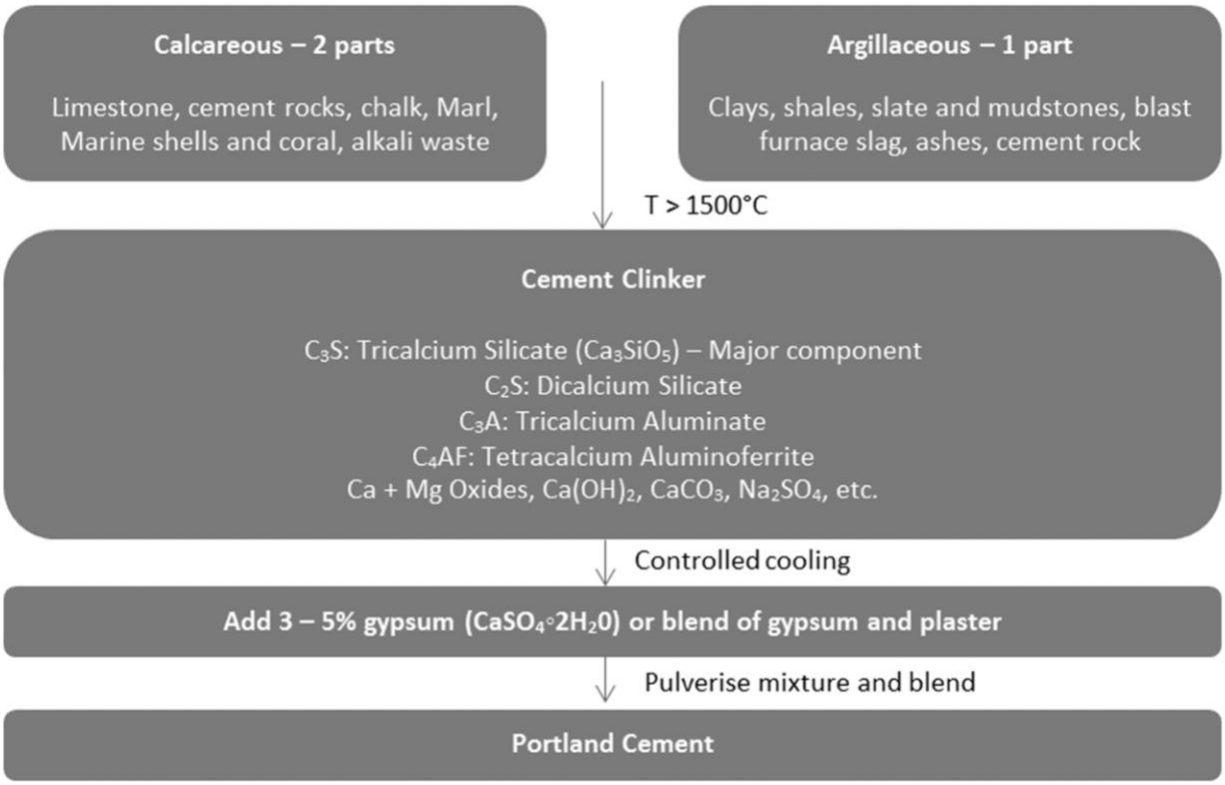

Figure 11. Portland Cement Production Workflow (Ichim, 2015)

The composition of Portland cement is shown in **Table 4.**

Table 4. Composition of Portland cement (Fink, 2015).

Compound	Percentage
Calcium oxide CaO	60-69
Silicon dioxide SiO_2	18-24
Aluminium oxide Al_2O_3 and Titanium oxide TiO_2	4 8
Iron oxide Fe_2O_3	1 8
Magnesium oxide MgO	<5
Sulfur trioxide SO_3	<3
Potassium oxide K_2O	<1
Natrium oxide Na_2O	<1

Cement used in the oil and gas industry is manufactured in accordance with the American Petroleum Institute. There are 8 cement classes, and 3 grades include ordinary (O), moderate sulfate-resistant (MSR), and high sulfate-resistant (HSR). The different cement classes are (American Petroleum Institute, 2010):

- Class A – Used in depths with less than 6000 ft when special properties are not required.
- Class B – used in depths with less than 6000 ft with requirements for moderate to HSR.
- Class C – used in depths with less than 6000 ft with requirements for high early strength (Higher C3A) and HSR.
- Class D – used in depths between 6000 ft and 10000 ft with requirements for MSR and HSR to counter moderately high temperatures and pressures.
- Class E – used in depths between 10000 ft and 14000 ft under high temperature and high-pressure conditions for MSR and HSR.
- Class F – used in depths between 10000 ft and 16000 ft under extremely high temperature and high-pressure conditions for MSR and HSR.
- Class G and H – used in depths with less than 8000 ft. Accelerators and retarders cover a range of depths and temperatures for both MSR and HSR. Class G cement has a finer particle size than Class H, which is coarser and requires more water for mixing.

2.5.2 Components and Products

The chemical composition of cement can be divided into four main mineral components (**Table 5**). These mineral components hydrate after mixing with water in order to form a rigid structure. S stands for silica, C for burnt lime or calcium oxide, A for alumina, and F for iron oxide (Aïtcin and Flatt, 2016). C3S hydration is a fast reaction that results in the formation of Calcium-silicate hydrate gel, which contributes to early cement strength during curing. C3A hydration reaction produces the required heat energy for the hydration reaction. C2S reaction with water is slow but influences the long-term strength of the rigid cement structure. C4AF effect on the physical properties is minor in both the short and long term. Therefore, the hydration of cement leads to the liberation of heat, change in volume, and mechanical bonding (Aïtcin and Flatt, 2016). The other hydration products that contribute to the cement properties include crystalline Calcium hydroxide ($Ca(OH)_2$), monosulfoaluminoferrite, and trisulfoaluminoferrite hydrates.

Table 5. Major Components that form the cement rigid structure.

Compound	Formula	Designation
Tricalcium silicate	3CaO.SiO2	C3S
Tricalcium aluminate	3CaO.Al2O3	C3A
Dicalcium silicate	2CaO.SiO2	C2S
Tetracalcium aluminoferrite	4CaO.Al2O3.Fe2O3	C4AF

Some of the reactions are generic to all kinds of cement, as suggested by equations (1)-(4).

$$CO_2 + H_2O \leftrightarrow H^+ + HCO_3^- \quad (1)$$

$$Ca(OH)_2 + H^+ + HCO_3^- \leftrightarrow CaCO_3 + SiO_2 \cdot H_2O \quad (2)$$

$$C - S - H + H^+ + HCO_3^- \leftrightarrow CaCO_3 + SiO_2 \cdot H_2O \quad (3)$$

$$2H^+ + CaCO_3 \leftrightarrow Ca^{2+} + H_2CO_3 \quad (4)$$

During hydration, cement is mixed with water with different percentages based on their requirements. The clinker components react with the water, precipitation hydrated products responsible for cement strength. It also affects the development of internal porosity. Depending on the water-to-cement ratio, the components, additives, and the curing conditions, the time it takes the cement to reach its strength can vary. Portland and oilfield types of cement settle and harden in both dry and wet environments (e.g., in air or water) (Nelson, 1990). The hydration of cement leads to mechanical bonding, heat liberation, and change of volume, depending on the curing conditions (Aïtcin and Flatt, 2016). During hydration, the cement slurry experiences shrinkage estimated to be between 1% and 8% of the absolute volume, also known as a chemical contraction (Keating et al., 1989). According to Powers' (1958), The cement paste must have a w/c ratio of at least 0.42 to reach complete hydration, and water can be classified as reactive, forming a solid gel (Powers, 1958). This produces the bonding properties of the cement and the non-reactive forming gel water glued to the hydrated cement paste. **Figure 12** shows the chemical contraction mathematical model for samples mixed at a 0.42 w/c ratio in a dry and wet environment. It is observed that during hydration in a dry environment, the relative volume of air increases with time, whereas in a wet environment, water enters the network of pores.

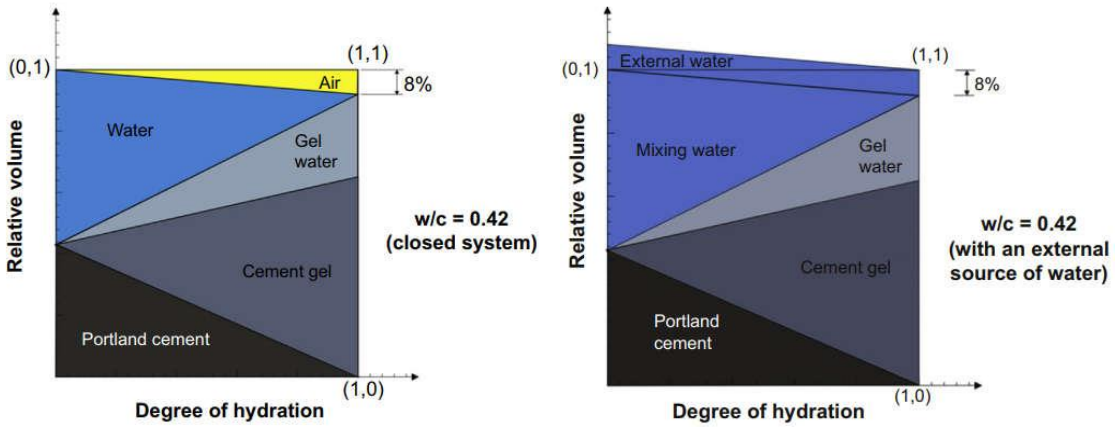

Figure 12. Relative Volume of Cement Components During Hydration in a Dry Environment (Left) and Under Water (Right) (Aïtcin and Flatt, 2016).

The hydration of Portland cement involves dissolution and precipitation in a complex chemical system, resulting in the formation of hydrates and the hardening of the cement. The hydration products are the following:

Table 6. Hydration products from cement curing.

Product	Designation	Formula
Calcium silicate hydrate	CSH	$3CaO.2SiO_2.3H_2O$
Calcium hydroxide	CH	$Ca(OH)_2$
Trisulfoaluminoferrite hydrates	AFt	$[Ca_3(Al,Fe)(OH)_6.12H2O]_2.X_3.nH_2O$
Monosulfoaluminoferrite hydrates	AFm	$[Ca2(Al,Fe)(OH)_6]_2.X.nH_2O$

Calcium silicate hydrate (CSH), a gel, is cement's most common hydration product. Calcium hydroxide (CH) is a crystalline phase also called portlandite. These two are responsible for the strength of the cement sheath. Trisulfoaluminoferrite hydrates (AFt), have ettringite as the most important phase. The hydration of C3A is essential in the early stage of hydration. It influences the mechanical and rheological properties of cement. This is because C3A's reaction with water is fast due to the precipitation of irregular hexagonal platelets of calcium aluminate hydrates on the clinker surface. Calcium sulfate is added to the clinker during its production process, leading to ettringite precipitation. Once the sulfate is completely used up, ettringite can react with the remaining C3A, forming monosulfoaluminate (Aïtcin and Flatt, 2016).

2.5.3 Hydration Process

The cement hydration process is exothermic due to the significant heat increase caused by the reaction between cement and water. Measuring the temperature makes it possible to estimate how far cement is in the hydration process. There are 5 stages of the hydration process shown in **Figure 13** that include Dissolution (I), Induction (II), Acceleration (III), Deceleration (IV), and Diffusion (V). After the initial mixing, the cement and water come in contact with each other, and this is where it reaches the highest temperature (Phase I). It is due to aluminate C3A reacting with water, calcium, and sulfate ions to form ettringite, causing a release of energy forming the

initial peak. The dormancy phase slows down the reaction as the access to water is not as good as during mixing. The amount of hydrated concrete increases steadily and remains fluid. Phase II ends with the initial set of concrete. During the next phase (III), heat increase occurs due to calcium silicate (C3S and C2S), which creates the silicate hydrate CSH. It can rapidly reach internal temperatures of 70-80 ^{o}C, and during this phase, there is also a significant risk of cracks if high variations occur. Phase IV is speed reduction; after the maximum temperature has been reached and the availability of free particles is reduced, there is a decrease in the heat flow rate. The fourth phase ends with the desired strength, and the concrete can be removed. The hydration process is now slowed down and will continue to finish the remaining available cement and water particles. The cement will now finish the hydration process and reach final strengths over more extended periods.

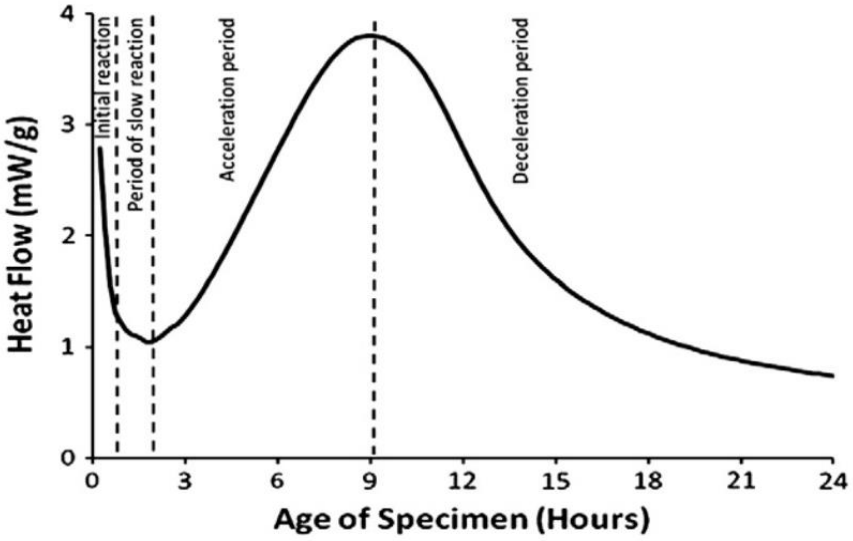

Figure 13. Heat Flow vs. Hydration time in cement. Dissolution or initial reaction (I), Induction or period of slow reaction (II), Acceleration period (III), Deceleration period (IV), and Diffusion (V) (Bullard et al., 2011)

Mechanisms of C3S (alite hydration) dominate the hydration kinetics of cement as it is the main component. Reactions between C3S and water begin immediately upon wetting, contributing to early heat flow. C3S continues to dissolve until reaching equilibrium calcium and silicate

concentrations in solution (Stein, 1974). C3S dissolution rates decelerate very quickly while the solution is still undersaturated, Garter et al. (2002) provided a detailed description of the proposed mechanisms responsible. C3S, hydration has two stages: formation of a silicate hydrate phase followed by the conversion into CSH once sufficiently concentrated with calcium. Reactions lead to poorly amorphous structured crystalline phase CSH and crystalline phase CH (portlandite). The growth mechanism is closely related to the development of CSH structure either as the aggregation of nanoscale particles (Allen et al., 2007; Jennigs et al., 2007) or as large but defective sheets of silicate layers (Gartner, 1997). Gartner et al. (2002) proposed four mechanisms for the accelerating hydration rate after the delay period in nucleation and growth observed in **Table 7.**

Table 7. Possible mechanisms of the onset of the nucleation and growth period (Gartner et al., 2002)

Hypothesis/mechanism	Brief description
Nucleation and growth of C–S–H	Nucleation and growth of a stable C–S–H happen at the end of the slow reaction period and are rate-controlling during the acceleration period as a metastable protective layer of hydrate becomes chemically unstable and exposes the high-solubility C_3S.
Growth of stable C–S–H	Nuclei of stable C–S–H, already formed during initial reaction, grow at a nearly exponential rate. C–S–H growth is rate controlling. No metastable hydrate barrier layer is invoked.
Rupture of initial barrier	Metastable C–S–H barrier layer is semipermeable. Solution inside is close to saturation with respect to C_3S. Osmotic pressure leads to its rupture
Nucleation of portlandite (CH)	Nucleation and growth of portlandite become rate-controlling (and thus indirectly control the rate of growth of C–S–H)

Mechanisms of C3A (aluminate) is the other phase that affects the hydration process kinetics. The reaction of C3A in the absence of calcium sulfate is very fast, and unlike alite there is no period of slow reaction, and the setting is almost instantaneous (Bullard et al., 2011). This is undesirable as the time to set the concrete is needed; therefore sources of calcium sulfate such as

gypsum (CaSO4·2H2O) or anhydrite (CaSO4) are commonly added to cement to control the reaction of the aluminate (Bullard et al., 2011). During the initial reaction, ettringite (C3A·3CaSO4·32H2O) is the main hydrate phase; after when calcium sulfate has all been consumed calcium monosulfoaluminate becomes the main product phase.

Gutteridge and Dalziel (1990) measured the hydration reaction of cement phases mixed individually over 100 days. The consumption of the phases was measured using X-ray diffraction analysis, where the mass composition of the cement was 68% C3S, 14% C2S, 6% C3A, 7% C4AF, and 2% calcium sulfate. **Figure 14** shows the hydration reaction plots for all phases except the C2S, with most of the reactions happening between 0 and 100 days.

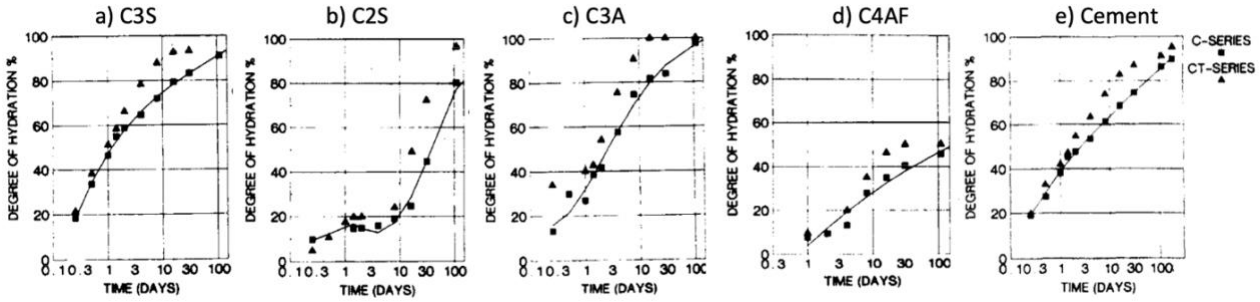

Figure 14. Hydration of a)C3S, phases b)C2S, c) C3A, d)C4AF, and e)Cement over 100 days (Gutteridge and Dalziel, 1990)

2.5.4 Porosity definition and sizes

When water is consumed during the reactions in the hydration process, cement porosity is affected. Solid cement is composed of randomly aggregated particles; it is both porous and permeable (Powers, 1958). Porosity depends on various factors, including cement clinker, w/c ratio, mixing method, and curing conditions. Cement can be classified by size into three main categories depending on the categories of pores, according to Muller (2014). Compaction or air voids (μm to mm) commonly created during mixing or air entrainment agents. Capillary porosity (>10 nm to μm) remaining spaces not occupied by hydration products or unreacted cement

grains. Some of these can originate from chemical shrinkage, where the bulk volume of hydration products is smaller than the volume of the initial components. Gel pores (>10 nm) are the intrinsic porosity of CSH. **Figure 15** shows the range of pore sizes of the different categories of cement described by different authors.

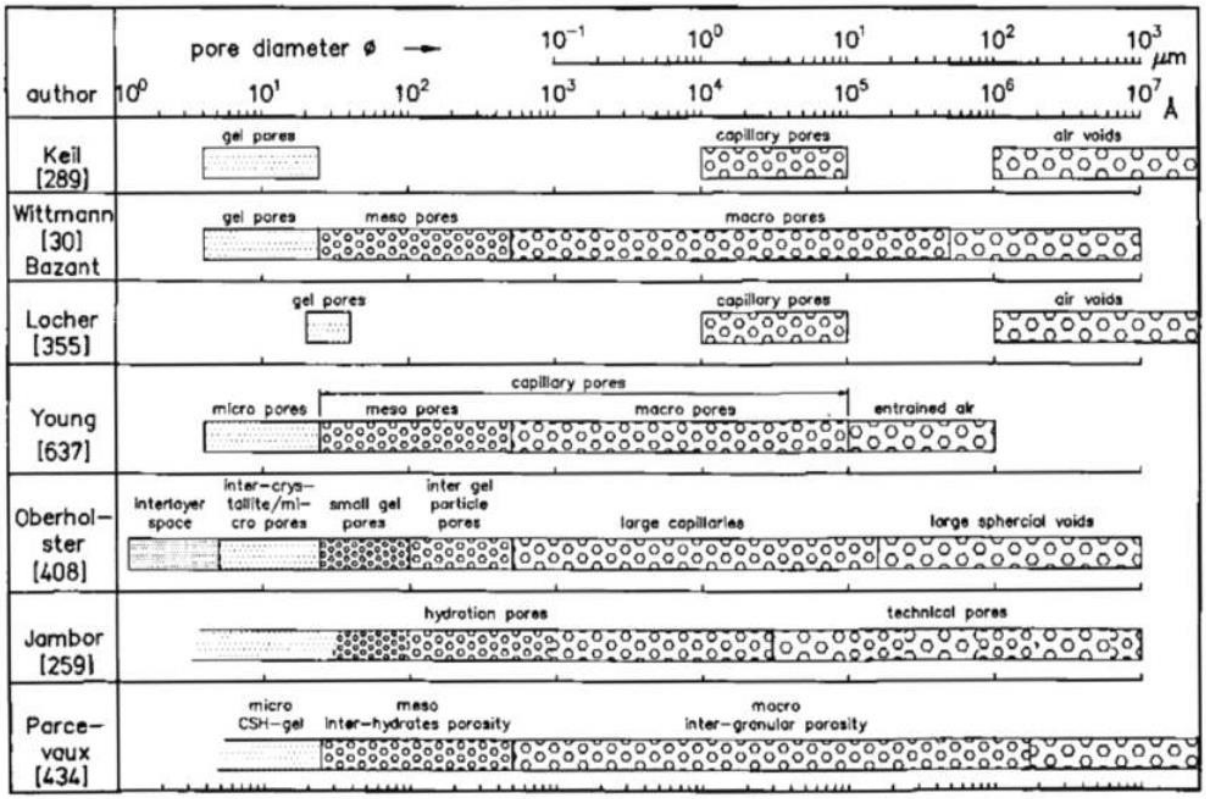

Figure 15. Porosity and the sizes ranges of the different categories of cement per different authors (van Bruegel, 1991)

It has been proven in a number of studies that permeability is dependent on the porosity of cement (Lafhaj et al., 2006). The relationship seems natural as a higher number of pores with a larger size would allow fluid to flow through it faster than the opposite. Porosity-permeability relationships are derived from a simple model with the assumption that the fluid flow of the pores is equivalent to a set of parallel circular channels (Lafhaj et al., 2006; Udegbunam et al., 1999). In cement, pores fall into two categories: open and closed pores. Open pores are connected to the outside surfaces. Closed pores are not connected to the outside surfaces. Therefore, open

pores are the predominant pore type controlling permeability among interconnected pores. It is expected that the interconnected porosity would have a more significant effect on the water permeability, whereas the open porosity would have a greater effect on the cement strength (Li et al., 2021).

2.6 Cement System Well Integrity Failures

The study of mechanical well integrity is essential to understand the distribution around a wellbore and in the annulus. Stress analysis is a critical part of the cement sheath design process. The mechanical response of cement under different load scenarios needs to be studied to determine the key controlling parameters that affect well integrity. Laboratory and modeling studies done by a number of research studies have shown that a principal cause of damage is the stresses induced by varying downhole conditions (Goodwin and Crook, 1992; Bosma et al., 1999; Eshiet and Sheng, 2014). In storage wells, changes in pressure and temperature will induce stress on the cement sheath (Wu et al., 2014).

2.6.1 Failure modes

Failure modes of cement systems include debonding of interfaces between casing and cement or between cement and rock, shear damage, radial cracking, and disking, as observed in **Figure 16** (Bois et al., 2010). Tangential stress or hoop stress is a normal stress in the tangential direction. Radial stress is perpendicular to the symmetry of the wellbore. These stresses determine the conditions of the casing, cement and rock (Bai et al., 2015). Debonding is caused by shrinkage during cement hydration and depressurization or temperature decrease inside the casing. Cement compression failure occurs if its compressive strength is exceeded. Compressive shear damage results from unequal or large differences in principal stresses. This difference result from a decrease in the tangential compressive stress that occurs during cement shrinkage. Radial cracking occurs due to hydration volume reduction in the construction phase of the well or over-

pressurization or temperature increase inside the casing. Typically the tangential stresses are compressive. A change in downhole conditions might turn the hoop stress into tensile. If the tangential stresses exceed the cement tensile strength, a failure in traction occurs. Finally, disking occurs by axial contraction of the cement sheath when cement cannot slide at its inner or outer boundaries (Bois et al., 2010).

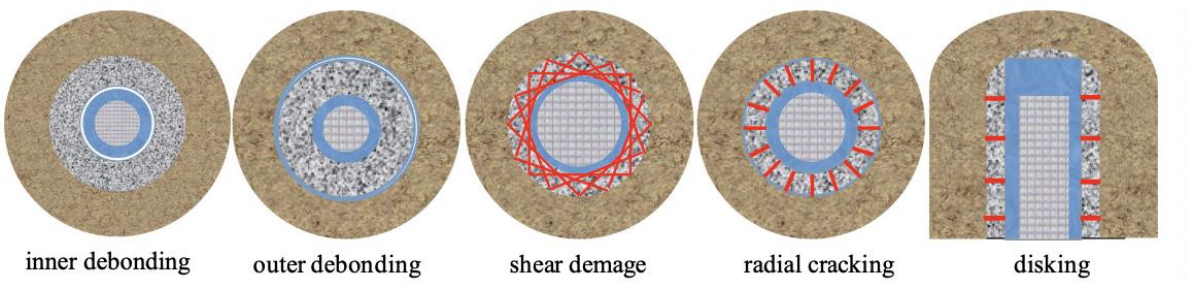

Figure 16. Cement sheath failure modes (Bai et al., 2015)

2.6.2 Downhole conditions changes

Downhole conditions can vary, especially in storage wells where injection and production cycles can generate changes in pressure and temperature, inducing stresses on the cement sheath. Bai et al. (2015) provide a detailed description of different scenarios of downhole condition changes. An inner pressure increase inside the casing can cause an increase in radial and axial stress. This may occur due to drilling, perforations, stimulation, or injection. It may even turn into tensile stress due to the decrease in tangential stress. An increase in pressure can cause compressive stress across two interfaces (casing/cement or cement/formation) and provide good well integrity. On the other hand, radial cracking can occur if the tensile stress failure in the tangential direction exceeds the tensile strength. An inner pressure decrease can increase the tangential compressive stress. This may occur due to a low mud weight utilized during drilling. It will decrease the radial and axial compressive stress and may turn them into tensile stress. The interface between casing and cement is the weakest point in the composite system. Microannuli

can provide weak points for interface failure due to tensile stress. The result will be debonding if the tensile stress exceeds the bond strength of the two interfaces.

A temperature increase occurs during the production of the fluid from the formation as downhole temperature increases with depth. This can cause an increase in compressive stresses and lead to cement failure when the yield strength is exceeded. On the other hand, a temperature decrease can occur due to injection phases, as the injection fluid may be at a lower temperature. This can decrease the radial, axial and tangential stresses. In addition, compressive stresses may turn to tensile stresses. Since the tensile strength is extremely low, there can be potential damage to the interface or even debonding (Bai et al., 2015).

Furthermore, for a rigid formation (high Young's modulus), a pressure or temperature increase can cause the compressive stresses to exceed the cement compressive strength; when the cement is squeezed between the two interfaces, a failure in compression may occur (Wu et al., 2014). A pressure or temperature increase inside the wellbore will push the casing outward for a soft formation (low Young's modulus) or rigid cement. If the rock is not rigid enough to hold the push, thus the casing and cement sheath expands outward, which increases the diameter. Such deformation will stretch the cement, creating tangential stresses; if the tangential stresses exceed the cement's tensile strength, a failure in traction occurs (Wu et al., 2014). Microannulus: will occur if the cement sheath loses its hydraulic bond with the casing and/or the formation. Pressure or temperature decrease inside the wellbore is another phenomenon that can cause the creation of the microannulus.

A cement sheath with characteristics that can withstand these stress levels is needed. Studies have shown that cement with a low Young's modulus and low expansion properties is the best option for mechanical durability and resistance to stress. Wu et al. (2014) suggests flexible and expanding cement technology based on a particle-size distribution technique with a trimodal

particle-size design. The trimodal particle-size design system uses an engineered blend comprising at least three engineered particle sizes (coarse, medium, and fine) that fit together to reduce the void space, decreasing the water requirements during mixing and thus increasing the slurry solid contents to yield the optimized overall slurry properties. Reduces chances of microannuli.

3. EXPERIMENTAL DESIGN AND METHODOLOGY

This section focuses on the experimental methodology's materials, design, experiments, and assumptions. Explanations and justifications are provided, including a detailed description of the equipment used. This study provides a comparison of experimental tests to highlight the effects hydrogen can have on cement during aging. Samples are cured in two different environments, based in distilled water and another in water saturated with hydrogen gas (H_2). The samples were then characterized using different physical and chemical tests such as Unconfined Compressive Strength (UCS), Fourier Transform Infrared Spectroscopy (FTIR), Porosity and Permeability (PP), Nuclear Magnetic Resonance (NMR), Scanning Electron Microscopy (SEM) and Energy Dispersive X-Ray Spectroscopy (EDS). UCS was measured using a universal testing machine to measure the strength of the cement. Fourier transform infrared spectroscopy (FTIR) was performed to monitor the amount of hydrated product. The analytical characterization of the samples cured in the different environments was compared using a Scanning Electron Microscopy (SEM) analyzer to observe any difference in the microstructure. EDS provided an elemental decomposition of the sample to see any change in composition when comparing the two cases. Porosity was measured using two different methods. Nuclear Magnetic Resonance (NMR) was used to measure the porosity of the sample being fully saturated, while the permeameter used samples fully dried. Finally, permeability was measured using the permeameter, with helium gas being the closest in molecular weight to hydrogen. The aforementioned experiments provided a complete methodology to quantify the impact of hydrogen present in water during aging conditions by comparing results to base samples aged in pure water.

3.1 Sample Conditioning

In this study, neat Class H cement, a commonly used cement type, was used to fabricate the samples. Class H has a coarser grind that provides better retarding properties for cementing wells. A slurry density of 20 lbm/gal (3.4 gm/cc) was used with a water-cement ratio of 0.38 in accordance with ASTM C 109 (2004) to represent mixtures in the field. The total volume for the cement slurries used were kept constant at a mean value of 600 ml for consistency.

Cement samples were prepared using a commercial blender with a 3.5 hp (**Figure 17a**). The blender was configured to mix at a certain speed setting (rpm) during predefined times. Mixing conditions were done in accordance with API-10B2 (2013). 4000 RPM for 15 seconds, where all solid components were added to the liquid components in the blender. Then 35 seconds at a higher speed of 12000 RPM. The mixing energy under API-10B2 cement mixing recommendations is 5.9 kJ/kg. The mixing energy was kept constant for all the cement slurries throughout the study for consistency because the thickening time of the cement slurries has been investigated to decrease with an increase in mixing energy (Hibbert et al., 1995).

The cement samples were cast in the form of cylinders with a 1-inch diameter and 1.5-inch height for dimensions (**Figure 17b**). Soon after preparing the cylindrical cement samples, these were immediately submerged in a hot water bath to cure for 12 hours at temperatures of 140 ± 10 ^{o}F (**Figure 17c**). After the desired hydration periods, the hardened samples were placed in different environments to cure for different timeframes. Before performing any tests, samples were polished using fine sandpaper. Each batch consisted of twelve samples for each curing time and were prepared to provide reproducibility and provide sufficient data for accurate results. No pressure was imposed during curing; this was a limitation and a possibility for further studies.

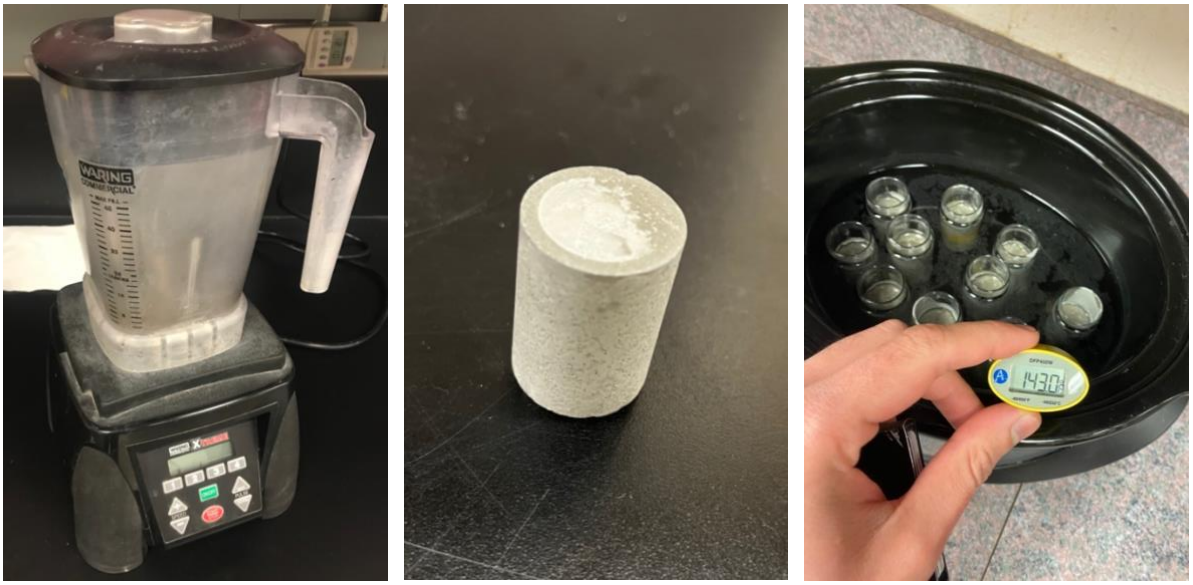

Figure 17. a) Blender used for mixing and cement sample preparation. b) Sample cylinder dimensions with a 1-inch diameter and 1.5-inch height. c) water bath for curing samples.

Six samples were then aged in each of the two different environments, the first consisting of base distilled water and the second consisting of water saturated with hydrogen gas (H2) with concentrations around 2 ppm. Hydrogen is generated through electrolysis, where water is split into hydrogen and oxygen using Proton Exchange Membrane (PEM) and a Solid Polymer Electrolytic (SPE). **Figure 18a** shows the hydrogen pitcher used to generate the environment consisting of water saturated with hydrogen. H_2, also called molecular hydrogen, is the most common form of hydrogen because of its stability with a neutral charge consisting of two protons and two electrons. Molecular hydrogen (H_2) is a neutral molecule when dissolved in water and should have no influence on the water's pH. Although, samples exposed to water saturated with hydrogen exhibited higher pH compared to samples exposed to water. The concentration of hydrogen and pH was measured using a portable hydrometer (**Figure 18b**).

Figure 18. a) Hydrogen pitcher used to generate hydrogen in water. b) portable hydrometer used to measure hydrogen content in water in ppm, temperature in C, and pH.

3.2 Mechanical Measurements

A compression universal testing machine (**Figure 19**) custom-made was used to determine the unconfined compressive strength (UCS) of the cement samples. Also known as uniaxial compressive strength, it measures the material's strength. It is defined as the maximum axial compressive strength a cylindrical sample can withstand along one axis under unconfined conditions. The testing machine applies a uniaxial load on the cylindrical cement sample at a constant stress rate controlled by the test machine. In this experiment, the compressive strength of the cement samples was measured using a loading rate of 0.6 MPa/min in accordance with ASTM C 109 (2004). The data acquisition system records the applied load (lbf), and each cylindrical sample was loaded until failure, where the peak load was obtained. To statistically capture any variance, at least 5 specimens from each sample batch were used in this test. Then, the compressive strength is calculated by dividing the maximum applied load by the measured surface area of the cylindrical samples, which were in complete contact with the load-bearing

plate of the load frame. The strength of the cement is directly related to the development of the microstructure in the bulk or surface by the hydration reaction of the cement with water during curing (Jo et al., 2018; Neville, 2011). Results were recorded and reported to the first 3 decimals and averaged among all samples from the same test at the same time as per API RP 10B-2. UCS tests were run on samples cured for 7, 28, 84, and 168 days.

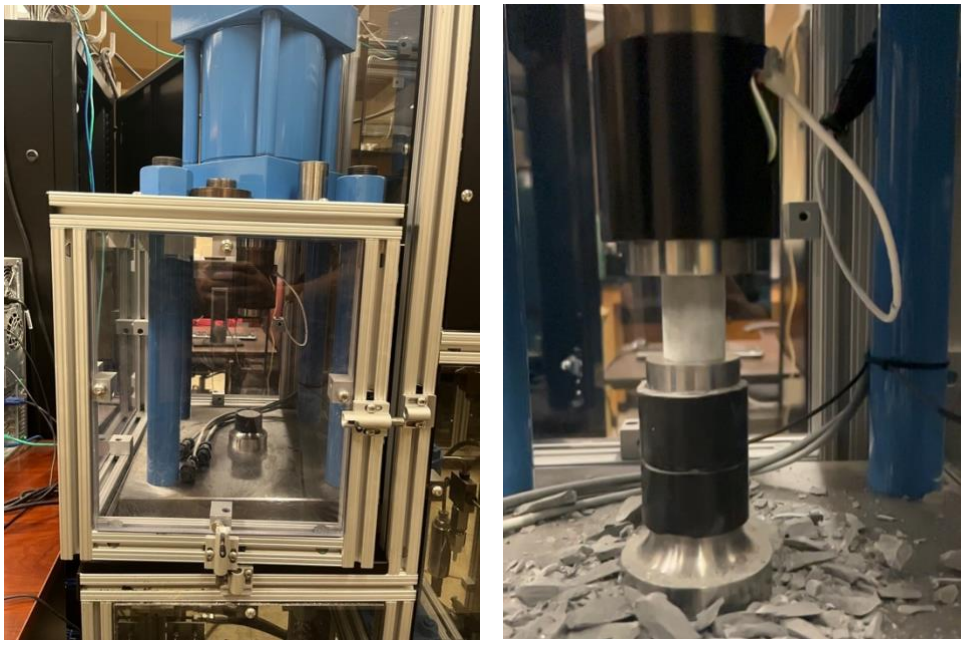

Figure 19. Unconfined Compressive Strength Testing Machine.

3.3 Petrophysical Measurements

Porosity is an essential factor in Petrophysical properties. It is directly related to the mechanical properties of cement. Experimental work has been done on the effect of porosity on the mechanical properties of cement (Mai and Cotterell, 1985). The porosity of the cement can determine its strength, supported experimentally by variations of the air content (Osbaeck, 1985) or the removal of large pores from the cement pastes (Kendall et al., 1983). Cement compressive strength varies with porosity; consequently, the higher number of voids (higher porosity) within the structure can lead to a lower compressive strength (**Figure 20**). Other properties such as Poisson's ratio, Young's modulus, and fracture toughness are also affected by porosity. The

weakest links are pores, voids, and cracks, providing starting points for crack initiation and further growth (Kunther et al., 2017). Maximum-sized pores do not determine the flexural strength; a crack will initiate at the largest pore or bonded cement interface (Mai and Cotterell, 1985).

Ghafoori and Dutta (1995) stated that most of the pores in cement are formed by the spaces left between the coarse aggregates that distinguish between porosity and air-void content. Therefore there is a variation between total and effective porosity. Total porosity accounts for all the porosity connected or non-connected within the cement. The strength of the cement is affected overall by the volume of its overall voids (Neville, 2011). Effective porosity is the pore volume of the interconnected pore space. Pores can have a wide variety of ranges from nano to micro-scale (Lian, 2011). In addition, the water/cement ratio is another predominant factor in the initial porosity during the hydration process. 0.25 is used as the ratio of hydration by weight, and the non-evaporable water reduces to approximately 0.75 of the original volume after chemically hydrating the cement (Neville, 2011). A lower water/cement ratio will yield to higher UCS and vice versa (**Figure 20**), while composition remains identical for all samples.

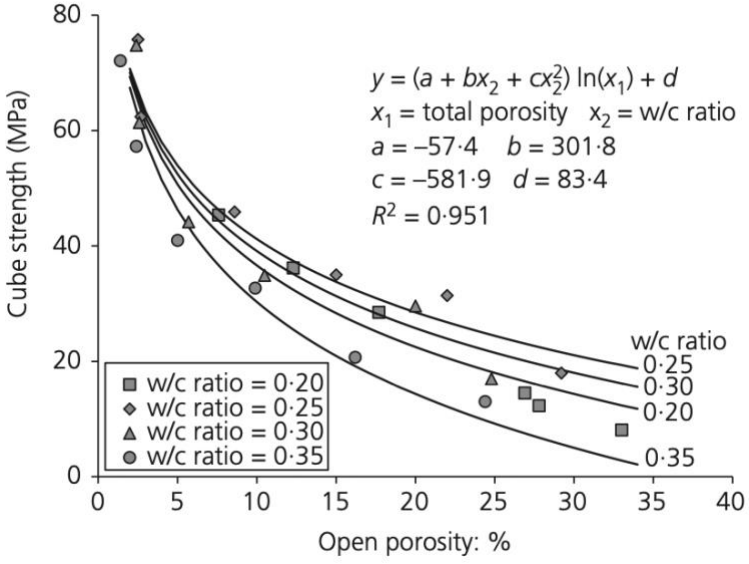

Figure 20. **The combined effect of porosity and w/c on cement compressive strength (Li et al., 2021)**

Accurate porosity testing is quite challenging due to its unique complex microstructure. A known method is mercury intrusion porosimeter (MIP), which is effective for observing the pore configuration in normal cement. MIP method is not feasible for porosity cement testing because a large number of connected voids within porous cement can cause mercury leakage. Vacuum sealing apparatus is more appropriate for porosity measurement in laboratory testing (Huang and Shu, 2010). AP608 porosimeter and permeameter were used for these measurements (**Figure 21**). It uses Boyle's Law to measure porosity. This vacuum-sealed apparatus flows helium through the porous cement to obtain the measurements. Helium was used as the gas, being the closest to hydrogen in terms of molecular size. However, helium is an atom, and hydrogen is a molecule; only then helium's molar mass is twice the other. As an atom, helium move has only translational kinetic energy (forward and backward via cartesian degrees of freedom), while hydrogen can also rotate with 2 degrees of freedom, also having rotational kinetic energy. Thus, on average, hydrogen will have 1.67 times the kinetic energy of helium. This validates the results using helium, providing a good estimation. Helium flows from one end to the other of the cement within the core holder. A confining pressure (overburden pressure) is applied. After, a large thermally stable reservoir is pressurized. The reservoir discharge valve is opened, allowing the helium to flow into the sample to measure porosity. Prior to performing the measurements, samples were polished to ensure proper contact between the cap for accurate testing avoiding misleading measurements. In addition, samples need to be dried in the oven for 24 hours at temperatures around 180 ^{o}F.

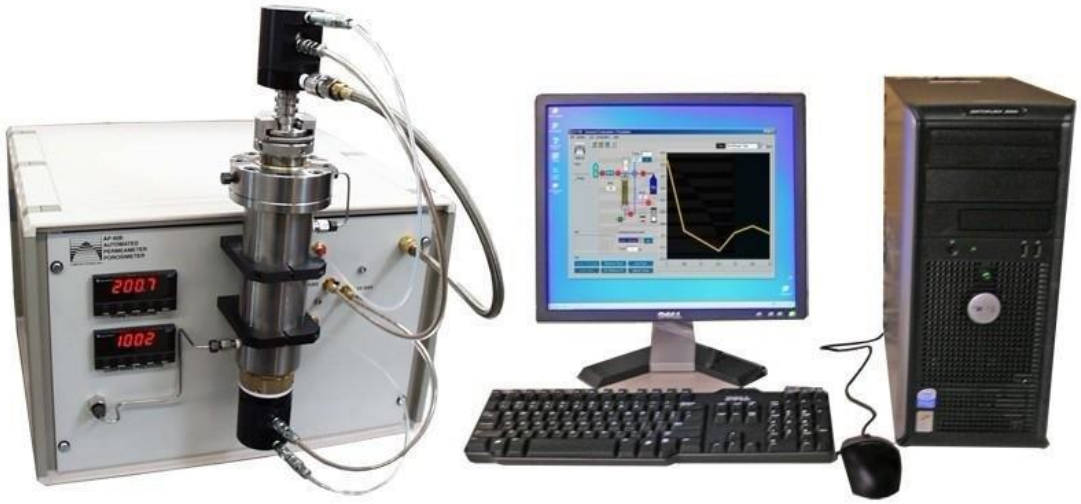

Figure 21. AP608 instrument to measure porosity and permeability. It uses helium, Boyle's Law to measure porosity, and an unsteady state technique to measure permeability.

Permeability is the unique ability of a fluid to penetrate through the porous media. It depends on the porosity of cement as a higher number of porous spaces with a larger size would allow fluid to flow through it faster than a lower number of porous spaces with a smaller size (**Figure 22**). A simple method to measure permeability in laboratory conditions steady-state method, the use of gas as a pore fluid instead of water for the permeability has many advantages. First, gas flow meters cover a wide range of flow rates, allowing the measurement of a wide range of permeabilities. Second, nitrogen and helium gases are chemically inert, ignoring geochemical effects, so only permeability variation caused by a change in confining pressure needs to be considered. Third, the compressibility and viscosity of gas are less sensitive to changes in temperature, so permeability measurement errors due to these three factors are less likely (Tanikawa and Shimamoto, 2009). However, permeability when using gas is higher than water permeability (Faulkner and Rutter, 2000) due to Klingenberg's effect on pore-pressure dependence. Gas slippage at the pore wall causes gas permeability to vary with the molecular weight of the gas and pressure. Klingenberg correction overcomes this, which is quite important

for cement due to its low permeability. AP608 porosimeter and permeameter automatically measure permeability; at the same time, it measures porosity. It is also a function of confining pressure (overburden pressure). The pressure decline is monitored during permeability measurements with a digital gauge. An unsteady state technique is used to measure permeability.

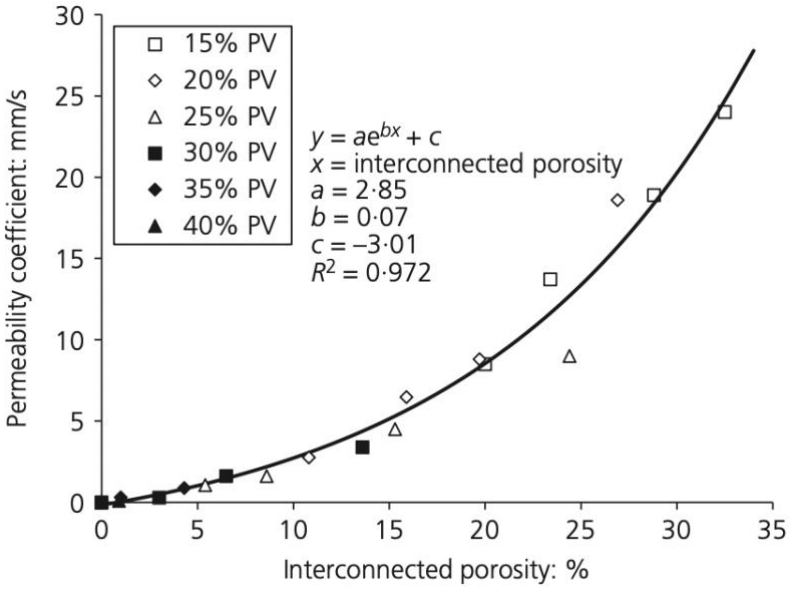

Figure 22. Effect of porosity on permeability at different paste volumes (PV) (Li et al., 2021)

Nuclear Magnetic Resonance (NMR) is a widely used tool in the oil and gas industry to measure petrophysical properties. Its greatest advantage is that it can measure the response to fluid directly. NMR can provide measurements of porosity and free plus bound water. Estimates of permeability can be obtained using NMR data and empirical correlations (Coates, 1999). The amplitude of H is used to estimate the porosity of the surrounding formation or fluid content, and the relaxation times are used to evaluate the pore size distribution. Water within the sample contains protons that have a net magnetic moment and spin. This can align parallel to a magnetic field subjected using magnets. Sufficient pulse duration causes the protons to tip at a 90-degree angle. When the pulse is removed, the protons begin to relax. A series of 180-degree pulses are used to realign the protons. When the proton comes in contact with a mineral surface, it relaxes

and changes its orientation. Therefore, in smaller pores, relaxation is faster than in larger pores. Surface relaxivity dominates, and the signal decay rate is inversely proportional to the size of the pores where the protons are. For more information regarding the basic principles of NMR please refer to Coates (1999) and Dunn et al. (2002).

A GeoSpec2 NMR system produced by Oxford Instruments was used to measure the NMR porosity of the samples (**Figure 23**). This equipment operates at a frequency of 2 MHz. During cement hydration, water is an integral component that can affect the microstructure and various properties, including porosity and pore size distribution. This is the reason why NMR measurement on cement can be advantageous. After the curing time of the sample, these were immediately removed from the aqueous curing environment and placed in a glass vial for NMR testing. The glass vial was covered with a Teflon lit to prevent fluid evaporation during the testing. Accurate T_2 measurements depend on the static magnetic field strength and the length of the echo spacings. Combined with T_1, these can provide insightful information on water in micropores, solid gel, and solids representing hydroxy groups ($Ca(OH)_2$).

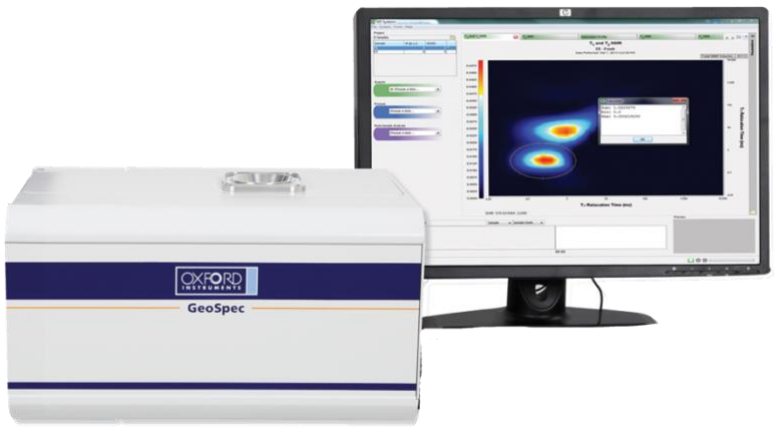

Figure 23. GeoSpec2 Nuclear Magnetic equipment by Oxford Instruments used to measure porosity

During hydration, part of the water enters the structure of the newly formed mineral while the other adsorbable water remains in contact with the surface as hydration and hardening continue (Schreiner et al., 1985). These two types of water can be distinguished as they have different relaxations. The exact role of various water fractions in the overall hydration process of cement is quite complex. The pore wall relaxation is greatly affected by paramagnetic impurities such as iron and manganese (Bryar et al., 2000). This causes relaxation processes to become more complex in NMR experiments due to the induced magnetic field. Since spins in different magnetic field strengths with different frequencies can cause dephasing and loss of signal (Schutle and Holthausen, 2019). Dephasing is caused by a constant difference in a magnetic field strength that can be accounted for with adjustments in the echo spacing, allowing accurate measurement of T_2 relaxation. Extensive research has been done on cement hydration, enabling the attribution of T_2 to different pore water species (McDonald et al., 2010).

3.4 Acoustic Velocities Measurements

Seismic elastic waves are categorized as P-waves and S-waves. P-waves also referred to as compressional waves, are the primary waves that travel faster because there is more resistance to deformation along the axis of the propagating wave. Compressional waves can travel through both solids and fluids medium. S-waves also known as shear or transverse waves, travels slower than compressional waves. Also, shear waves only propagate through solids due to the perpendicular motion of the particles along the axis of the propagating wave. As elastic waves travel through solids the speed depends on the densities and elastic properties of the cement. Elastic wave velocities are created by the applied force upon the mass as proposed by Newton's second law of motion (Goodman, 1989). Hence, elastic waves velocities can be described as a function of mechanical properties (Gomez et al., 2010; Si et al., 2016). Mechanical properties represent the elastic and inelastic behavior of a material under pressure. The elastic moduli are comprised of Young’s modulus, Poison’s ratio, Bulk’s modulus, and Shear’s modulus. Velocities

are dependent on the ratio of rock moduli to density. Seismic velocities, compressional wave (Vp), and shear wave (Vs), of anisotropic material, are a function of the elastic moduli (1-3):

$$V_p = (E/\rho)^{0.5} \quad (1)$$

$$V_s = (G/\rho)^{0.5} \quad (2)$$

$$V_p/V_s = [(1-v)/(0.5-v)]^{0.5} \quad (3)$$

where E represents Young's modulus, p is the Bulk's density, G is the Shear's modulus, and v is Poisson's ratio. Knowing Vp and Vs and density allows us to calculate any of the other moduli for an isotropic material.

To measure the compressional wave (Vp), and shear wave (Vs) a pulse transmission setup was used (**Figure 24**). Pulse transmission is a simple technique to measure the velocity of sound waves through rocks and fluids. A transducer acts as a transmitter generating a voltage that is applied to the piezoelectric crystal. This expands creating a mechanical or acoustic wave. The wave propagates through the length of the sample. On the other opposite end, there is a receiving piezoelectric crystal. The distortion causes the crystal to output a voltage that is amplified and recorded on the digital oscilloscope. A trigger signal is generated simultaneously with the start of the excitation signal to provide a zero-time reference. The measurement consists of getting the transit time, tt required to traverse a sample of length, l, then the associated velocity can be calculated. The measurements are a function of increasing confining pressure (overburden pressure). An increase in the confining pressure compresses the pore space resulting in a reduction of porosity, thereby increasing density, and an increase in moduli or the resistance to deformation.

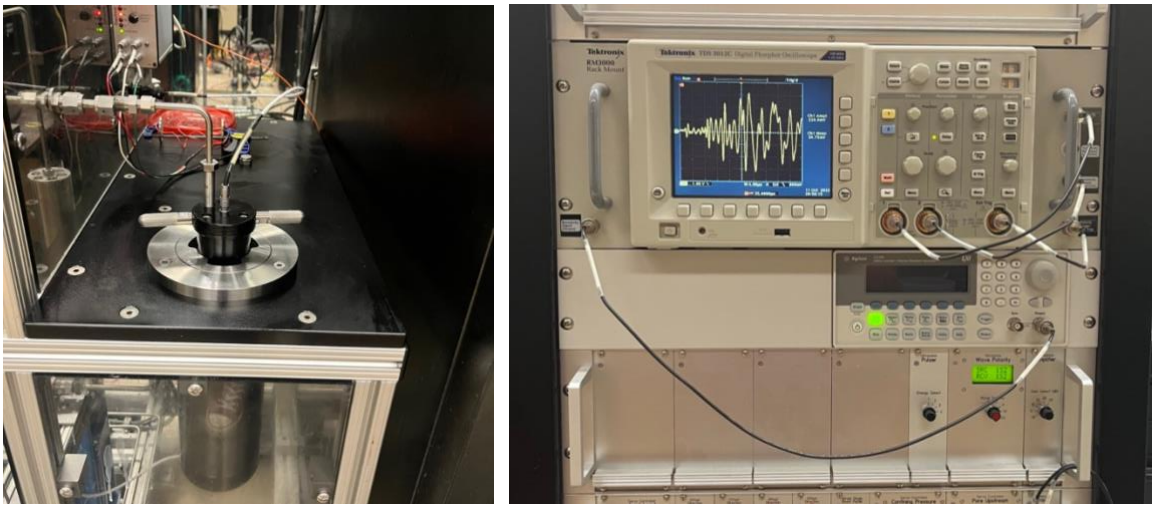

Figure 24. Acoustic velocities setup consists of a a) pressure vessel that contains the samples in the left and b) he pulse transmission (transmitter, digital oscilloscope, amplifier) in the right.

3.5 Compositional Measurements

Compositional measurements were performed in order to compare and determine if hydrogen generates any compositional change in cement. Fourier Transformed Infrared Spectroscopy (FTIR) and Energy Dispersive X-Ray Spectroscopy (EDS) allowed comparison between the samples and see any change within the main components and any change wt% of the elements in the cement.

FTIR is an infrared spectroscopy method that can determine and quantify mineralogy. The concept is based on passing an infrared beam through a sample, the sample absorbs radiation, and the rest is transmitted passing through the sample to the detector. The signal is measured in the detector resulting in a spectrum. It measures how much light a sample absorbs at each wavelength. The technology relies on the excitation of mineral bond vibrations in the infrared band. Absorption, emission, and reflection spectra arise from molecular bonds' vibrational and rotational energy states. If the radiation frequency matches the molecule's vibrational frequency, then absorption takes place. There are multiple vibrational modes in three dimensions; this will cause each molecule or mineral to have several absorption frequencies, a characteristic spectrum, or a fingerprint. Beer's Law governs absorbance.

The FTIR equipment is Nicolet 6700 from Thermo Scientific (**Figure 25**). This normal dispersive emits the infrared source as it passes through a sample made with a dispersive element to a detector. The dispersive element uses potassium bromide because it is an intensive neutral material that can extend the wavelength region to 400 cm-1. The samples are prepared using 0.005gr of the mixed samples through a set of processes with 0.30 gr of potassium bromide. Before being measured, the spectrum of potassium bromide is measured and zeroed out. This is done to avoid measuring the spectrum of potassium bromide. Therefore, it will only capture the sample spectrum when the measurement is done. The raw data is collected as a transmission spectrum and converted to an absorbance using the following equation (1):

$$A = -log_{10}(T/100) \quad (1)$$

FTIR software allows performing quantitative analysis. This requires a dataset built with mixtures of carefully weighed known minerals. The software can perform a partial least squares analysis of the diagnostic portions of the collected spectra; a series of regression coefficients are used to relate the magnitudes of absorbance at characteristic frequencies to the quantity of mineral present. Comparing this, the software can generate the weight percentages of minerals present as the output.

Figure 25. Nicoet 6700 Fourier Transformed Infrared Spectroscopy (FT-IR) Thermo Scientific equipment used to observe mineralogy.

FTIR spectra can analyze cement and infer something about its hydration based on the absorbance peaks and wavelength location. The relative peak intensity ratio of the IR bands is an indicator of the amount of hydrated product (Chakraborty et al., 2016). Peaks at 3650, 3400-3500, 2900, 1650, 1425 and 980 cm-1. These are due to the O−H stretching of calcium hydroxide at 3650, Si−O stretching of polymeric silicate (C−S−H) at 980 (Garcia et al., 2009). **Table 9** shows a band assignment with wavelength for common elements of cement from studies performed by Garcia et al. (2009).

Table 8. Band assignment for cement components (Garcia Lodeiro et al., 2009)

Band	Gel N0 (cm^{-1})	Assigned to	Band	Gel N2 (cm^{-1})	Gel N4 (cm^{-1})	Gel N10 (cm^{-1})	Assigned to
1	3635	ν OH ($Ca(OH)_2$)					
2	3439	ν OH (H_2O)	a	3432	3436	3438	ν OH (H_2O)
3	1631	δ OH (H_2O)	b	1635	1630	1626	δ OH (H_2O)
4	1470	ν_3 CO (CO_3^{2-})	c	1489	1424	1424	ν_3 CO (CO_3^{2-})
5	1417	ν_3 CO (CO_3^{2-})	c*	1463	–	–	ν_3 CO (CO_3^{2-})
–	–	–	d	–	1033	1109	ν Si–O
6	966	ν Si–O (C–S–H) Q^2	e	966	970	968	ν Si–O (C–S–H) Q^2
7	865	ν_2 CO (CO_3^{2-})	f	867	872	871	ν_2 CO (CO_3^{2-})
8	815	ν Si–O (C–S–H) Q^1	g	813	–	–	ν Si–O (C–S–H) Q^1
9	667	δ Si–O–Si	–	–	–	–	–
		–	h	–	709	710	ν_2 CO (CO_3^{2-})
10	590	δ Si–O–Si	–	–	–	–	–
–	–	–	i	664	665	666	δ Si–O–Si
11	491	δ Si–O–Si	j	491	–	–	δ Si–O–Si
12	453	δ Si–O (SiO_4 Td)	k	452	453	449	δ Si–O (SiO_4 Td)

Energy Dispersive X-Ray Spectroscopy (EDS) is an analytical measurement from the Scanning Electron Microscope (SEM). A Thermo Quattro S field emission environmental Scanning Electron Microscope (FE-ESEM) equipment was used as observed in **Figure 26**. This technique is used for elemental analysis or chemical characterization of the samples. It relies on the interaction of some source of X-ray excitation and a sample where the fundamental principle is that each element has a unique atomic structure generating a unique set of peaks on its electromagnetic spectrum. There are 4 components in the EDS setup that include an excitation source, an X-ray detector, a pulse processor, and an analyzer. A beam of electrons is focused on

the sample to generate the emission of characteristic X-rays from a specimen. Therefore only perform the analysis on the section receiving the beams. Then multiple regions at a lower magnification were recorded to determine and quantify the full chosen range of characteristic X-rays. EDS analysis was performed simultaneously with the Scanning Electron Microscope (SEM) imaging presented in the upcoming section.

3.6 Imaging Measurements

Scanning Electron Microscope (SEM) produces images of a sample by scanning the surface with a focused beam of electrons. The electrons interact with atoms in the sample, producing various signals containing surface topography and composition information. SEM with a back-scattered electron mode was utilized to observe the microstructure of the cement samples. A Thermo Quattro S field emission environmental Scanning Electron Microscope (FE-ESEM) was used to perform the microstructure imaging of the different samples observed in **Figure 26**. For accurate imaging, back-scattered electron mode was used. Prior to analyzing the microstructure, samples were sputter-coated with platinum to remove any bound water and avoid any charge. Samples were analyzed at multiple magnifications ranging from 1k to 12k. Before coating the samples and utilizing SEM, these needed to be prepared. After the desired period of hydration, samples were removed from the aqueous curing environment and placed in an oven for 24 hours at temperatures around 180 ^{o}F prior to the experiment. However, it is known to have an adverse effect due to the removal of bound water of some hydrated products and decomposition (Knapen and Van Gemert, 2009). Finally, it is a known problem that samples exposed to environments may exhibit changes in the outer sections but no change in the inner center of the samples. Two samples for each of the different sample configurations were used. For uniformity and to explore the difference throughout the testing samples, these were cut in half using a piece of mechanical equipment. Therefore, SEM imaging was done in the innermost center of the sample.

Figure 26. Thermo Quattro S field emission environmental Scanning Electron Microscope (FE-ESEM) used for Scanning Electron Microscopy (SEM) and Energy Dispersive X-Ray Spectroscopy (EDS). Cut samples placed before testing.

4. RESULTS AND ANALYSIS

This section provides results from the different testing performed, from mechanical testing, petrophysical testing, acoustic velocities, compositional testing, and imaging. It provides an analysis of each test performed and the proposed hypotheses accompanying the data and results gathered. Finally, an in-depth discussion of these results from the testing.

4.1 Sample Associated Error in the Dimensions

The cement samples were cast in a cylinder glass mold to form cylinders with a 1-inch diameter and 1.5-inch height for dimensions. The molds were sprayed with a mold release to prevent any adherence of the cement with the mold walls and facilitate sample extraction. For the samples, the standard error of the height measurements calculated was ± 0.420 mm with a standard deviation of ± 2.45 mm, whereas for the diameter, the standard error is ± 0.015 mm with a standard deviation of ± 0.090 mm. The reason for such variability in height is during cement slurry pouting into the small molds; it was difficult to control the exact amount. Thus, the height irregularities among the samples. The glass mold cylinders are standardized, and their diameter does not show notable variations. The overall area led to a standard error of the cylindric samples of ± 2.160 mm^2.

4.2 Mechanical Testing

4.2.1 Unconfined Compressive Strength Results

An experimental program was performed to measure the unconfined compressive strength of the cement samples. After samples were cured for 12 hours at 140 ± 10 ^oF, these developed consistencies and strength. The logic was to allow samples to hydrate and pass the first hydrations phases before exposure to the different environments. These were then moved to base distilled water and water saturated with molecular hydrogen gas for curing the designed

timeframes. Once the curing time was due, these were removed and polished for mechanical unconfined compressive strength testing. Two batches were prepared for testing, each comprised of 3 or 4 samples for each test type. Therefore, each curing timeframe had 7 samples tested. The average difference between the samples had a percentage difference of 4.2% in the 7 days, and the highest difference was 14.3% observed in the longest time of 168 days. The average values, standard deviation, and standard error can also be found within **Table 9**.

Table 9. Unconfined Compressive Strength (UCS) average, standard deviation, and standard error for different curing times of 7, 28, 84, and 168 days.

Unconfined Compressive strength (MPa) cement samples cured for different timeframes (Days)				
Hydrogen (H)	**7 days**	**28 days**	**84 days**	**168 days**
Average	24.838	30.042	37.032	54.007
Standard deviation	3.015	4.502	6.702	6.992
Standard error	1.348	1.702	2.533	2.855
Water (W)	**7 days**	**28 days**	**84 days**	**168 days**
Average	23.811	27.510	30.755	47.305
Standard deviation	1.702	2.716	2.659	8.356
Standard error	0.761	1.027	1.005	3.411

Figure 27 presents the average unconfined compressive strength of samples cured in base distilled (W) and water saturated with molecular hydrogen (H) after curing for 7, 28, 84, and 168 days. It is known that the strength of cement increases with an increase in curing time due to the hydration products being formed (Abalaka and Okoli, 2013). Results showed that the unconfined compressive strength of samples exposed to water saturated with molecular hydrogen, irrespective of curing time, was significantly higher than samples cured in base distilled water. It was inferred that the presence of molecular hydrogen in the cement system affects the mechanical properties of cement. There is a direct relationship between cement microstructure development during hydration and its mechanical strength. Potential explanations are discussed in the upcoming sections.

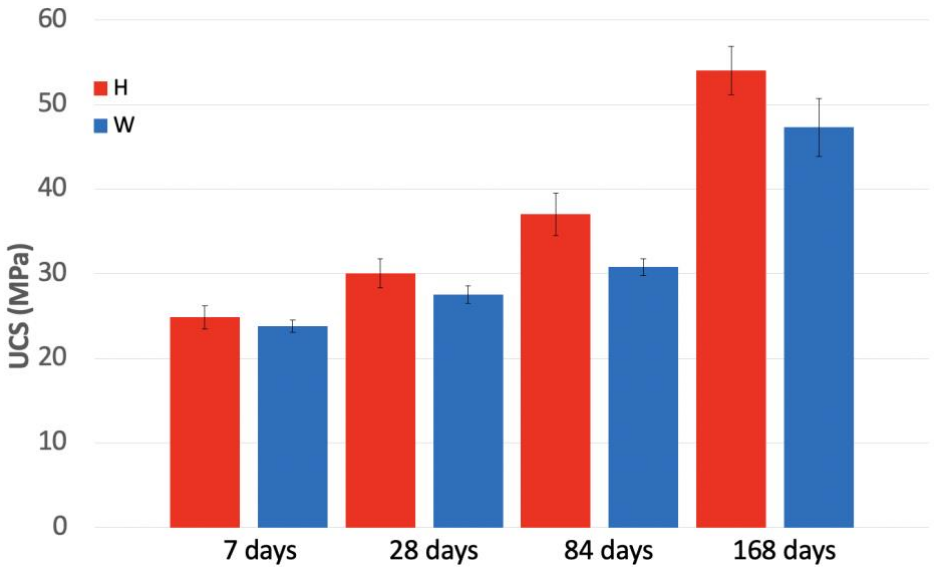

Figure 27. Unconfined Compressive Strength (UCS) comparison of samples exposed to water with molecular hydrogen (H) vs. base distilled water (W) over different curing times of 7, 28, 84, and 168 days.

4.3 Petrophysical Testing

4.3.1 Porosity and Permeability Results

Porosity is a property essential for cement as it is directly related to compressive strength and other mechanical properties. Two samples from each curing setting from the batch prepared for UCS were separated to run petrophysical testing. To test for porosity and permeability samples in the AP608 equipment, these needed to be dried in the oven for 24 hours at temperatures around 180 ^{o}F. **Figure 28** shows the average results obtained from the porosity measurements. It was observed that samples exposed to molecular hydrogen present in the aqueous environment showed a consistently lower porosity compared to the samples cured in water over the different curing times of 7 days, 28 days, 84 days, and 168 days. The percentage difference observed was 2.6% (0.83% porosity) in the shortest curing time and 6.1% (1.61% porosity) in the longest curing time.

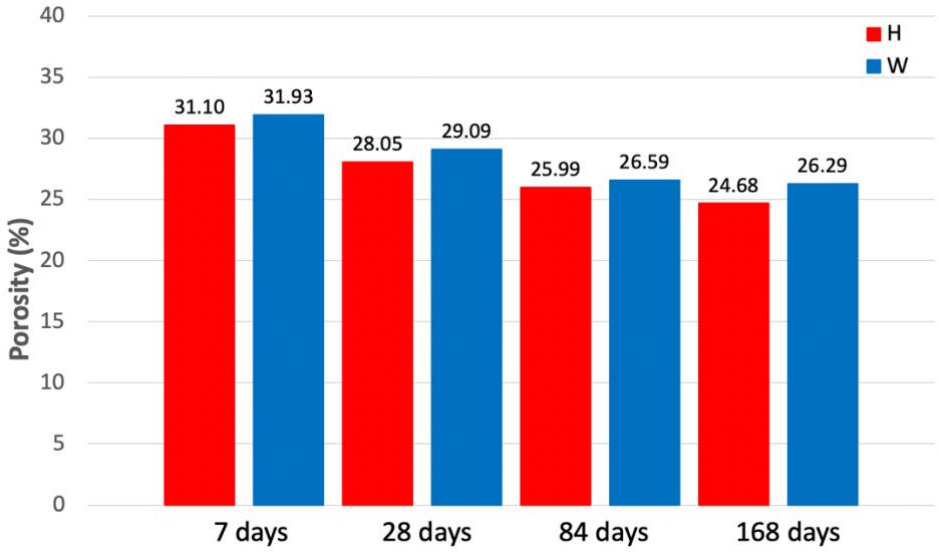

Figure 28. AP608 Porosity comparison of samples exposed to water with molecular hydrogen (H) vs. base distilled water (W) over different curing times of 7, 28, 84, and 168 days.

The porosity decreased in samples exposed to molecular hydrogen can coherently be an explanation for the higher compressive strength observed in the previous section. **Figure 29a** shows the relationship between UCS with porosity and curing time. **Figure 29b** shows the relationship between the average values of UCS from mechanical testing with the obtained porosity. It can be observed that at higher porosity and shorter curing times, both samples behave quite similarly. Nevertheless, at the longer curing times and lower porosity values, there seems to be a difference showing hydrogen exposed samples showing a much higher UCS in the long term.

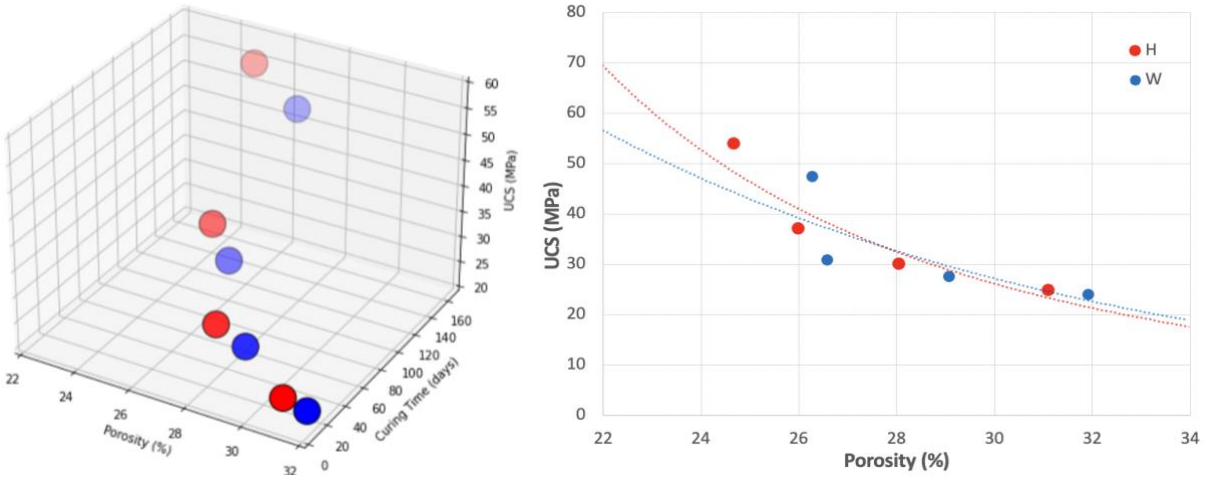

Figure 29. a) Relationship between UCS (MPa) with Porosity (%) and Curing Time (days) on the right b) UCS (MPa) against Porosity (%). Hydrogen exposed (H) samples in red and Base Water (W) in blue on the left.

Permeability is dependent on porosity, as the number of interconnected pores can produce a more permeable cement. For UHS, a major concern is that hydrogen can permeate cement sheaths. As hydrogen is such a small gas, it is a concern. For common Class H and G cement used in well construction, no published test results guarantee these would be tight enough to contain the hydrogen gas over long timeframes. Permeability results from AP608 testing with helium gas showed a similar proportional trend compared to porosity. Permeability results showed samples exposed to hydrogen present in the curing environment showed a consistently lower permeability than the samples cured in water over the different curing times of 7 days, 28 days, 84 days, and 168 days (**Figure 30**). The difference was 20.9% (0.092md) in the shortest curing time and 4.2% (0.007md) in the longest curing time.

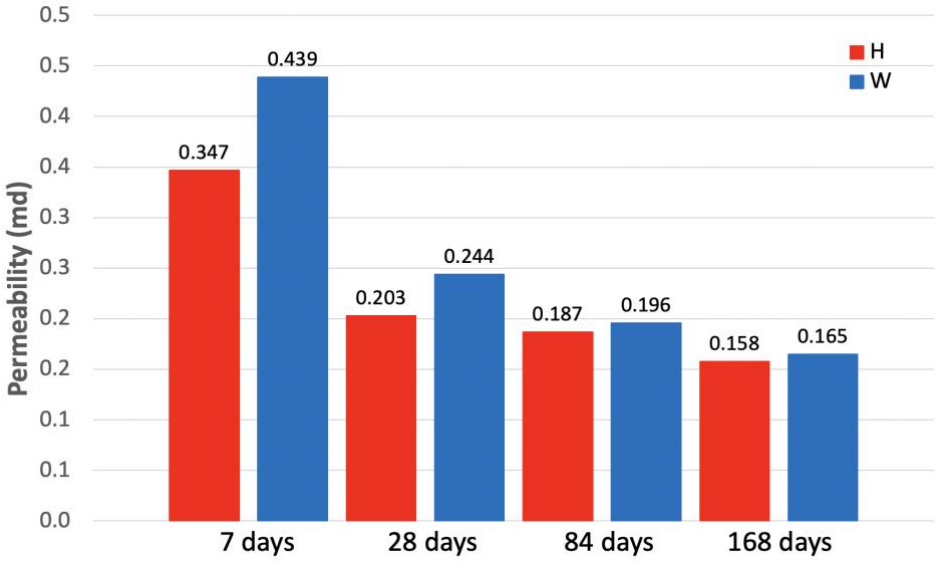

Figure 30. Permeability comparison of samples exposed to water with molecular hydrogen (H) vs. base water (W) over different curing times of 7, 28, 84, and 168 days.

Figure 31a shows the relationship between porosity and permeability with UCS. Samples with lower porosity and lower permeability have higher UCS. It was noted that the most significant difference between the permeability occurred in the shortest curing time, where the shortest difference between porosity was previously observed. A possible explanation is cement is not completely hardened, yet we are able to see a difference in both porosity and permeability even in the shortest timeframes. It was observed in **Figure 30** that show that permeability was lower for hydrogen-exposed samples in all timeframes. **Figure 31b** shows the relationship between permeability and porosity. However, this plot trend shows that based distilled water samples have a lower permeability at lower porosity. This is misleading due to the lack of points. The few number of points used for the analysis was a limitation of this study.

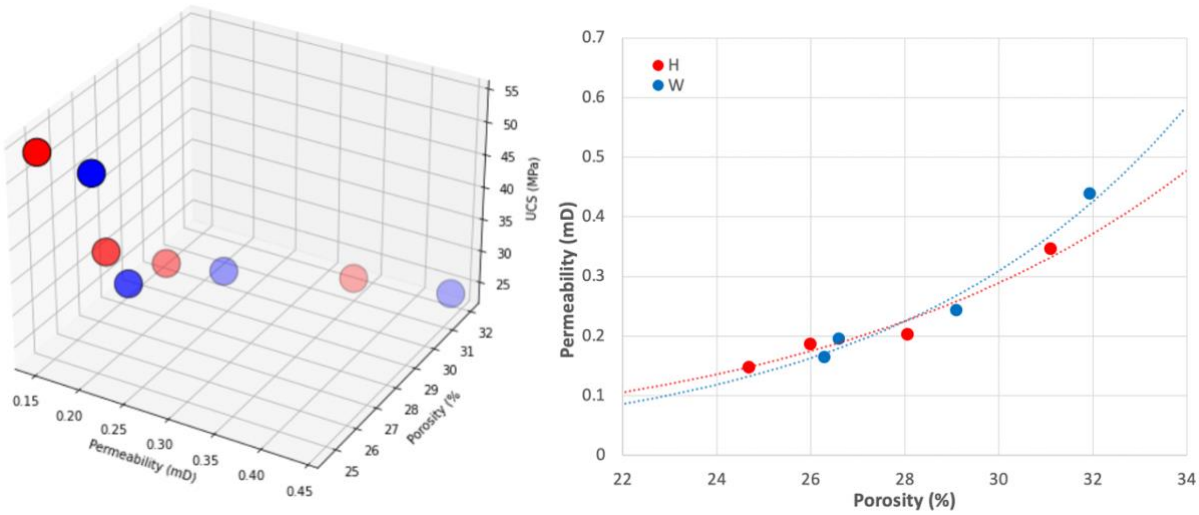

Figure 31. a) Relationship between UCS (MPa) with Permeability (mD) and Porosity (%) on the right b) Permeability (mD) against Porosity (%). Hydrogen exposed (H) samples in red and Base Water (W) in blue on the left

4.3.2 Nuclear Magnetic Resonance Results

By measuring T2 relaxation time from NMR equipment, we are able to estimate the amount of pore space present in the cement without affecting the fluid present in the pores. Relaxation is dominated by the relaxation of the molecules in contact with a surrounding pore surface. **Figure 32** shows the average results obtained from the NMR porosity measurements on saturated samples. It was observed samples exposed to hydrogen present showed a consistently lower porosity compared to the samples cured in water over the different curing times of 7 days, 28 days, 84 days, and 168 days. The observed difference in the shortest curing time was 0.07% (0.29% porosity) and 1.3% (0.42% of porosity) in the longest curing time. These results match the porosity trend from the dry porosity results from the AP608.

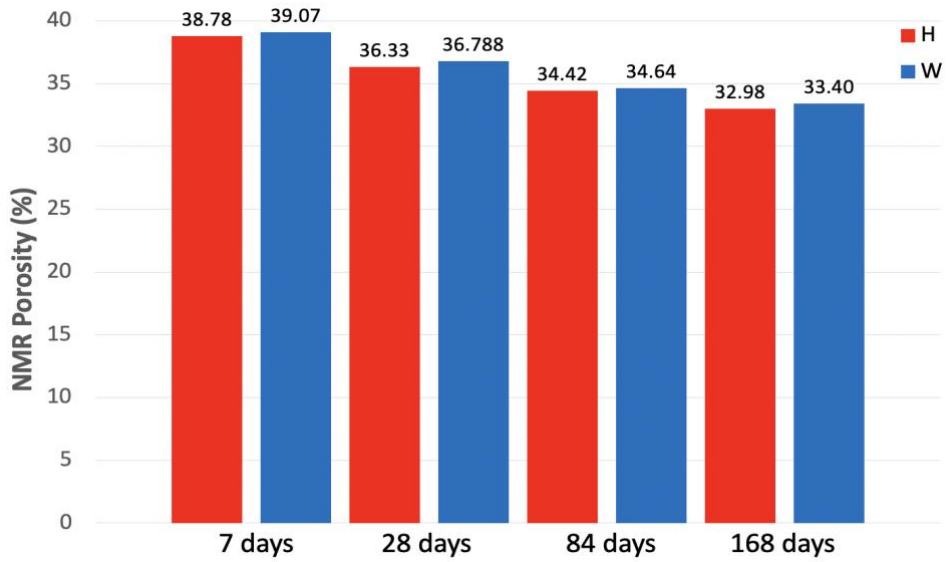

Figure 32. NMR Porosity comparison of samples exposed to water with molecular hydrogen (H) vs. base water (W) over different curing times of 7, 28, 84, and 168 days.

Figure 33 shows the linear relationship between porosity from NMR measurements with porosity from AP608. It is important to mention that NMR measurements are with saturated wet samples, while AP608 tests are with dried samples. Nevertheless, results seem proportional and consistent, providing support to the porosity values obtained. The difference in porosity values is due to AP608 equipment measuring the effective porosity of interconnected pores. Also, AP608 requires confining pressure which reduces the pores space, while NMR tests do not require any confining pressure. In addition, AP608 porosity samples were oven-dried; expulsion of water induces additional confining pressures that may lead to pore size reduction (Cruz et al., 2020).

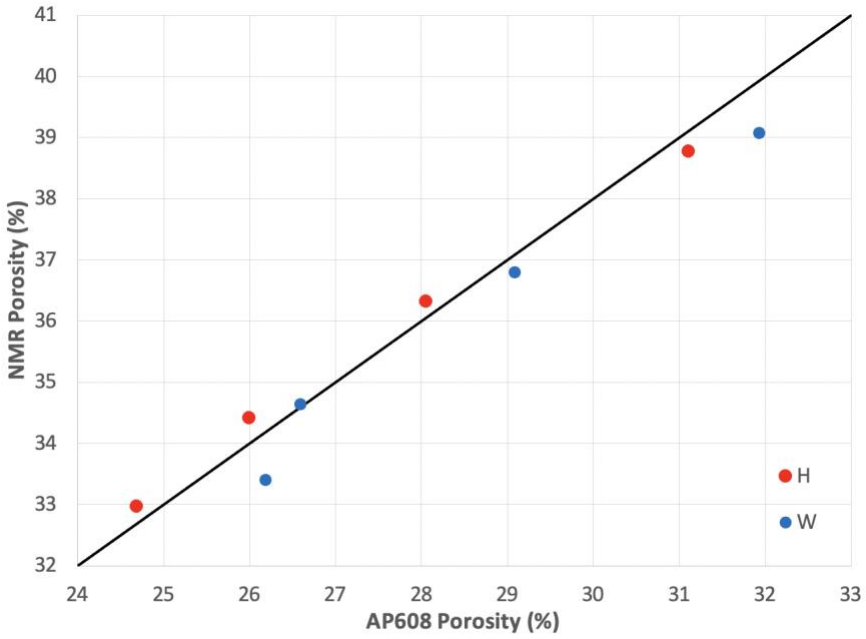

Figure 33. The linear relationship between NMR porosity and AP608 porosity.

Figure 34-37 shows the comparison of NMR T_2 relaxation between the two cases in all the different curing times. Results obtained showed minimal displacement in the overall pore size distribution between both cases. Only the shortest curing time shows a small displacement of based distilled water (W) samples towards the right compared to hydrogen-exposed (H) samples (**Figure 34**). It was observed that hydrogen exposed (H) showed a decrease in large pore spaces at a T_2 Relaxation time of around 1 ms. This is particularly evident in the 128-day samples (**Figure 37**). This is the main cause of the lower porosity in hydrogen-exposed samples. This may be due to a mineral being formed in the larger pore spaces, which can also hold water within the surface of the newly formed mineral, causing the shift in the decrease of larger pores (1 ms) and increase in smaller pores (0.4 ms). Capillary pressure is the difference across the two fluids causing the formation of the mineral in the larger pores space. This is because hydrogen in a two-phase porous media will move to the larger pores.

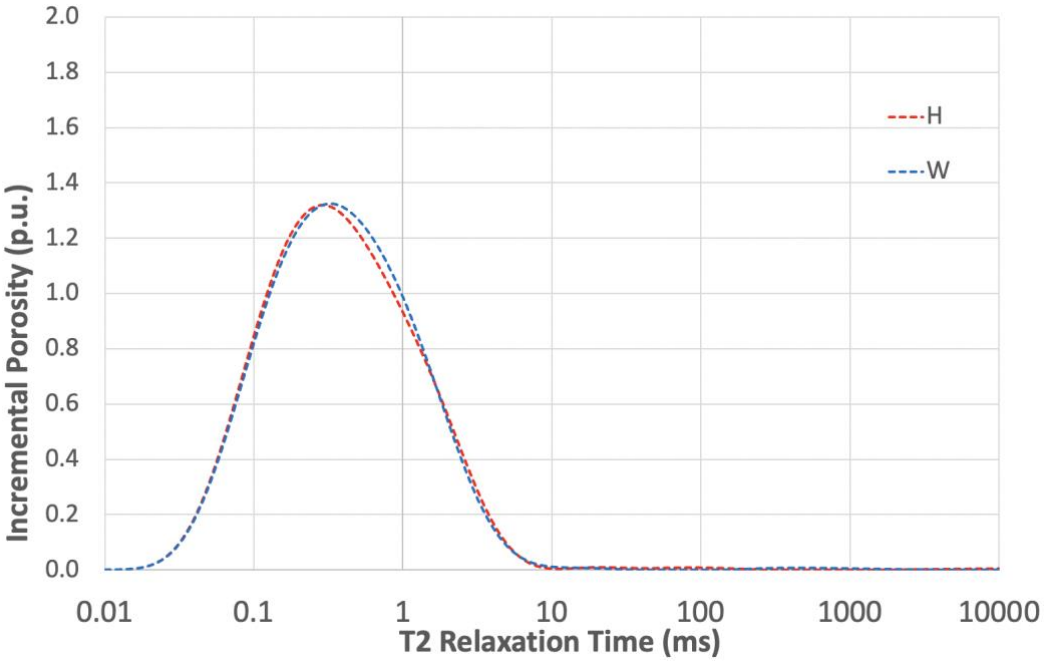

Figure 34. NMR incremental porosity against T2 relaxation time for samples cured for 7 days.

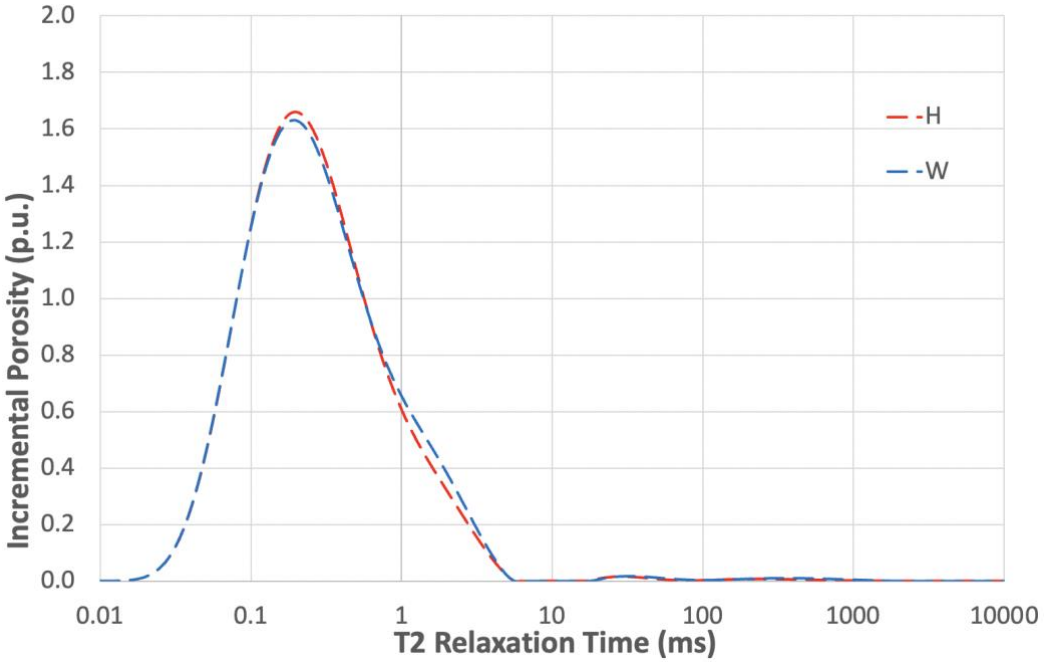

Figure 35. NMR incremental porosity against T2 relaxation time for samples cured for 28 days.

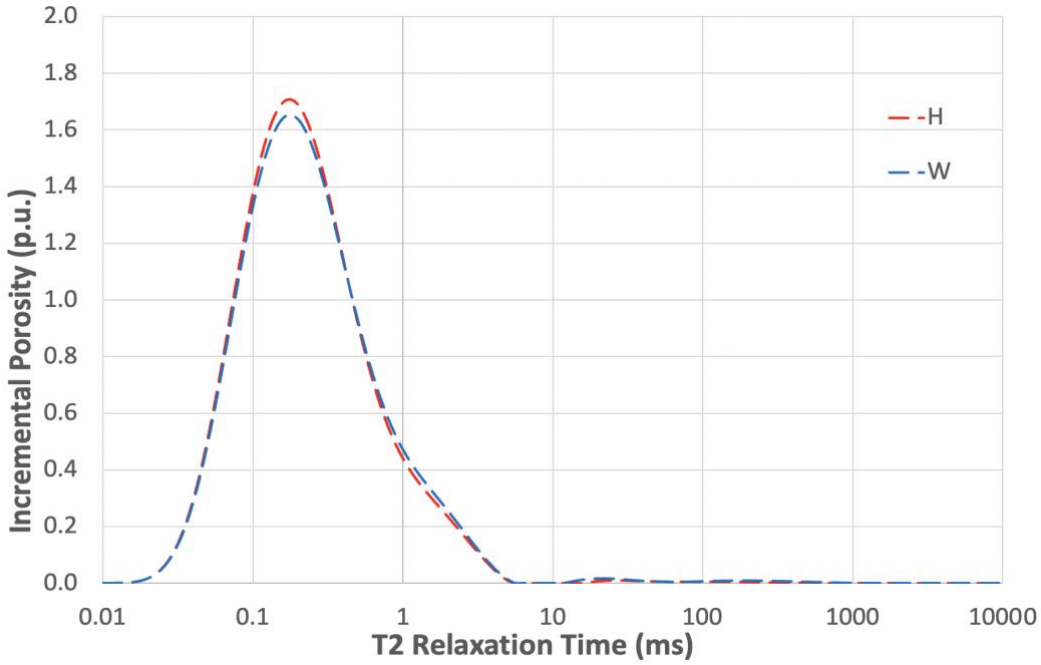

Figure 36. NMR incremental porosity against T2 relaxation time for samples cured for 84 days.

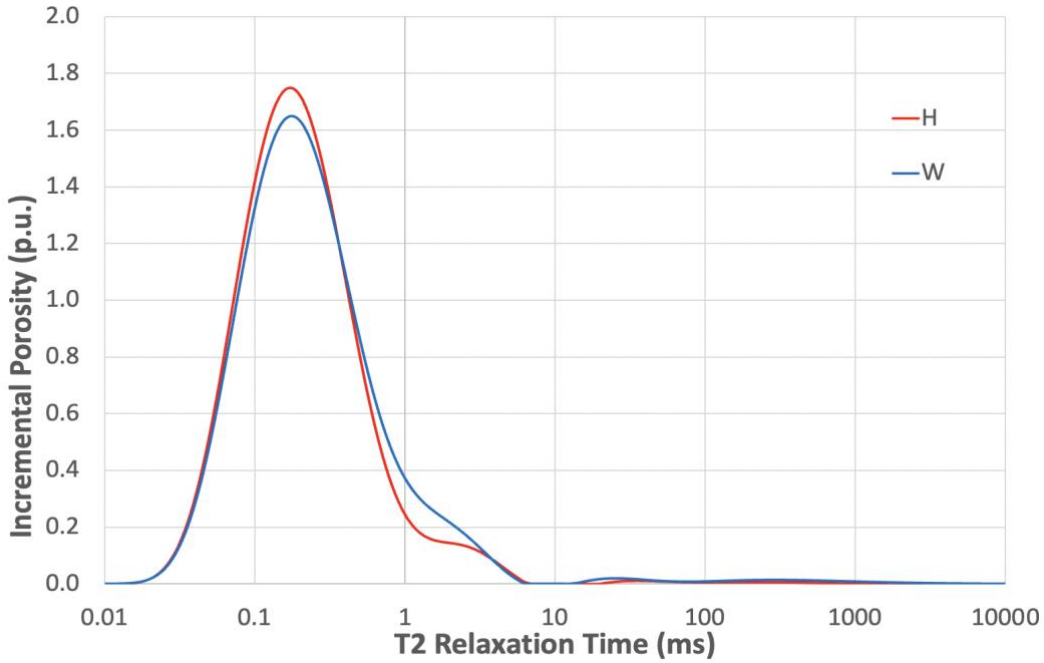

Figure 37. NMR incremental porosity against T2 relaxation time for samples cured for a) 168 days (top left), b) 84 days (top right), c) 28 days (bottom left), d) 7 days (bottom right).

4.4 Acoustic Velocities Testing

Acoustic Velocities measurements of Vp and Vs were performed using the equipment presented in the previous chapter. The software from the same manufacturer allows us to pick up the arrival times of the compressional waves and perpendicular two-shear waves. These were manually picked carefully and consistently. Within all samples, there was no variation be the two measured shear waves. Two samples from each curing setting from the batch prepared for AP608 porosity and permeability were also used to run these measurements. Previous sections describe the porosity within a bulk volume of cement that potentially contains fluids. Existing pore fluid and wettability affect acoustic propagations. Therefore, saturation and wettability need to be considered. Compressional waves travel faster in fluids than in air. For this reason, we focused on dry velocities to see only the effect from the cement sheath and have more concise representative measurements. **Figure 38** and **Figure 39** shows the acoustic velocities of the two differently cured samples over different timeframes. It was observed that hydrogen-exposed samples showed higher compressional and shear wave velocities compared to samples cured in base water.

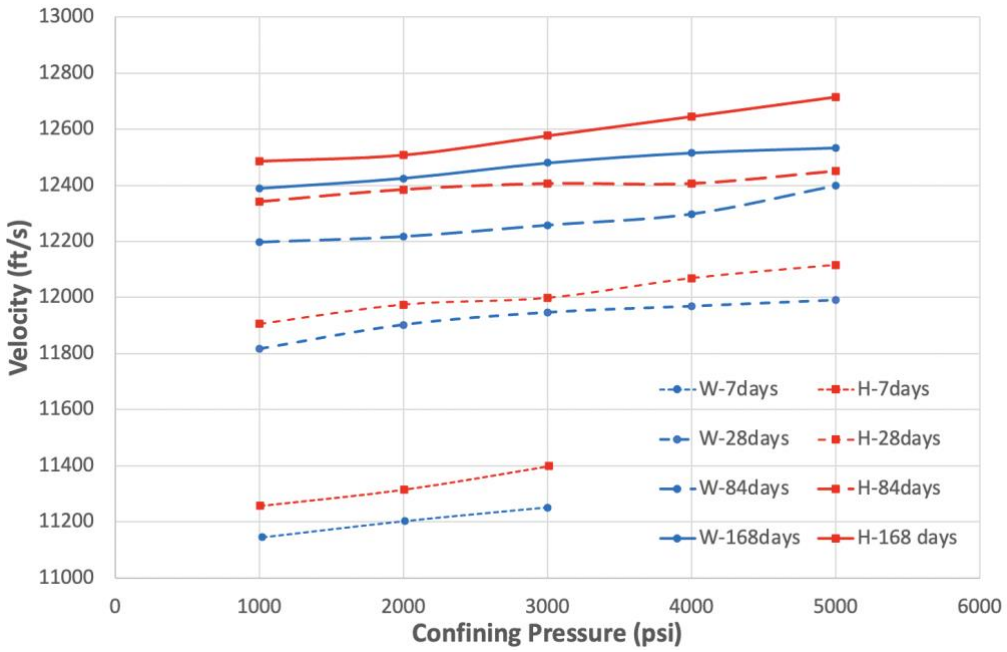

Figure 38. Compressional waves (P-waves) velocities comparison of samples exposed to water with molecular hydrogen (H) vs. base water (W) over different curing times of 7, 28, 84, and 168 days.

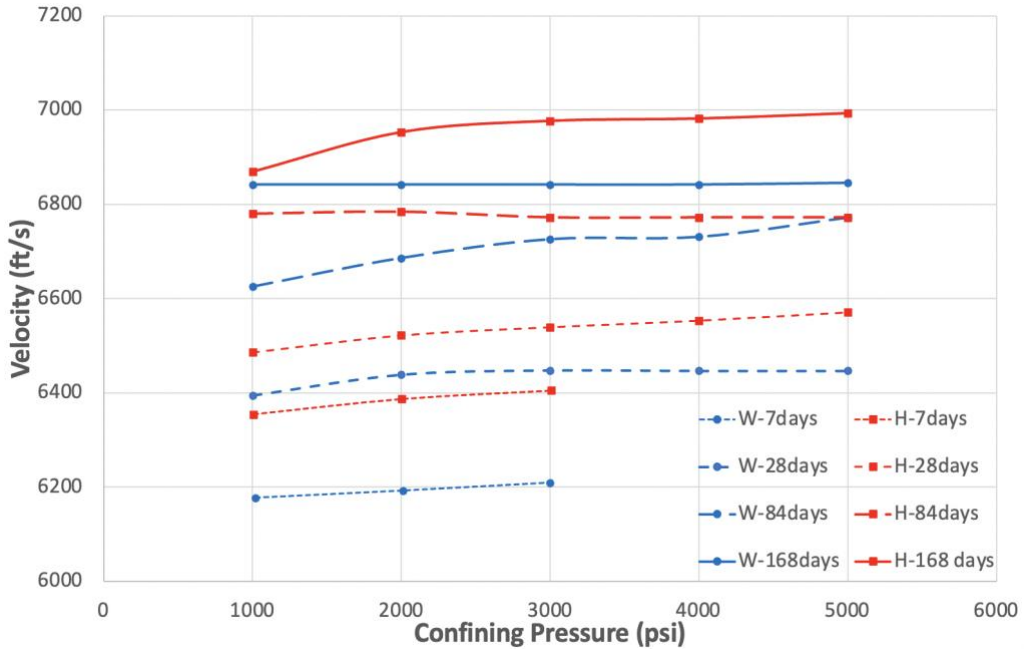

Figure 39. Shear waves (S-waves) velocities comparison of samples exposed to water with molecular hydrogen (H) vs. base water (W) over different curing times of 7, 28, 84, and 168 days.

There is a direct relation between seismic waves and porosity found in the literature (Dobrin and Savit, 1960). Nevertheless, results obtained from these empirical equations are either overestimated or underestimated because it is only applied to certain rock features and are merely assumptions (Hamada and Joseph, 2020). **Figure 40b** shows the relationship between UCS and compressional wave velocities, and **Figure 40a** includes porosity. In porous media, elastic wave velocity is attenuated by density and pore fluid (ElKatatny et al., 2018; Xu et al., 2015; Hamada and Joseph, 2020). Compressional waves travel faster in fluids than in air. It is known that lower compressional velocity is observed in materials with high porosity because the wave energy travels much slower in empty pore spaces. Compressional waves that travel through a more compacted cement will induce higher vibrations towards the particles, hence increasing the velocity.

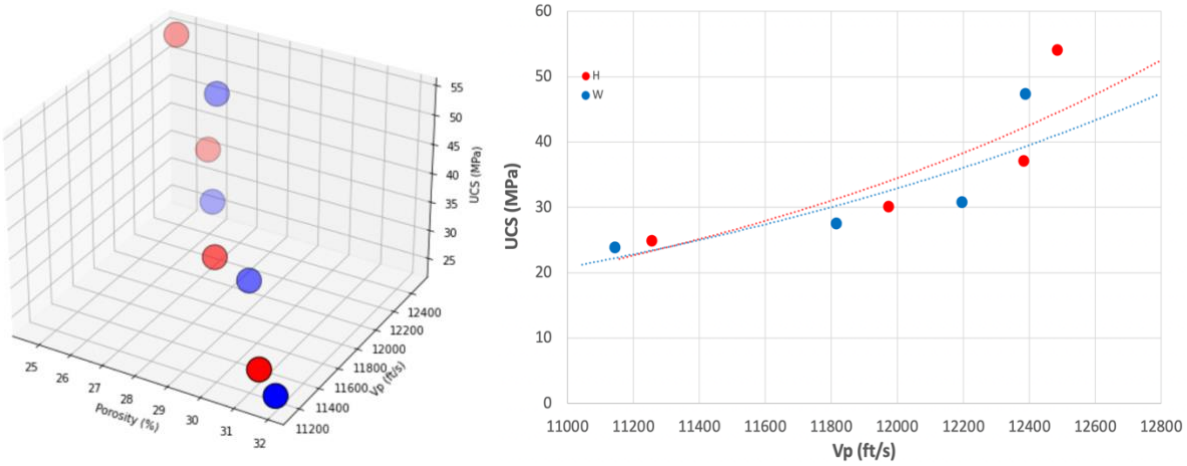

Figure 40. a) Relationship between UCS (MPa) with Compressional wave velocity Vp (ft/s) and Porosity (%) on the right. b) UCS (MPa) against Vp (ft/s). Hydrogen exposed (H) samples in red and Base Water (W) in blue on the left.

Acoustic waves velocities can be used to compare elastic properties under dynamic conditions. Nevertheless, results obtained from these empirical equations are either overestimated or underestimated because (Hamada and Joseph, 2020). **Figure 41-43** shows the results from the calculations, where in most instances hydrogen exposed samples exhibit slightly lower Poisson ratio (**Figure 43**). In addition, a higher Young's modulus (**Figure 41**) and higher Shear's modulus (**Figure 42**). During the life of a well, cement is subjected to a number of stresses that can lead to failure, and cement failure is directly related to the elastic properties of cement. During UHS the well is subject to a number of injection and production cycles, therefore, a flexible cement is desired to avoid the possibility of having any sort of cement failure. Cement is considered flexible the more force it can withstand. Stiff cement needs a higher load to deform it compared to a soft cement. Hydrogen-exposed samples exhibit a more rigid structure as they exhibited a higher elastic property, such as Young's modulus showing a more rigid behavior compared to distilled water cured samples. This can be an issue as for UHS, a flexible cement would be desired to withstand all the injection/production cycles throughout the entire life of the well. Flexible cement requires a higher Poisson's Ratio and a lower Young's Modulus. Nevertheless, the difference is too small to consider it to be detrimental. Different cement

formulations might behave differently; therefore, it is important to consider that although molecular hydrogen might increase cement's strength, it will make it stiffer, which is undesirable. In the longest curing time, with a percentage difference of 4.7%, 5.0%, and 1.8%, respectively.

Figure 41. Young Modulus (E) comparison of samples exposed to water with molecular hydrogen (H) vs. base water (W) over different curing times of 7, 28, 84, and 168 days

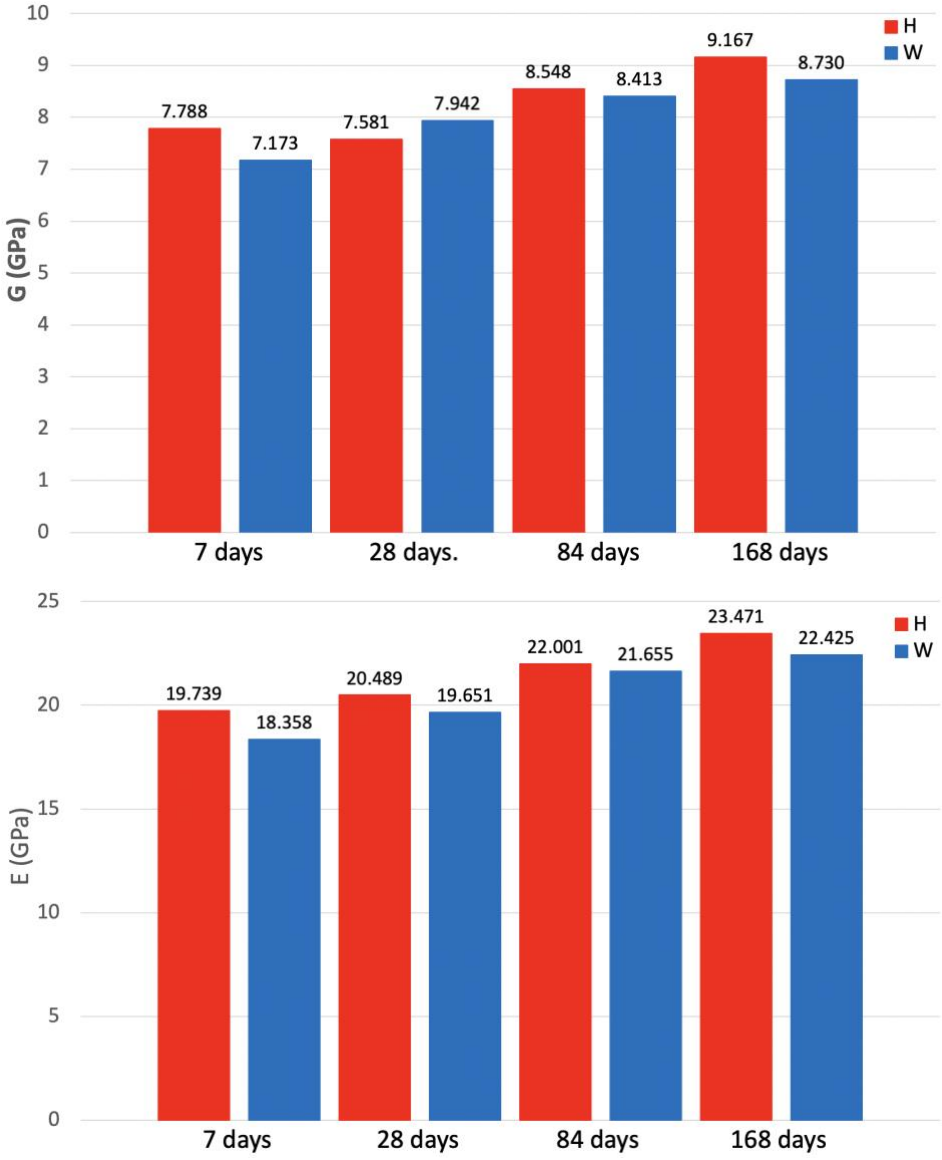

Figure 42. Shear Modulus (G) comparison of samples exposed to water with molecular hydrogen (H) vs. base water (W) over different curing times of 7, 28, 84, and 168 days

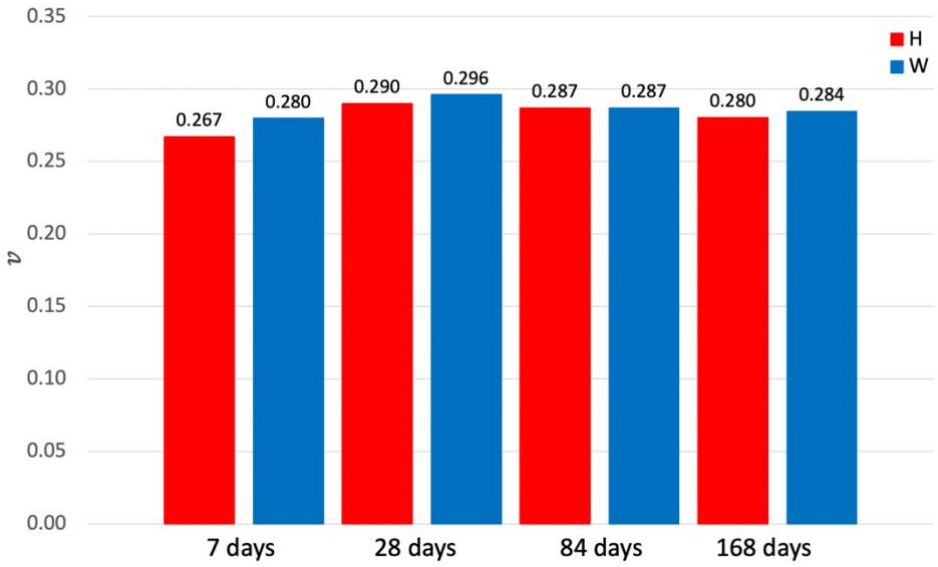

Figure 43. Poisson ratio comparison of samples exposed to water with molecular hydrogen (H) vs. base water (W) over different curing times of 7, 28, 84, and 168 days

4.5 Cement compositional Analysis

4.5.1 Fourier Transform Infrared Spectroscopy

To compare the two different environments, compositional analysis was done to see what components varied, causing the difference in UCS. Fourier Transformed Infrared Spectroscopy (FTIR) can be used to observe the amount of hydrated product. **Figure 44** shows the FTIR spectra of the samples cured in different environments over different timeframes. The FTIR spectra of all samples were similar but with distinct peaks in the same position with different intensities. Relevant peaks are in 3650, 3400-3500, 2900, 1650, 1425 and 980 cm-1 positions. The O−H stretching of calcium hydroxide appears at 3650, H−C stretching of methyl or methylene group at 2900, Si−O stretching of polymeric silicate (CSH) at 980 (Trezza, 2007). The bands related to Si–O stretching, Si–O–Si bending, and SiO4 tetrahedral deformation identify a predominant silicate chain structure. The silicate vibration regions of C-S-H spectra are centered at ~970 cm−1. They are assigned to Si–O stretching vibrations of the Q2 tetrahedra,

with their mean frequency varying systematically with the C/S ratio (Yu, 1999). The intensities of the carbonate bands at 1400–1500 correspond to the asymmetric stretching (v3) of CO2 and the 875 cm−1 (Yu, 1999). The variation in the peak area ratio at 3650 cm-1 of O-H stretching of $Ca(OH)_2$ and at 872 of Si−O of CSH are indications of variation between the main hydrated products (Jo and Chakraborty, 2015; Jo et al., 2015).

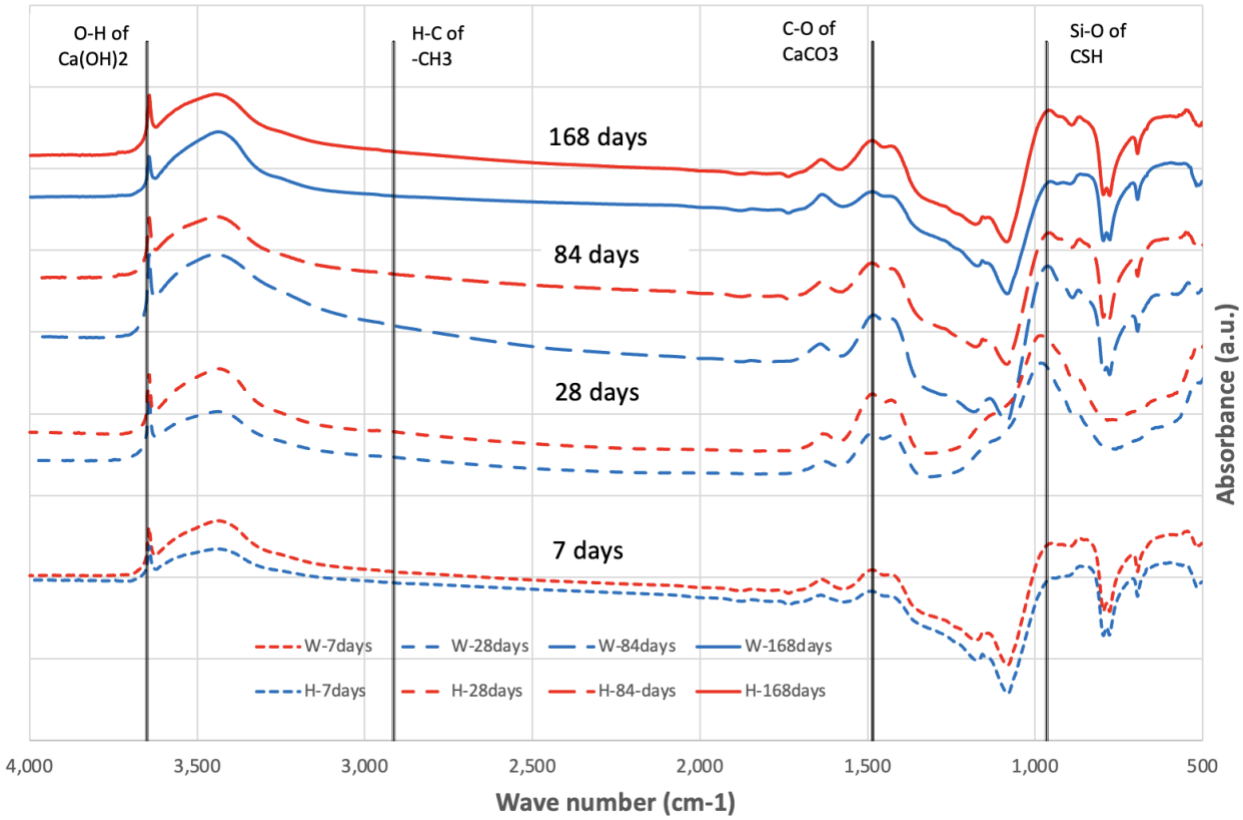

Figure 44. Fourier Transformed Infrared Spectra comparing samples exposed to water with molecular hydrogen (H) vs. base water (W) over different curing times of 7, 28, 84, and 168 days.

The relative peak intensity ratio of the IR bands is an indicator of the amount of hydrated product that includes CH and CSH (Jo and Chakraborty, 2015; Chakraborty et al., 2013). Portlandite (CH) is the naturally occurring form of $Ca(OH)_2$. Two of the main components are responsible for the strength of cement. Deconvolution and fitting of the FTIR spectra were done to get the peak area of the products. These provided an alternative comparison method to see composition

differences between the two cases at different timesteps. The relative peak area ratios were calculated using O-H stretching from portlandite (CH) and Si-O stretching of tobermorite (CSH) divided by the respectively peak of the methyl or methylene group. **Figure 45** shows the relative peak area ratio of Si-O/H-C, and **Figure 46** of O-H/H-C as a function of time. It was observed, irrespective of the curing time, that samples exposed to hydrogen exhibited higher ratios compared to base distilled water. This shows that the amount of hydrated product was higher in all the different timeframes. During the first 28 days, the results showed an increase in the amount of CSH in the Si-O/H-C. This is due to the cement hardening in early hydration of the first 28 days. On the other hand, the ratio O-H/H-C showed there is a continuous increase over all timeframes. This phenomenon indicates the continuous development of portlandite and ettringite over time. This is a possible explanation of why the difference in UCS between the two cases was smaller in the shortest curing time than the difference between the two cases in the longest curing time. The higher presence of ettringite and portlandite causes an increase in the strength of cement.

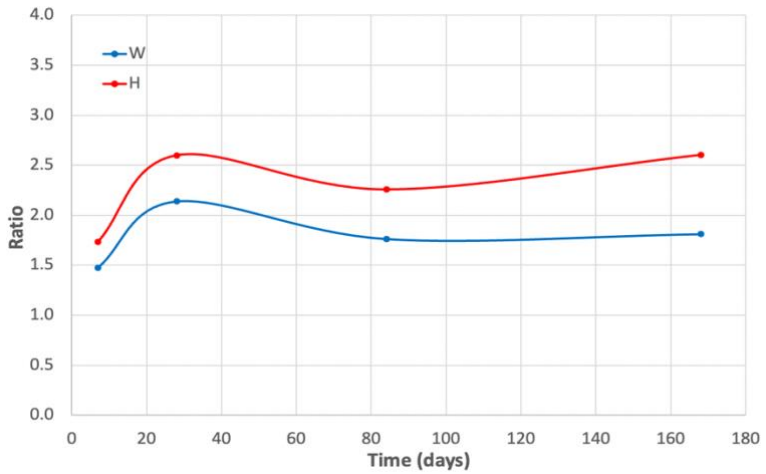

Figure 45. Peak area ratio of Si-/H-C comparing samples exposed to water with molecular hydrogen (H) vs. base water (W) over different curing times of 7, 28, 84, and 168 days.

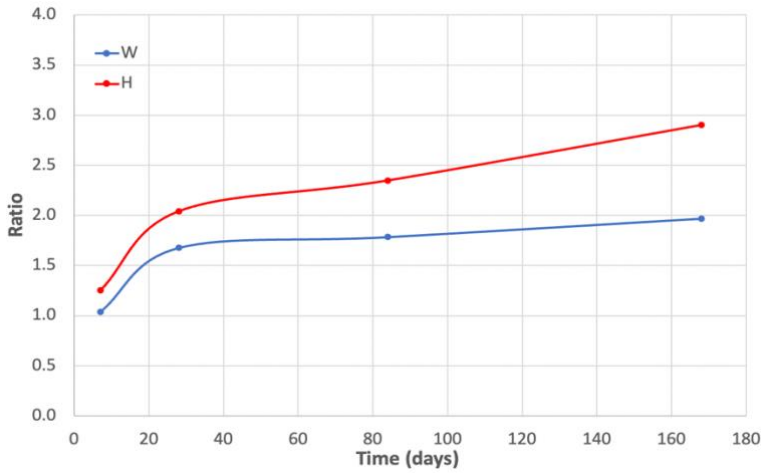

Figure 46. Peak area ratio O-H/H-C comparing samples exposed to water with molecular hydrogen (H) vs. base water (W) over different curing times of 7, 28, 84, and 168 days.

4.5.2 Energy Dispersive X-Ray Spectroscopy

Energy Dispersive X-Ray Spectroscopy (EDS) technique is used to observe the weight percentage of the elements from the sample to determine and quantify the full chosen range of characteristic X-rays. This is an additional analysis performed from the SEM. **Table 10** shows the weight percentage (wt%) of the samples from the EDS analysis. All samples contain the same elemental composition as both are class H cement. Nevertheless, a difference in the wt% was observed in both cases. It is observed that samples exposed to hydrogen showed higher Silicon (Si), lower Calcium (Ca), and a higher Ca/Si overall for all the different timeframes. An increment of the Ca/Si ratio reduces the silicate chain length and the interlayer spacing (Garcia Loderiro et al., 2009; Li et al., 2019). In addition, it can also be noted that the wt% of Magnesium (Mg), Aluminum (Al), including their ratios Mg/Ca and Al/Ca, was higher in samples exposed to hydrogen. Aluminum present may act as a substitute for silicon. According to the literature, CSH behavior depends on its structure, which is affected by Ca/Si and the uptake of aluminum and magnesium (Bakharev et al., 2001; Kamali and Ghahremaninezhad, 2018). The result indicates a higher presence of CSH and a higher presence of CH.

Table 10. wt % of elements from EDS analysis for the two cases over different curing times of 28, 84, and 168 days.

wt % of elements from EDS analysis									
Curing time	**Sample**	**C**	**O**	**Mg**	**Al**	**Si**	**S**	**Ca**	**Fe**
1 month	*Water*	2	48.5	0.8	1.2	7.8	0.9	34.1	2.6
	Hydrogen	2.8	50.9	1.1	1.4	8.4	1.4	30.3	2.3
3 month	*Water*	1.7	41.5	0.6	0.8	8.2	1	42.4	1.4
	Hydrogen	1.8	44.5	0.8	0.8	8.4	0.9	39.9	1.4
6 month	*Water*	2.1	42.8	1	1.1	8.2	0.9	37.9	3.7
	Hydrogen	2.5	43.9	1.3	1.3	8.9	1.1	35.8	3.2

4.6 Cement Imaging

4.6.1 Scanning Electron Microscopy

The microstructure of the cement samples was analyzed and compared using SEM. **Figure 47** shows the SEM images of the two compared cases over 28, 84, and 168 days. The microstructure showed a slight difference in the amount of CSH; samples exposed to hydrogen had a smaller amount of CSH. Nevertheless, this was not widely observed, and the same in all cases. It was observed in **Figure 47b** that samples exposed to hydrogen showed a more compacted microstructure than samples cured in water shown in **Figure 47a**. Also, these had more empty black pore spaces. Crystalline structures resembling portlandite were found within the pores in samples exposed to hydrogen **Figure 47**. In **Figure 47d**, it can be observed that this crystalline-shaped structure was found to be sparse throughout the pore spaces of the sample. Similarly, these crystalline needle structures were also found in the samples exposed to water, as seen in **Figure 47c**, yet in smaller amounts. This can be seen in **Figure 47f**, where these crystalline needle structures representing portlandite and ettringite are found in a larger amount within this large pore filling it almost completely.

In conclusion, samples exposed to hydrogen showed a higher presence of crystalline structures representing portlandite and ettringite within some of the pore space of all samples over the different timeframes. In addition, the interrupted pore space was found to decrease within the microstructure; this would explain why the porosity was found to be lower in samples exposed to hydrogen. In addition, the unconfined compressive strength increases gradually with the increase in curing time due to the development of dense microstructure in the bulk of the cement (Jo et al., 2018). As stated in the previous section, unconfined compressive strength is directly related to porosity, and having more portlandite and ettringite reduces the pore space and provides more strength.

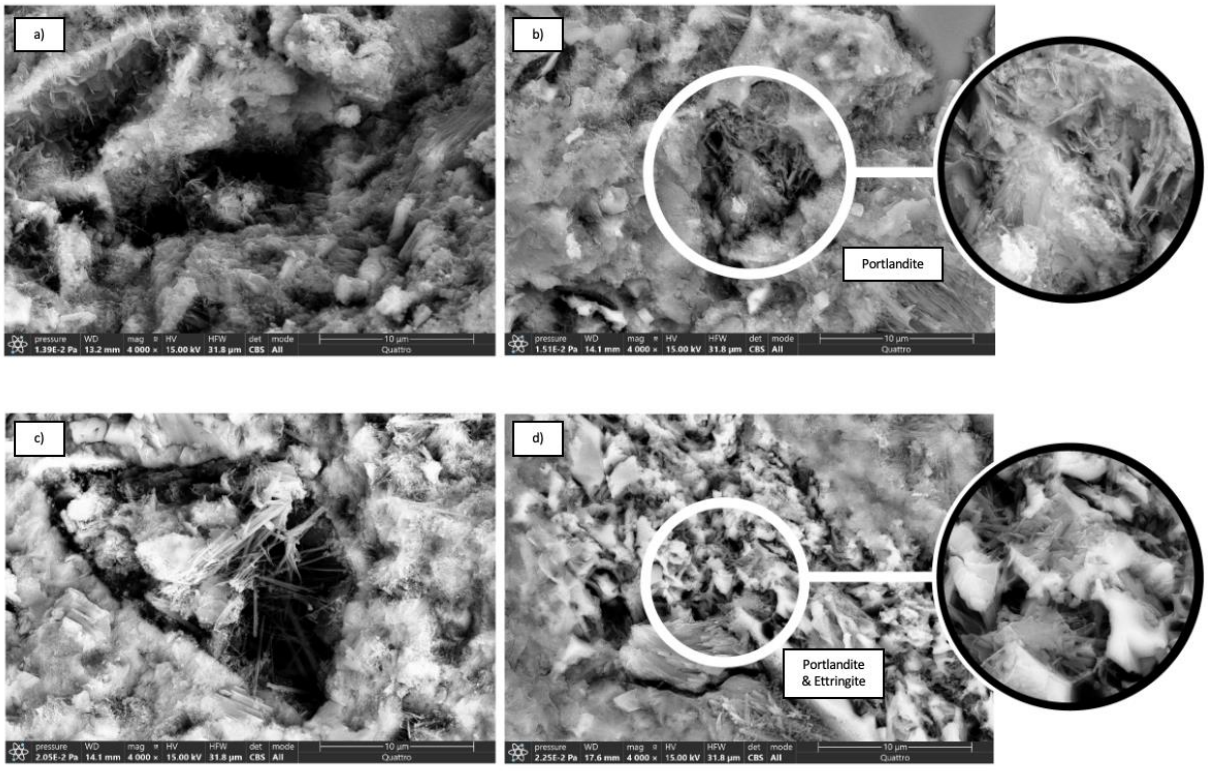

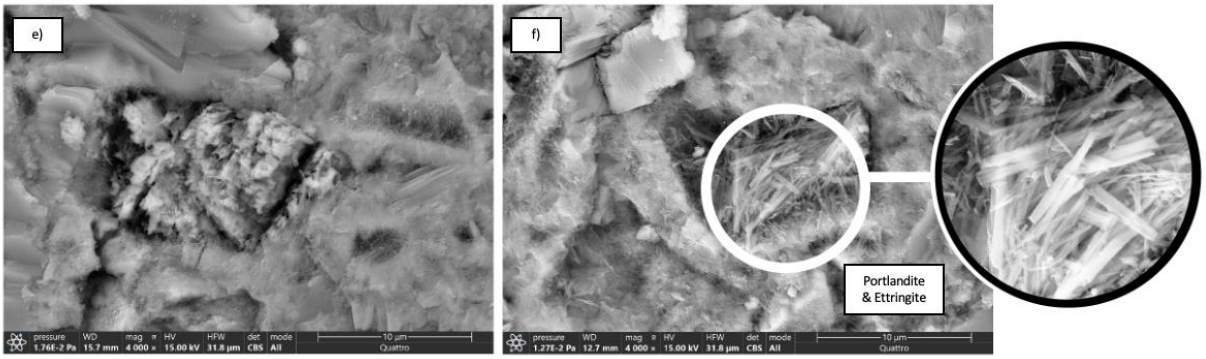

Figure 47. Scanning Electron Microscopy (SEM) imaging shows a) base water-exposed samples and b) hydrogen-exposed samples at 28 days. c) base water exposed samples and d) hydrogen exposed samples at 84 days. e) base water-exposed samples and f) hydrogen-exposed samples at 168 days.

5. DISCUSSION

It has been demonstrated in the section of Results and Analysis that the presence of molecular hydrogen during curing in aqueous conditions can affect the mechanical properties of cement. It can cause the cement product to show higher unconfined compressive strength, which is desirable in terms of well integrity. It ensures the cement is capable of withstanding pressure and stresses in the subsurface to provide adequate isolation intervals of interest. This indicates that the difference increases with exposure time. It was observed in the compositional analysis and imaging that portlandite and ettringite amounts were higher in samples exposed to hydrogen. It was also noted that the amount was higher in samples cured for the longest time showing these hydrated products (portlandite and ettringite) increase over time when hydrogen is present. Therefore, it can be inferred that these components are causing the difference in UCS.

Porosity was found lower in samples exposed to hydrogen. Porosity is directly related to UCS strength. Portlandite and ettringite are two components responsible for the strength of cement. The higher presence of these hydrated products is causing a lower porosity and generating a higher UCS. NMR porosity also exhibited the same results showing a lower porosity in samples exposed to hydrogen. In addition, using NMR we can see a decrease in the larger pores in samples exposed to hydrogen compared to samples exposed to base distilled water. Plus, there is an increase in the smaller pores. A possible explanation is that hydrated product is being generated within the larger pores, causing that reduction of the larger pores and increased capillary small pores. It was observed in the microscopic imaging using SEM (**Figure 47**) that has ettringite and portlandite are in large amounts found within large pore spaces. Plus, **Figure 48** shows a microscopic image comparison at a lower magnification. From a wide perspective of the samples, it can be observed that the number of larger black pore spaces is lower in samples exposed to hydrogen. Further showing and explaining the difference in porosity.

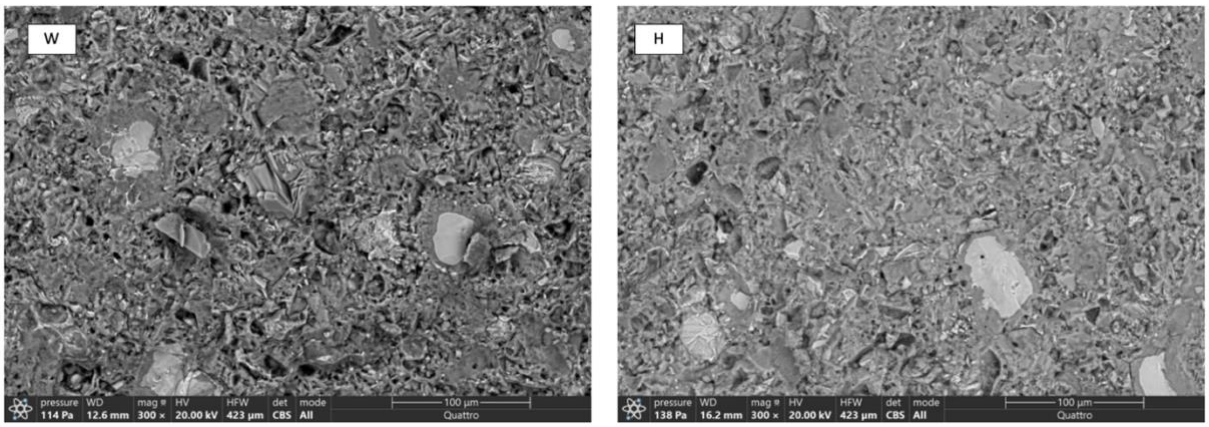

Figure 48. Scanning Electron Microscopy (SEM) imaging showing base distilled water exposed samples (W) and hydrogen exposed sample (H) at 28 days. Showing the difference in larger pores from a lower magnification of 300 (100 μm).

Something relevant was observed in the samples exposed to hydrogen. When taking the samples before testing, it was observed on the outer surface that some crystalline structures formed in hydrogen-exposed samples. **Figure 49** shows this occurrence during the experiments. This happened on the surface of the sample where there is direct contact with the curing environment. The same occurrence may occur within the sample where the crystalline structures were found within the pore space. However, this is simply an assumption based on observation. There is no concise proof of the matter.

Figure 49. Samples after curing. The left is base water exposed samples, and the right is hydrogen exposed samples. It can be observed that hydrogen-exposed samples exhibit some crystals within the outer surface of the samples.

Permeability is directly related to porosity, then the lower permeability in samples exposed to hydrogen can be due to the formation of hydrated product in the larger pores. Permeability is another essential property to consider in UHS, as the cement barrier needs to avoid any leakage or loss of stored gas by permeation. Strong hydrogen diffusion can lead to potential leaks generated by hydrogen permeation through the cement barrier (Carden and Patterson, 1979). Improving completion operations and barrier systems are prerequisites for UHS implementation to control hydrogen leakage (Bai et al., 2015; Bai et al., 2014). The maximum leakage rate tolerated is 150 kg/day, while 50 kg/day is defined as the lowest limit (Crotogino, 1995). No studies show class H would be sufficiently tight for hydrogen storage in the published literature.

A higher UCS is a desired mechanical property. For UHS, the well will be subjected to multiple cyclical injection and production periods. These periods cause changes in pressures and stresses. During the life of a well, cement can fail due to compressional or tangential stresses. In addition, due to injection and production phases, pressure and temperature will change cyclically during UHS. Studies have shown that cement sheath with a low Young's modulus and low expansion properties is desirable for mechanical durability and stress resistance (Wu et al., 2014). Although the amount of hydrated product (portlandite and ettringite) increases the compressive strength of cement, results obtained by measuring acoustic velocities showed an increase in Young's modulus, which would be detrimental for well integrity as flexible and expanding cement would be needed. This would also increase the risk of creating micron annuli between the cement and casing (Baumgarte et al., 1999).

The main explanation for the difference between the samples of both environments is that hydrogen acts with unreacted components to generate more hydrated products. FTIR results can support the statement regarding the higher formation of products in samples exposed to hydrogen. Due to the difference observed in early curing times, it can be said that hydrogen accelerated hydration. It was observed how the absorbance ratio of O-H (**Figure 46**) increased

over time while the absorbance ratio of Si-O (**Figure 45**) only increased during the first 28 days and then remained constant. Cement takes 28 days to fully hydrate, although, in an aqueous environment, it can continue developing more strength over time. Analyzing the results showed that more hydrated product (ettringite and portlandite) was formed over time in hydrogen-exposed samples. From the ratios observed in **Figure 45-46**, it can be concluded that the amount of portlandite and ettringite increased over time due to the presence of hydrogen.

A limitation of the study is that samples were exposed to hydrogen after the first 12 hours of the hydration cycle, which is the deceleration period of the cement settling. This is relevant for new wells. Yet, this period is known for conversion from ettringite to monosulphate. In other words, the concern is if the observed results would happen in a sample that has been fully hydrated for 28 days. This would be relevant for older wells repurposed for hydrogen storage. For this reason, the same experiments were run in a batch of cement samples that were cured for 28 days under the same conditions. After 28 days, half the samples were placed in a curing environment saturated with hydrogen (H) and the other with base distilled water (W). Results of UCS, Porosity from AP608 and NMR, FTIR, and Acoustic Velocities can be observed in **Figures 50-53**. These results exhibit a similar trend to those observed in the previous section. This validates the claim that hydrogen presence in an aqueous environment will react with fully hydrated cement's unreacted cement components, causing the formation of more hydrated products. This is relevant for old wells, showing that hydrogen can also generate more ettringite and portlandite in fully hydrated cement. Thus shows, hydrogen does not affect well integrity of cement in old wells rather, it also increases cement strength.

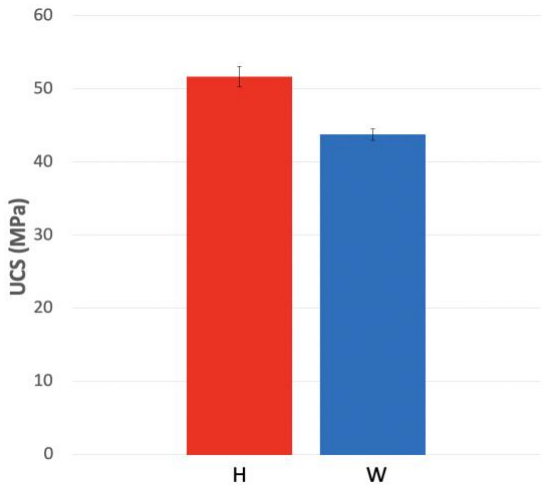

Figure 50. Mechanical Testing Results showing Unconfined Compressive Strength (UCS) of samples after 28 days curing in the same environment and 28 days exposed to either water with molecular hydrogen (H) or base water (W).

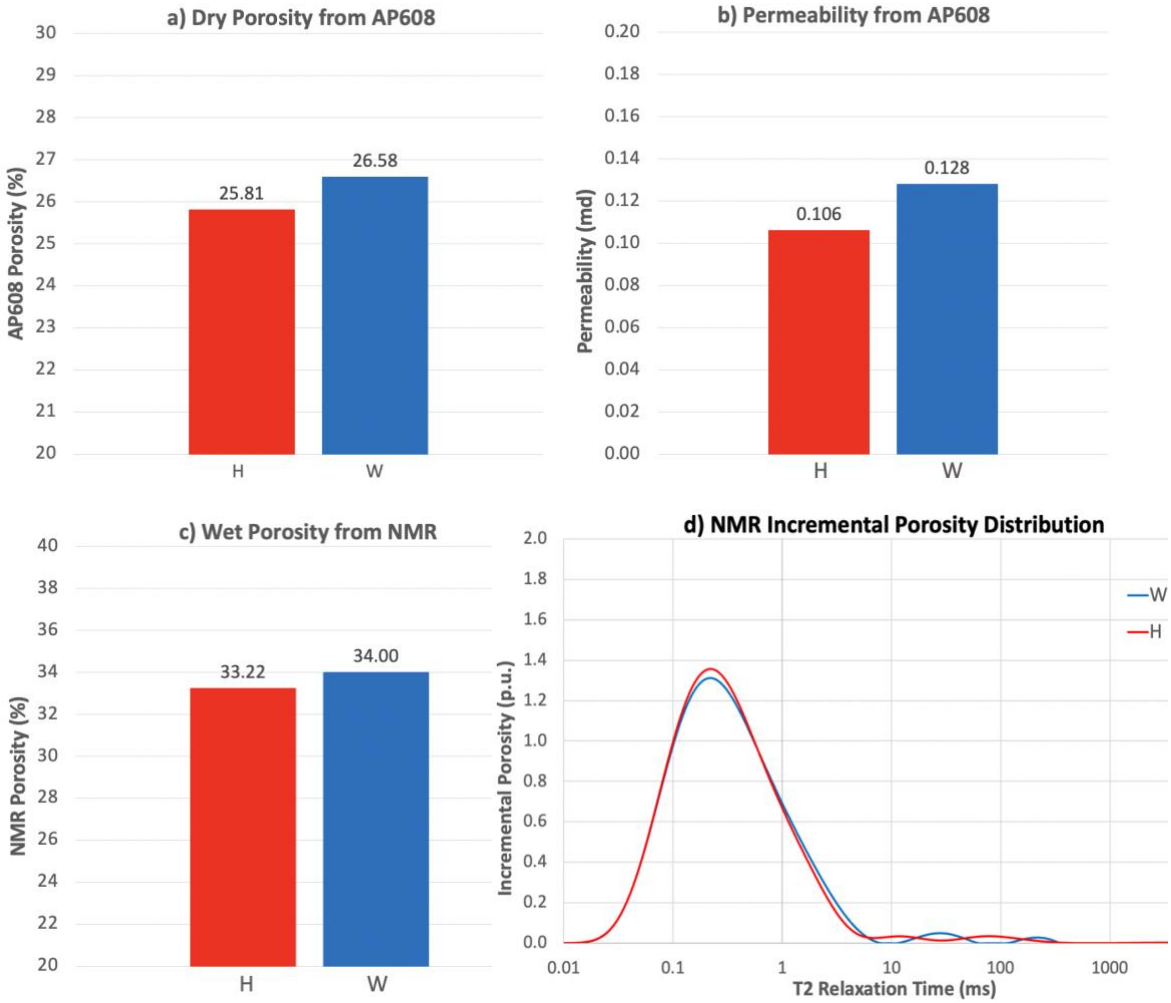

Figure 51. Petrophysical Testing Results showing a) AP608 Porosity, b) AP608 Permeability, c) NMR Porosity, and d) NMR incremental porosity vs. T2 relaxation of samples after 28 days curing in the same environment and 28 days exposed to either water with molecular hydrogen (H) or base water (W).

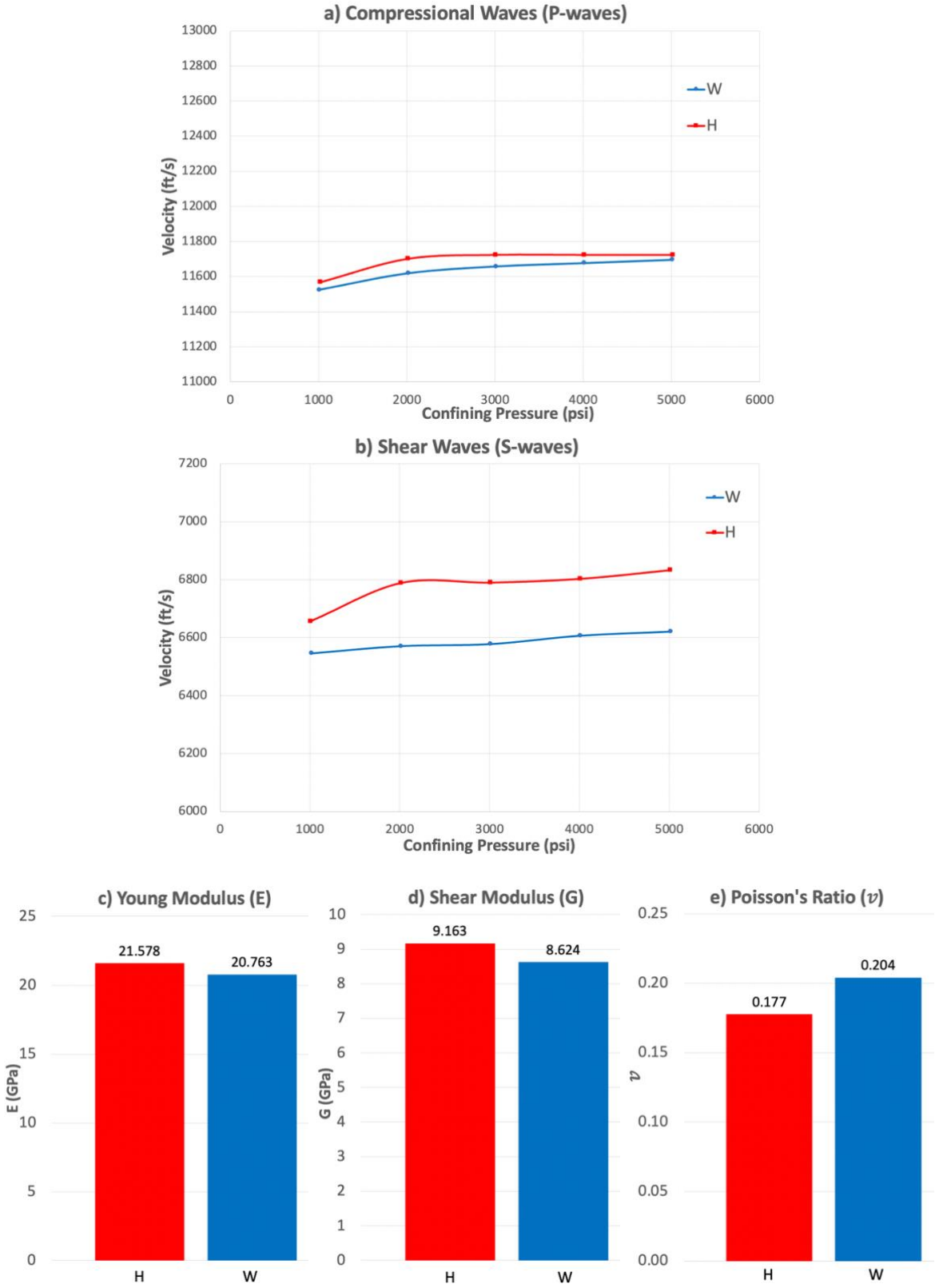

Figure 52. Acoustic Velocities Testing Results showing a) Compressional waves and b) Shear waves, c) Young Modulus (E), d) Shear Modulus (G), and e) Poisson ratio of samples after 28 days curing in the same environment and 28 days exposed to either water with molecular hydrogen (H) or base water (W).

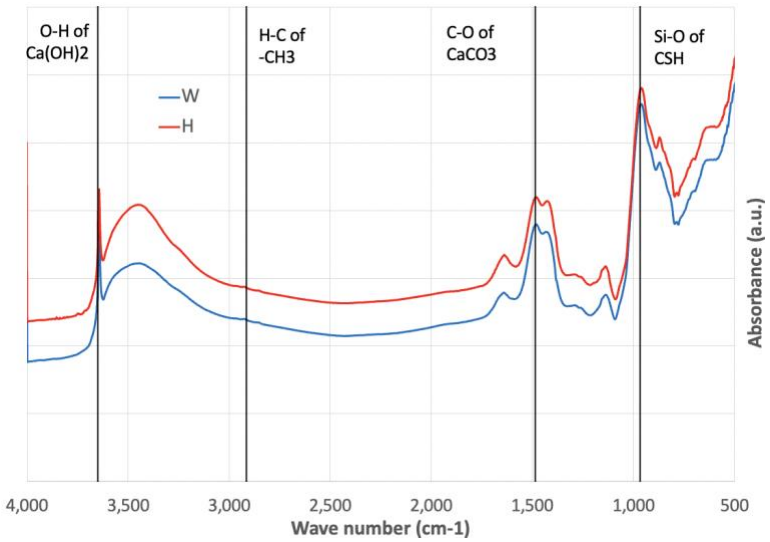

Figure 53. Compositional Analysis showing FTIR spectra of samples after 28 days curing in the same environment and 28 days exposed to either water with molecular hydrogen (H) or base water (W).

Figure 54 shows the T_1-T_2 distribution maps for the 28 days cured plus 28 days exposure samples. It can be observed in the water samples (**Figure 54b**) that there is a more spread distribution with a higher number of large pores contributing to the overall porosity. On the hydrogen-exposed samples, it can be observed less distribution of larger pores and more concentration in the smaller pores. This visual representation of the NMR T_1-T_2 distribution shows the small variation change in samples exposed to hydrogen.

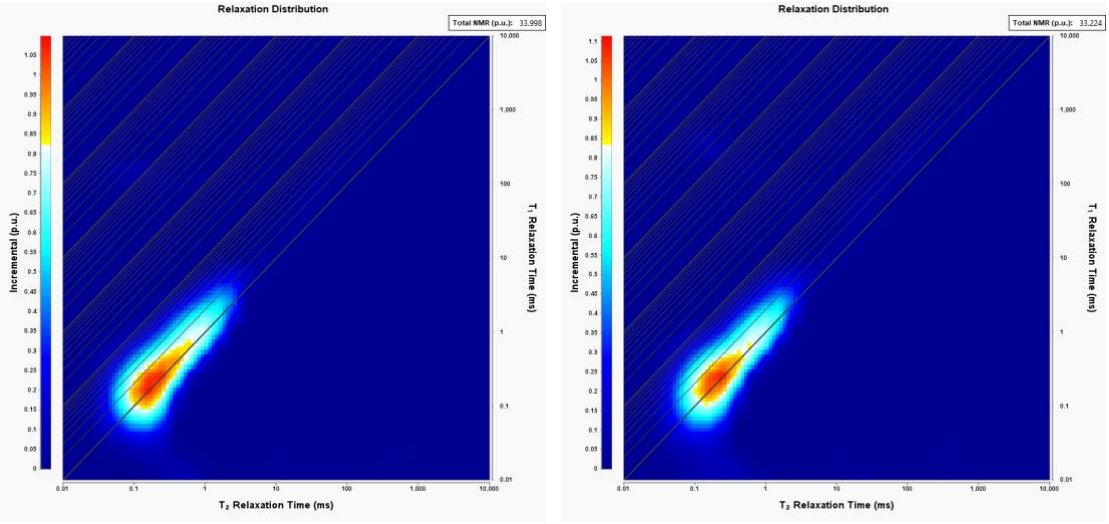

Figure 54. Nuclear Magnetic Resonance (NMR) T1-T2 Relaxation Distribution with Incremental Porosity of samples after 28 days curing in the same environment and 28 days exposed to either water with molecular hydrogen (H) in the right or base water (W) in the left.

Calcium silicate hydrate (CSH or tobermorite) is the main binding element responsible for cement strength. Tobermorite is an amorphous phase with a layer structure (Battocchio et al., 2012). An increment of Ca/Si ratio leads to a reduction of the silicate chain length and the interlayer spacing (Renaudin et al., 2009; Garcia Lodeiro et al., 2009). The Ca/Si, Al/Si, and Mg/Si ratios have effects on the structure of the CSH but also on the carbonation resistance (Bakharev et al., 2001, Renaudin et al., 2009; Garcia Lodeiro et al., 2009). Carbonation is the chemical degradation of cement due to CO_2 presence in an aqueous environment. This is a mentioned issue in literature. During UHS, if it is found in the rock mineral and the formation fluids, it can generate an acidic environment; this can cause the dissolution of cement's major binding components (CH and CSH). Black et al. (2007) indicated that CSH with a low Ca/Si ratio had better carbonation resistance. Li et al. (2019) showed a CSH with a low Ca/Si ratio had better carbonation resistance, an increase in Al/Si ratio showed no effect on carbonation resistance, and Mg/Si ratio helped increase carbonation resistance. Hydrogen-exposed samples exhibited a lower Ca/Si ratio in all timeframes. It can be inferred that cement samples exposed to hydrogen that have developed more hydrated products will have higher resistance against carbonation.

Imaging was a valuable tool for observing the microstructure of the samples. It supported the hypothesis that more hydrated products are formed within the larger pores. It was observed that portlandite and ettringite were formed. Now ettringite can improve strength development. But on the other hand, secondary delayed ettringite formation is known to be a problem when appearing in cement. Secondary delayed ettringite formed after the hardening of the slurry. It can lead to expansion, internal stress, and cement degradation (Kutchko et al., 2011; Collepardi, 2003). When hydrated cement is placed in an environment containing high sulfate concentrations, the calcium monosulfo-aluminate hydrate and the portlandite present in the cement paste will react with the sulfate ions coming from the environment. This can lead to

secondary delayed ettringite formation. Sulfate attack from H2S exposure can cause secondary ettringite formation as the acid penetrates the cement pores and forms voluminous water-insoluble crystal products that expand. The size of the crystal grows, causing pressure to increase inside the cement pores resulting in cracks and fractures. This hydrated product formation would destroy the cement's strength. Nevertheless, during this study, ettringite formed seems to contribute to cement strength and not deteriorate it. Cement exposed to water for a long period of time may cause primary ettringite to dissolve and recrystallize in voids. This case seems to be causing secondary ettringite formation over time with no destructive impact. In addition, there is no additional sulfate attack that may lead to ettringite formation, meaning sulfate comes from the original cement composition. Therefore, it is unreacted material that is reacting in the aqueous environment saturated with molecular hydrogen, which is causing the behavior observed in this study.

Nevertheless, it is hard to ensure the same behavior across the whole cement in the well. Testing with a small 1.5-inch by 1-inch cement can be quite different compared to a 4000-ft column of cement. On a large scale, due to hydrogen properties, it is expected hydrogen will have a higher effect in the top section of the cement. Thus, the impact will occur only in certain sections of the well. This suggests that more heterogeneity exists on a larger scale compared to a small laboratory scale.

6. SUMMARY AND CONCLUSIONS

This study compared two curing conditions of neat class H cement commonly used in the oil & gas industry. The first includes base distilled water, and the second is the same water with the presence of molecular hydrogen. Molecular hydrogen is meant to be present in the subsurface during underground hydrogen storage operations. This study aimed to understand the interactions between hydrogen and cement during setting. This are relevant for new wells. Results showed that hydrogen presence in water could cause the cement to show higher unconfined compressive strength, lower porosity and permeability, higher elastic moduli, and change in the composition and microstructure. The behavior during setting was observed in all samples, from the shortest timeframe of 7 days to the longest of 168 days. The impact was most significant in the longest exposure time. In the discussion, we observed similar results in a fully set cement. This is relevant for old wells that could be repurpose for storage. The followings are the outcomes of this study:

- Hydrogen-exposed samples exhibited a higher UCS compared to base water. The percentage difference of 4.2% (1.03 MPa) in the shortest curing time of 7 days and 14.3% (6.70 MPa) in the longest curing time of 168 days.
- AP608 porosimeter showed a lower porosity in samples exposed to hydrogen by a percentage difference of 2.6% (0.83% porosity) in the shortest curing time and 6.1% (1.61% porosity) in the longest curing time.
- Directly related to porosity permeability showed a lower value for samples exposed to hydrogen compared to samples exposed to pure water. The difference was 20.9% (0.092md) in the shortest curing time and 4.2% (0.007md) in the longest curing time.

- Similar porosity trends among the cases were observed in the NMR tests. The observed difference in the shortest curing time was 0.07% (0.29% porosity) and 1.3% (0.42% of porosity) in the longest curing time.
- NMR T2 distribution showed a reduction of larger pores and an increase of smaller pore spaces in samples exposed to hydrogen, meaning there was a minimal shift in the pore size distribution. The maximum observed difference showed a porosity increase of 5.6% in the smaller pores and a decrease of 23.6% in the larger pores.
- Acoustic velocities showed hydrogen-exposed samples to have a higher Youngs Modulus, higher Shear Modulus, and Poisson ratio. In the longest curing time, with a percentage difference of 4.7%, 5.0%, and 1.8%, respectively. Stiffer and less flexible may be detrimental because, during UHS, of multiple cycles of injection and production. Nevertheless, the observed difference is too low to be detrimental to the integrity of the storage.
- The comparison between compositional analysis among the two cases was observed in the FTIR analysis showed that hydrogen presence increases the amount of hydrated product (portlandite and ettringite) formed within the cement sheath.
- The observed presence of this crystalline needle-shaped structure in the SEM confirmed the presence of portlandite and ettringite and showed the formation of these minerals within some of the larger pores.
- EDS analysis from SEM provided similar results by observing the weight percentage of the minerals in the samples.

The conclusions presented were based on observations made during this research and applied to the different cement samples used in the analysis. It is important to remember that cement can have varying responses to several factors.

However, the general behavior of cement is assumed to be comparable over the different timeframes. Results demonstrate that molecular hydrogen presence in water can generate more portlandite and ettringite by reacting with unreacted components generating these minerals within the larger pore spaces, causing an increase in the cement's unconfined compressive strength. This behavior was observed during cement setting related to new wells constructed for storage purposed and fully set cement related to old wells repurposed for storage.

7. RECOMMENDATIONS AND FUTURE WORK

Underground Hydrogen Storage is an undeveloped technology that has recently started gaining attention due to its applications in the future. Yet, the lack of projects and actual real data make it difficult to see what problems it may face. From literature, the number of publications regarding UHS has been increasing. However, there a very few numbers of publications oriented to well integrity. Cement is one of the main components of well integrity, which is needed to ensure proper containment of fluid throughout the storage life. This study focused on understanding the behavior of cement exposed to molecular hydrogen in aqueous conditions by comparing the variance from a neat Class H sample. Results showed that molecular hydrogen presence could affect the properties of cement. Nevertheless, there were a number of limitations that occurred during this study. Therefore, these are the recommendations for future research:

- Subsurface conditions are exposed to elevated pressure and temperature. Further research would include developing a setup to consider temperature and pressure as variables to simulate subsurface conditions more accurately.
- Hydrogen concentrations are an important variable as the hydrogen generator only runs for a certain period of 2 hours. It is required to constantly restart it. This has caused something concentrations to drop below 1 ppm. Future work would vacuum seal the curing environment to have even concentrations of hydrogen and prevent hydrogen from escaping.
- Hydrogen generator equipment is quite small, which causes a delay in testing as samples are curing for long periods. A bigger setup is required to be able to cure more samples simultaneously to provide more results, as cement can be quite variable.
- Cement was exposed to hydrogen after developing a hard constituency and the majority of its strength after 12 hours. Nevertheless, cement samples are still in the fourth phase

of hydration. This was a poor experimental design, so for future work, it is recommended to leave the cement to cure for at least 24 hours before moving to different environments.

- This study was narrowed to class H cement, which is commonly used in oil and gas applications. Future work should consider expanding to class G cement and other commonly used types.
- The use of numerical chemical models can be done to better understand reactions that may occur in cement during hydration and exposure to hydrogen. This would provide a better foundation to see which components are responsible for the behavior and formulate suggestions for future types of cement to be used in UHS.
- Mechanical testing can be expanded beyond uniaxial compressive strength. As in the subsurface, the well is subjected to a number of pressures from multiple regimes. Using triaxial testing setups is recommended.
- For UCS using stress-strain gauges to measure the change in width and reduction in height can provide insightful information regarding the cement's mechanical behavior, obtaining a more accurate Poisson’s ratio and Youngs' modulus.
- Further expanding mechanical testing can be done using Tensile Strength tests such as the Brazilian test.
- Developing a better experimental procedure with more samples tested and longer exposure and curing times would increase the veracity of the results and provide additional information on the behavior of cement during UHS.
- For FTIR, the deconvolutions excel sheet was built to fit this purpose and compare results. Yet, for a better understanding of the curves and what they represent aside from the ones discussed in this study would provide valuable compositional information that might have been overseen during this study. For this, it is recommended the use more advanced commercial software.

- NMR is a technique that can be quite valuable in understanding the petrophysical behavior of cement. Performing NMR porosity measurements in all samples would provide additional support. In addition, the use of T_1-T_2 tests in all samples from all the different curing times is recommended to compare pore distributions better.
- Porosity and Permeability tests in cement are massively time-consuming. Nevertheless, it is recommended to perform Helium Porosity and Permeability tests in the AP608 for all samples in all curing timeframes to increase certainty. In addition, considering multiple confining pressures.
- Due to hydrogen properties and small particle sizes, literature mentions that permeation can be a problem during UHS. Developing cement permeation tests using hydrogen gas can provide information regarding this issue, as it can be detrimental and lead to potential leaks.
- Carbonation is caused to an acid environment in the subsurface. No literature investigates the behavior of cement with hydrogen gas present in an acid environment.

NOMENCLATURE AND ACRONYMS

Abbreviations and Acronyms

Symbol	Description	Units
Al_2O_3	Aluminum Oxide	--
LBF	Applied load	lbf
$Ca(HCO_3)_2$	Calcium Bicarbonate	--
$CaCO_3$	Calcium Carbonate	--
CCS	Carbon Capture and Storage (CCS)	--
CO_2	Carbon Dioxide	--
CaO	Calcium Oxide	--
C_2S	Dicalcium Silicate	--
L or D	Dimensions (length or Dimaeter)	mm
EDS	Energy Dispersive X-Ray Spectroscopy	Wt%
FTIR	Fourier Transform Infrared Spectroscopy	cm^{-1}
EIA	U.S. Energy Information Administration	--
H_2S	Hydrogen Sulfide	--
IRB	Iron-Reducing Bacteria	--
HPHT	High Pressure High Temperature	--
HIC	Hydrogen Blistering	--
MD	Measured Depth	Ft
CH_4	Methane	--
MIP	Mercury Intrusion Porosimeter	--
H	Molecular Hydrogen	Ppm

NMR	Nuclear Magnetic Resonance	--
LR	Loading Rate	MPa/min
W	Weight	gr
O&G	Oil and Gas	--
P	Pressure	psi
Perm	Permeability	Md
ϕ	Porosity	%
CH	Portlandite or Calcium Hydroxide	--
PEM	Proton Exchange Membrane	--
RGD	Rapid Gas Decompression	--
RPM	Revolutions Per Minute	rpm
SEM	Scanning Electron Microscopy	--
SiO_2	Silicon Dioxide	--
SPE	Solid Polymer Electrolytic	--
SRB	Sulfate-Reducing Bacteria	--
T	Temperature	°F or °C
C_4AF	Tetracalcium Aluminoferrite	--
C_3S	Tricalcium Silicate	--
C_3A	Tricalcium Aluminate	--
CSH	Tobermorite or Calcium Silicate Hydrate	--
UCS	Unconfined Compressive Strength	MPa
UGS	Underground Hydrogen Storage	--
UHS	Underground Hydrogen Storage	--
H_2O	Water	--

REFERENCES

Abalaka, A. E. and Okoli, O. G. 2013. Influence of curing regime on strength development of grade C60 concrete. *International Journal of Modern Engineering Research* **3**(2): 709- 714.

Ahmed, S., Patel, H., and Salehi, S. 2020. Numerical modeling and experimental study of elastomer seal assembly in downhole wellbore equipment: Effect of material and chemical swelling. *Polymer Testing* **89**:106608. https://doi.org/10.1016/j.polymertesting.2020.106608

Ahmed, S., Salehi, S., Ezeakacha, C., and Teodoriu, C. 2019. Experimental investigation of elastomers in downhole seal elements: Implications for safety. *Polymer Testing* **76**: 350-364. https://doi.org/10.1016/j.polymertesting.2019.03.041

Aïtcin, P.C., and Flatt, R.J. 2016. Science and Technology of Concrete Admixtures. Elsevier.

Al Ramadan, M., Salehi, S., Kwatia, G., et al. 2019. Experimental Investigation of Well Integrity: Annular Gas Migration in Cement Column. *Journal of Petroleum Science and Engineering.* https://doi.org/10.1016/j.petrol.2019.04.023.

Allen, A.J., Thomas, J.J., and Jennings, H.M. 2007. Composition and density of nanoscale calcium–silicate–hydrate in cement, *Nat. Mater*. **6**: 311–316.

American Petroleum Institute. 2010. *ANSI/API Spec 10A - Specification for Cements and Materials for Well Cementing.* Washington, D.C.: American Petroleum Institute.

Amid, A., Mignard, D., and Wilkinson, M. 2016. Seasonal storage of hydrogen in a depleted natural gas reservoir. *Int. J. Hydrog. Energy* **41**(12): 5549-5558. https://doi.org/10.1016/j.ijhydene.2016.02.036.

API RP 10B-2. 2013. Recommended Practice for Testing Well Cement. American Petroleum Institute (API).

ASTM C 109/C 109M. 2004. Standard test method for compressive strength of hydraulic cement mortars. American Society for Testing and Materials. West Conshohocken, Pennsylvania.

Bai, M., Song, K., Sun, Y., et al. 2014. An overview of hydrogen underground storage technology and prospects in China. *Journal of Petroleum Science and Engineering* **124**: 132–136. http://dx.doi.org/10.1016/j.petrol.2014.09.037

Bai, M., Sun, J., Song., K., et al. 2015. Well completion and integrity evaluation for CO2 injection wells. *Renewable and Sustainable Energy Reviews* **45**: 556–564. http://dx.doi.org/10.1016/j.rser.2015.02.022

Bai, M., Zhang, Z., and Fu, X. 2016. A review on well integrity issues for CO2 geological storage and enhanced gas recovery. *Renew. Sust. Energ. Rev.* **59**: 920–926. http://dx.doi.org/10.1016/j.rser.2016.01.043

Bakharev, T., Sanjayan, J.G., and Cheng, Y.B. 2001. Resistance of alkali-activated slag concrete to carbonation. *Cement and Concrete Research* **31**(9): 1277-1283. ISSN 0008-8846. https://doi.org/10.1016/S0008-8846(01)00574-9

Barlet-Gouedard, V., Rimmele, G., Goffe, B, et al. Mitigation strategies for the risk of CO2 migration through wellbores. Paper presented at the IADC/SPE Drilling Conference, Miami, Florida, USA, February. https://doi.org/10.2118/98924-MS

Battocchio, F., Monteiro, P.J.M., Paulo J.M. Wenk, H.R. 2012. Rietveld refinement of the structures of 1.0 C-S-H and 1.5 C-S-H. *Cement and Concrete Research* **42**(11): 1534-1548. ISSN 0008-8846. https://doi.org/10.1016/j.cemconres.2012.07.005

Baumgarte, C., Thiercelin, M., and Klaus, D. 1999. Case Studies of Expanding Cement To Prevent Microannular Formation. Paper presented at the SPE Annual Technical Conference and Exhibition, Houston, Texas, October. https://doi.org/10.2118/56535-MS

Benato, A., and Stoppato, A. 2017. Energy and Cost Analysis of a New Packed Bed Pumped Thermal Electricity Storage Unit. *ASME J. Energy Resour. Technol.* **140**(2): 020904. https://doi.org/10.1115/1.4038197

Bois, A.P., Garnier, A., Galdiolo, G., and Laudet, J.B. 2010. Use of a mechanistic model to forecast cement-sheath integrity for CO2 storage. Paper presented at the SPE International Conference on CO2 capture, storage, and utilization, New Orleans, Nov 10–12.

Boopathy, R., and Daniels, L. 1991. Effect of pH on Anaerobic Mild Steel Corrosion by Methanogenic Bacteria. *Appl. Environ. Microbiol.* **57** (7): 2104-2108.

Bosma M.G.R, Ravi, K., van Driel, W., and Schreppers, J. 1999. Design approach to sealant selection for the life of the well. Paper presented at the Annual Technical Conference and Exhibition, Houston, Oct 3–6

Bryar, T.R., Daughney, C.J., and Knight, R.J. 2000. Paramagnetic effects of iron(III) species on nuclear magnetic relaxation of fluid protons in porous media. *J. Magn. Reson*. **142**: 74–85. https://doi.org/10.1006/jmre.1999.1917.

Bullard, J.W., Jennings, H.M., Livingston, R.A., et al. 2011. Mechanisms of cement hydration. *Cement and Concrete Research* **41**(12): 1208-1223. https://doi.org/10.1016/j.cemconres.2010.09.011.

Câmara, R.J.B., Carneiro, J.F., Câmara, G.A.B., et al. 2019. Methodology for Sub-commercial Calculation of the Potential Energy Storage Capacity of Hydrogen, Natural Gas, and Compressed Air in Salt Caves. *ASME J. Energy Resour. Technol.* **142**(4): 042007. https://doi.org/10.1115/1.4045351

Campion, R. P., Thomson, B., and Harris, J. A. 2005. Elastomers for Fluid Containment in Offshore Oil and Gas Production: Guidelines and Review. Technical Report No. RR-320, MERL Ltd for the Health and Safety Executive, U.K.

Carden, P.O., and Paterson, L. 1979. Physical, chemical and energy aspects of underground hydrogen storage. *International Journal of Hydrogen Energy* **4** (6): 559-569. ISSN 0360-3199. https://doi.org/10.1016/0360-3199(79)90083-1.

Chakraborty, S., Kundu, S. P., Roy, A., et al. 2013. Effect of jute as fiber reinforcement controlling the hydration characteristics of cement matrix. *Ind. Eng. Chem. Res*. **52**: 1252− 1260.

Chakraborty, S., Jo, B.W. and Sikandar, M.A. 2016. Hydration Mechanism of the Hydrogen-

Rich Water Based Cement Paste. *The Journal of Physical Chemistry C* **120**(15): 8198-8209. https://doi.org/10.1021/acs.jpcc.6b01444

Coates, George R., Lizhi Xiao, and Manfred G. Prammer. 1999. *NMR Logging Principles and Applications.* Houston: Halliburton Energy Services.

Collepardi, M. 2003. A state-of-the-art review on delayed ettringite attack on concrete. *Cem Concr Compos* **25**, pp. 401-407. https://doi.org/10.1016/S0958-9465(02)00080-X

Condon, J. B., and Schober, T. 1993. Hydrogen bubbles in metals. *J. Nucl. Mater.* **207**: 1-24. https://doi.org/10.1016/0022-3115(93)90244-S

Crotogino, F. 1996. SMRI reference for external well mechanical integrity testing/performance, data evaluation and assessment. Paper presented at the SMRI spring meeting, summary of final project report 95-0001 Short Class, Houston, TX, USA.

Cruz, F., Tinni, A., Brackeen, S, et al. 2020. Impact of Capillary Pressure on Total Porosity in Unconventional Shales. Paper presented at the SPE/AAPG/SEG Unconventional Resources Technology Conference, Virtual. https://doi.org/10.15530/urtec-2020-3117

Das, D., and Veziroğlu, T.N. 2001. Hydrogen Production by Biological Processes: A Survey of Literature. *Int. J. Hydrogen Energy*, **26**(1): 13–28. https://doi.org/10.1016/S0360-3199(00)00058-6

Dunn, K.J., D.J. Bergman, and G.A. Latorracca. 2002. *Nuclear Magnetic Resonance Petrophysical and Logging Applications.* Oxford: Elsevier Science Ltd.

Edlmann, K., Bensabat, J., Niemi, A., Haszeldine, R. S., and McDermott, C. I. 2016. Lessons learned from using expert elicitation to identify, assess and rank the potential leakage scenarios at the Heletz pilot CO2 injection site. *Int. J. Greenh. Gas Control* **49**: 473-487. https://doi.org/10.1016/j.ijggc.2016.02.018

Elkatatny, S., Mahmoud, M., Mohamed, I. et al. 2018. Development of a new correlation to determine the static Young's modulus. *J Petrol Explor Prod Technol* **8**: 17–30. https://doi.org/10.1007/s13202-017-0316-4

Edyvean, R.G.J., Benson, J., Thomas, C.J., et al. 1997. Biological Influences on Hydrogen effects in Steel in Seawater. Paper presented at the NACE-97206 presented at Corrosion97, New Orlean, U.S., March 9-14.

EIA. 2020. Monthly Energy Review, U.S. Energy Information Administration, Washington, DC.

Eshiet, K., Sheng, Y. 2014. Investigation of geomechanical responses of reservoirs induced by carbon dioxide storage. *Environ Earth Sci* **71**(9): 3999–4020

Faulkner, D. R. and Rutter, E. H. 2000. Comparisons of water and argon permeability in natural clay-bearing fault gouge under high pressure at 20°C. *Journal of Geophysical Research* **105**(7): 415–426. https://doi.org/10.1029/2000JB900134

Fernández, C., and Castaño, P. 2016. Compatibility Behavior of Elastomers for PCP Applications. Paper presented at the *CORROSION, NACE International*, Vancouver, British Columbia, Canada. NACE-2016-7106.

Fink, Johannes. 2015. *Petroleum Engineer's Guide to Oil Field Chemicals and Fluids.* 2nd. Elsevier.

Fronk, B. M., Neal, R., and Garimella, S. 2010. Evolution of the Transition to a World Driven by Renewable Energy. *ASME J. Energy Resour. Technol.* **132**(2): 021009. https://doi.org/10.1115/1.4001574

García Lodeiro, I., Macphee, D.E., Palomo, A., et al. 2009. Effect of alkalis on fresh C–S–H gels. FTIR analysis. *Cement and Concrete Research* **39**(3): 147-153. ISSN 0008-8846. https://doi.org/10.1016/j.cemconres.2009.01.003

Gartner, E.M. 1997. A proposed mechanism for the growth of C–S–H during the hydration of tricalcium silicate. *Cem. Concr. Res***. 27** (5): 665–672.

Gartner, E.M., Young, J.F. Damidot, D.A., et al. 2002. Hydration of portland cement. Structure and Performance of Cements, 2nd Edition, Spon Press, New York, pp. 57–113.

Gasda, S. E., Bachu, S. and Celia, M. A. 2004. Spatial characterization of the location of potentially leaky wells penetrating a deep saline aquifer in a mature sedimentary basin. *Environmental Geology* **46**(6-7): 707-720. https://doi.org/10.1007/s00254-004-1073-5.

Ghafoori, N., and Dutta, S. 1995. Laboratory investigation of compacted no-fines concrete paving materials. Journal of *Materials in Civil Engineering* **7**(3): 183-191. ISSN: 0899-1561. http://ascelibrary.org/journal/jmcee7

Ghosh, G., Rostron, P., Garg, R., et al. 2018. Hydrogen induced cracking of pipeline and pressure vessel steels: A review. *Engineering Fracture Mechanics* **199**: 609-618. ISSN 0013-7944. https://doi.org/10.1016/j.engfracmech.2018.06.018

Gomez, C.T., Dvorkin, J., and Vanorio, T. 2010. Laboratory measurements of porosity, permeability, resistivity, and velocity on Fontainebleau sandstones. *GEOPHYSICS* **75**(6): https://doi.org/191-204.10.1190/1.3493633

Goodman, R.E., 1989. Introduction to rock mechanics. Vol. 2 Wiley. New York.

Goodwin, K.J., Crook, R.J. 1992. Cement sheath stress failure. SPEDE, 291–296, Dec 1992

Gutteridge, W.A., and Dalziel, J.A. 1990. Filler cement: The effect of the secondary component on the hydration of Portland cement: Part I. A fine non-hydraulic filler. *Cement and Concrete Research* **20**(5): 778-782, ISSN 0008-8846 https://doi.org/10.1016/0008-8846(90)90011-L.

Hamada, G., and Joseph, V. 2020. Developed correlations between sound wave velocity and porosity, permeability and mechanical properties of sandstone core samples. *Petroleum Research* **5**(4): 326-338. ISSN 2096-2495. https://doi.org/10.1016/j.ptlrs.2020.07.001.

Heinemann, N., Booth, M.G., Haszeldine, R.S., et al. 2018. Hydrogen storage in porous geological formations – onshore play opportunities in the midland valley (Scotland, UK). *International Journal of Hydrogen Energy* **43** (45): 20861-20874. ISSN 0360-3199, https://doi.org/10.1016/j.ijhydene.2018.09.149.

Hemme, C., Van Berk, W. 2018. Hydrogeochemical Modeling to Identify Potential Risks of

Underground Hydrogen Storage in Depleted Gas Fields. Appl. Science **8** (11): 2282. https://doi.org/10.3390/app8112282

Hibbert, A.P., Kellingray, D.J. and Vidick, B. 1995. Effect of mixing energy levels during batch mixing of cement slurries. *SPE Drilling and Completions* **10**(1): 49-52. https://doi.org/10.2118/25147-PA.

Hirata, K., Iikubo, S., Koyama, M., Tsuzaki, K., and Ohtani, H. 2018. First-Principles Study on Hydrogen Diffusivity in BCC, FCC, and HCP Iron. *Metal Mater. Trans. A.* **49**: 5015–5022. https://doi.org/10.1007/s11661-018-4815-9

Hollis, A.P. 1984. Some Petroleum Engineering Considerations in the Changeover of the Rough Gas Field to the Storage Mode. *J. Pet. Technol.* **36:** 797–804. https://doi.org/10.2118/12932-PA

Huang, B., and Shu, X. 2010. Laboratory evaluation of permeability and strength of polymer-modified pervious concrete. *Construction and Building Materials* **24**. 818-823. https://doi.org/10.1016/j.conbuildmat.2009.10.025.

Ichim, A. 2015. Effect of Cement Thermal Properties on Heat Transfer in HP/HT Wells. Clausthal-Zellerfeld: Clausthal University of Technology.

ISO 16530-1, 2017. Petroleum and Natural Gas Industries—Well Integrity— Part 1: Life Cycle Governance.

Iverson, W. P. 1987. Microbial Corrosion of Metals. *Adv. Appl. Microbiol.* **32**: 1-36. https://doi.org/10.1016/S0065-2164(08)70077-7.

Jennings, H.M., Thomas, J.J., Gevrenov, J.S. and Constantinides, G. 2007. A multi- technique investigation of the nanoporosity of cement paste. *Cem. Concr. Res.* **37**: 329–336.

Jo, B.W., Chakraborty, S. A. 2015. Mild alkali treated jute fibre controlling the hydration behaviour of greener cement paste. *Sci Rep* **5**: 7837. https://doi.org/10.1038/srep07837

Jo, B.W., Chakraborty, S., Lee, Y.S. 2015. Hydration study of the polymer modified jute fibre reinforced cement paste using analytical techniques. *Constr. Build. Mater* **101**: 166−173. https://doi.org/10.1038/srep07837

Jo, B.W., Chakraborty, S., Sikandar, M.A. et al. 2018. Prediction of the Failure Stress of Hydrogen-rich Water Based Cement Mortar Using the Weibull Distribution Model. *KSCE J Civ Eng* **22**: 1827–1839. https://doi.org/10.1007/s12205-017-1560-3

Jones, R. R., and Carpenter, R. B. 1991. New Latex, Expanding Thixotropic Cement Systems Improve Job Performance and Reduce Costs. Paper presented at the *International Symposium on Oilfield Chemistry,* Anaheim, CA. https://doi.org/10.2118/21010-MS

Kabuth, A., Dahmke, A., Beyer, C. et al. 2017. Energy storage in the geological subsurface: dimensioning, risk analysis and spatial planning: the ANGUS+ project. *Environ Earth Sci* **76** 23 (2017). https://doi.org/10.1007/s12665-016-6319-5

Kamali M, Ghahremaninezhad A. 2018. A Study of Calcium-Silicate-Hydrate/Polymer Nanocomposites Fabricated Using the Layer-By-Layer Method. *Materials* **4**: 527.

https://doi.org/10.3390/ma11040527

Keating, J., D. J. Hannant, and A. P. Hibbert. 1989. Correlation Between Cube Strength, Ultrasonic Pulse Velocity, and Volume Change for Oil Well Cement Slurries.*Cement and Concrete Research* **19**(5): 715-726.

Kendall, K., Howard, A. J., Birchall, J. D., et al. 1983. The Relation between Porosity, Microstructure and Strength, and the Approach to Advanced Cement-Based Materials [and Discussion]. *Philos. Trans. R. Soc*. **310**: 139–153.

King, G. E., and Valencia R. T. 2014. Environmental Risk and Well Integrity of Plugged and Abandoned Wells. Paper presented at the *SPE Annual Technical Conference and Exhibition*, Amsterdam, The Netherlands. https://doi.org/10.2118/170949-MS

Kiran, R., Teodoriu, C., Dadmohammadi, Y., Nygaard, R., Wood, D., Mokhtari, M., and Salehi, S. 2017. Identification and evaluation of well integrity and causes of failure of well integrity barriers (A review). *J. Nat. Gas Sci. Eng.* **45**: 511-526. https://doi.org/10.1016/j.jngse.2017.05.009.

Kleinitz, W., and Boehling, E. 2005. Underground Gas Storage in Porous Media - Operating Experience with Bacteria on Gas Quality. Paper presented at the *SPE Europec/EAGE Annual Conference*, Madrid, Spain. https://doi.org/10.2118/94248-MS

Knapen, E., and Van Gemert, D. 2009. Cement hydration and microstructure formation in the presence of water-soluble polymers. *Cement and Concrete Research*, **39**(1): 6-13. ISSN 0008-8846. https://doi.org/10.1016/j.cemconres.2008.10.003.

Kunther, W., Ferreiro , S., and Skibsted, J. 2017. Influence of the Ca/Si ratio on the compressive strength of cementitious calcium–silicate–hydrate binders. *J. Mater. Chem. A* **5**: 17401-17412. https://doi.org/10.1039/C7TA06104H

Kutchko Duguid, A., and Scherer, G. 2010. Degradation of oilwell cement due to exposure to carbonated brine. *Int. J. Greenh. Gas Control*. **4**(3), pp. 546-560. https://doi.org/10.1016/j.ijggc.2009.11.001

Kutchko, B. G., Strazisar, B. R., Hawthorne, S. B., et al. 2011. H2S–CO2 reaction with hydrated Class H well cement: Acid-gas injection and CO2 Co- sequestration. *Int. J. Greenh. Gas Control* **5**(4): 880–888. https://doi.org/10.1016/j.ijggc.2011.02.008.

Lafhaj, Z., Goueygou, M., Djerbi, A., et al. 2006. Correlation between porosity, permeability and ultrasonic parameters of mortar with variable water/cement ratio and water content. *Cement and Concrete Research* **36**(4): 625-633. ISSN 0008-8846. https://doi.org/10.1016/j.cemconres.2005.11.009.

Lécolier, E., Rivereau, A., Ferrer, N., Audibert, A., and Longaygue, X. 2010. Durability of Oilwell Cement Formulations Aged in H2S-Containing Fluids. *SPE Drill & Compl* **25**: 90–95. https://doi.org/10.2118/99105-PA

Li, J., Yu, Q., Huang, H., and Yin, S. 2019. Effects of Ca/Si Ratio, Aluminum and Magnesium on the Carbonation Behavior of Calcium Silicate Hydrate. *Materials* **12**(8): 1268. https://doi.org/10.3390/ma12081268

Li, L.G., Feng, J.J., Zhu, J., et al. 2021. Pervious concrete: effects of porosity on permeability and strength. *Magazine of Concrete Research* **73**(2): 69-79. https://doi.org/10.1680/jmacr.19.00194

Lian, C., Zhuge, Y., and Beecham, S. 2011. The relationship between porosity and strength for porous concrete. *Construction and Building Materials* **25**(11): 4294-4298. ISSN 0950-0618. https://doi.org/10.1016/j.conbuildmat.2011.05.005.

Lockyear, C. F., Ryan, D. F., and Gunningham, M. M. 1990. Cement Channeling: How To Predict and Prevent. *SPE Drill Eng* **5**: 201–208. https://doi.org/10.2118/19865-PA

Loizzo, M., and Sharma, S. 2008. Assessing Long-term CO2 Containment Performance: Cement Evaluation in Otway CRC-1. Paper presented at the *SPE Asia Pacific Oil and Gas Conference and Exhibition*, Perth, Australia. https://doi.org/10.2118/115707-MS

Lord, A. S., Kobos, P. H., and Borns, D. J., 2014. Geologic Storage of Hydrogen: Scaling Up To Meet City Transportation Demands. *Int. J. Hydrogen Energy* **39**(28): 15570–15582. https://doi.org/10.1016/j.ijhydene.2014.07.121

Loto, C.A. 2017. Microbiological corrosion: mechanism, control and impact—a review. *The International Journal of Advanced Manufacturing Technology* **92**: 4241–4252. https://doi.org/10.1007/s00170-017-0494-8

Lovley, D. R., and Phillips, E. J. P. 1986. Organic-matter mineralization with reduction of ferric iron in anaerobic sediments. *Appl. Environ. Microbiol.* **51:** 683–689.

Mai, Y.W., Cotterell, B. 1985. Porosity and mechanical properties of cement mortar. *Cement and Concrete Research* **15**(16): 995-1002. ISSN 0008-8846. https://doi.org/10.1016/0008-8846(85)90090-0.

Mainguy, M., Longuemare, P., Audibert, A., and Lecolier, E. 2007. Analyzing the Risk or Well Plug Failure after Abandonment. *Oil Gas Sci. Technol.* **62**(3): 311-324. https://doi.org/10.2516/ogst:2007026

McDonald, P.J., Rodin, V., and Valori, A. 2010. Characterisation of intra- and inter-C-S-H gel pore water in white cement based on an analysis of NMR signal amplitudes as a function of water content. *Cement Concrete Res* **40**: 1656–1663. https://doi. org/10.1016/j.cemconres.2010.08.003

McPherson, M., Johnson, N., and Strubegger, M. 2018, The Role of Electricity Storage and Hydrogen Technologies in Enabling Global Low-Carbon Energy Transitions. *Appl. Energy* **216**: 649–661. https://doi.org/10.1016/j.apenergy.2018.02.110.

Michalski, J., Bünger, U., Crotogino, F., et al. 2017. Hydrogen generation by electrolysis and storage in salt caverns: Potentials, economics and systems aspects with regard to the German energy transition. *Int. J. Hydrog. Energy* **42**(19): 13427-13443. https://doi.org/10.1016/j.ijhydene.2017.02.102

Miyazaki, B. 2009. Well integrity: An overlooked source of risk and liability for underground natural gas storage. Lessons learned from incidents in the USA. *Geological Society London Special Publications* **313**(1): 163-172

Nelson, E.B. 1990. *Well Cementing.* 1st. Vol. 28. Elsevier Science.

Neville, A. M. 2011. Properties of Concrete. Fifth edition. Pearson Education Asia Pvt. Ltd., London.

NORSOK D-010. 2013. Well Integrity in Drilling and Well Operations, October 2010.

Nygaard, R., and R., Lavoie. 2010. Well Integrity and Workover Candidates for Existing Wells in the Wabamun Area CO2 Sequestration Project (WASP).Paper presented at the *Canadian Unconventional Resources and International Petroleum Conference*, Calgary, Alberta, Canada. https://doi.org/10.2118/137007-MS

Nygaard, R., Salehi, S., Weideman, B. et al. 2014. Effect of Dynamic Loading on Wellbore Leakage for the Wabamun Area CO2-Sequestration project. *Journal of Canadian Petroleum Technology* **53**(1): 69-82. https://doi.org/10.2118/146640-PA.

Osbaeck, B. 1985. The Influence of air content by assessing the pozzolanic activity of fly ash by strength testing. *Cement and Concrete Research* **15**(1): 53-64. ISSN: 0008-8846. http://www.sciencedirect.com/science/journal/00088846

Ottesen, S., and Kwakwa. K. A. 1991. A Multidisciplinary Approach to In-Situ Stress Determination and Its Application to Wellbore Stability Analysis. Paper presented at the SPE/IADC Drilling Conference, Amsterdam, Netherlands. https://doi.org/10.2118/21915-MS

Patel, H., Salehi, S., Ahmed, R., et al. 2019. Review of elastomer seal assemblies in oil & gas wells: Performance T evaluation, failure mechanisms, and gaps in industry standards. *Journal of Petroleum Science and Engineering* **179**: 1046 – 1062. https://doi.org/10.1016/j.petrol.2019.05.019

Pfeiffer, W. T., and Bauer, S. 2015. Subsurface Porous Media Hydrogen Storage – Scenario Development and Simulation. *Energy Procedia* **76:** 565-572. https://doi.org/10.1016/j.egypro.2015.07.872.

Powers, T.C. 1958. Structure and Physical Properties of Hardened Portland Cement Paste. *Journal of the American Ceramic Society* **41**(1): 1-6.

Pudlo, D., Ganzer, L., Henkel, S., et al.et al. 2013. The H2STORE Project: Hydrogen Underground Storage—A Feasible Way in Storing Electrical Power in Geological Media?" Paper presented at the Clean Energy Systems in the Subsurface: Production, Storage and Conversion, Berlin, Germany, May 21–23. https://doi.org/10.1007/978-3-642-37849-2_31

Pudlo, D., and Henkel, S. 2016. H2STORE and HyINTEGER—Studies on the Effect of Hydrogen Storage in (PORE) Underground Gas Reservoirs—An Overview. Paper presented at the 3rd HIPS-NET Workshop, Brussels, Belgium, June 23–24.

RAG Austria, 2020. Underground Sun Storage Final Report, 2017.

Reitenbach, V., Ganzer, L., Albrecht, D., et al. 2015. Influence of added hydrogen on underground gas storage: a review of key issues. *Environmental Earth Science* **73**: 6927–693. https://doi.org/10.1007/s12665-015-4176-2

Renaudin, G., Russias, J., Leroux, F., et al. 2009. Structural characterization of C–S–H and C–A–S–H samples—Part I: Long-range order investigated by Rietveld analyses. *Journal of Solid State Chemistry* **182**(12): 3312-3319. ISSN 0022-4596. https://doi.org/10.1016/j.jssc.2009.09.026.

Reuß, M., Grube, T., Robinius, M., et al. 2017. Seasonal Storage and Alternative Carriers: A Flexible Hydrogen Supply Chain Model. *Appl. Energy* **200**: 290–302. https://doi.org/10.1016/j.apenergy.2017.05.050.

Rickard, D. 2012. Sedimentary Iron Biogeochemistry. *Developments in Sedimentology* **65**, pp. 85-119. https://doi.org/10.1016/B978-0-444-52989-3.00003-9.

Sainz-Garcia, A., Abarca, E., Rubi, V., and Grandia, F., 2017. Assessment of feasible strategies for seasonal underground hydrogen storage in a saline aquifer. *Int. J. Hydrog. Energy* **42**(26): 16657-16666. https://doi.org/10.1016/j.ijhydene.2017.05.076

Salehi, S., Ezeakacha, C. P., Kwatia, G., and Ahmed., R. 2019. Performance verification of elastomer materials in corrosive gas and liquid condition. *Polym. Test.* **75**: 48–63. https://doi.org/10.1016/j.polymertesting.2019.01.015

Santra, A., Reddy, B. R., Liang, F. and Fitzgerald, R. 2009. Reaction of CO2 with Portland cement at Down- hole Conditions and the role of Pozzolanic Supplements. Paper presented at the *SPE International Symposium on Oilfield Chemistry*, Woodlands, TX, USA. 10.2118/121103-MS

San Marchi, C., Somerday, B.P., Tang, X., and Schiroky, G.H. 2008. Effects of alloy composition and strain hardening on tensile fracture of hydrogen-precharged type 316 stainless steels. *Int. J. Hydrog. Energy* **33**(2): 889-904. https://doi.org/10.1016/j.ijhydene.2007.10.046

Schulte, R., and Holthausen, M.R. 2019. A phenomenological approach on the influence of paramagnetic iron in cement stone on 2D T1-T2 relaxation in single-sided 1H nuclear magnetic resonance. *Cement and Concrete Research* **120**: 279-293. ISSN 0008-8846. https://doi.org/10.1016/j.cemconres.2019.03.027.

Schreiner, L.J., Mactavish, J.C., Miljkovic, J.C. 1985. NMR Line Shape-Spin-Lattice Relaxation Correlation Study of Portland Cement Hydration. *Journal of the American Ceramic Society* **68**(1): 10-16. https://doi.org/10.1111/j.1151-2916.1985.tb15243.x

Shahid, M., Bidin, N., and Mat, Y. 2012. Production and Enhancement of Hydrogen From Water: A Review. *ASME J. Energy Resour. Technol.* **134**: 034002. https://doi.org/10.1115/1.4006432

Shang, D., Pei, P., and Zuo, Y. 2020. Techno-Economic Feasibility Analysis of Pumped Storage Hydroelectricity in Abandoned Underground Coal Mines. *ASME J. Energy Resour. Technol.* **142**(12): 122001. https://doi.org/10.1115/1.4047406

Sharan, P., Kitz, K., Wendt, D., McTigue, J., and Zhu, G. 2020. Using Concentrating Solar Power to Create a Geological Thermal Energy Reservoir for Seasonal Storage and Flexible Power Plant Operation. *ASME J. Energy Resour. Technol.* **143**(1): 010906. https://doi.org/10.1115/1.4047970

Shi, Z., Jessen, K., and Tsotsis, T. T. 2020. Impacts of the subsurface storage of natural gas and hydrogen mixtures. *Int. J. Hydrog. Energy* **45**(15): 8757-8773. https://doi.org/10.1016/j.ijhydene.2020.01.044

Si, W. Di, B., Wei, J., et al. 2016. Experimental study of water saturation effect on acoustic velocity of sandstones. *Journal of Natural Gas Science and Engineering* **33**: 37-43. ISSN 1875-5100. https://doi.org/10.1016/j.jngse.2016.05.002.

Simon, J., Ferriz, A. M., and Correas, L. C. 2015. HyUnder—Hydrogen Underground Storage at Large Scale: Case Study Spain. *Energy Procedia* **73**: 136–144. https://doi.org/10.1016/j.egypro.2015.07.661

Stein, H.N. 1972. Thermodynamic considerations on the hydration mechanisms of Ca3SiO5 and Ca3Al2O6, *Cem. Concr. Res.* **2** (2): 167–177.

Strazisar, B., Kutchko, B., and Huerta, N. 2009. Chemical Reactions of Wellbore Cement Under CO2 Storage Conditions: Effects of Cement Additives. *Energy Procedia* **1**(1): 3603-3607. https://doi.org/10.1016/j.egypro.2009.02.155

Tanikawa, W., Shimamoto, T. 2009. Comparison of Klinkenberg-corrected gas permeability and water permeability in sedimentary rocks. *International Journal of Rock Mechanics and Mining Sciences* **46**(2): 229-238. ISSN 1365-1609. https://doi.org/10.1016/j.ijrmms.2008.03.004

Tarkowski, R., 2019. Underground Hydrogen Storage: Characteristics and Prospects. *Renew. Sustain. Energy Rev.* **105**: 86–94. https://doi.org/10.1016/j.rser.2019.01.051.

Taylor, J.B., Alderson, J.E.A., Kalyanam, K.M., et al. 1986. Technical and economic assessment of methods for the storage of large quantities of hydrogen. *Int. J. Hydrog. Energy* **11**(1): 5-22. https://doi.org/10.1016/0360-3199(86)90104-7.

Teodoriu, C., Reinicke, K.M., Fichter, C., Wehling, P., and Clausthal T. U. 2010. Investigations on Casing-Cement Interaction with Application to Gas and CO2 Storage Wells. Paper presented at the *SPE EUROPEC/EAGE Annual Conference and Exhibition*, Barcelona, Spain. https://doi.org/10.2118/131336-MS

Thiercelin, M.J., Dargaud, B., Baret, J.F. et al. 1998. Cement design based in Cement mechanical response. *SPE Drill. & Compl* **13**(4): 266-273. https://doi.org/10.2118/52890-PA.

Trezza, M.A. 2007. Hydration study of ordinary portland cement in the presence of zinc ions. *Materials Research* **10**(4): 331-334. ISSN 1980-5373. https://doi.org/10.1590/S1516-14392007000400002.

Truche, L., Jodin-Caumon, M.C., Lerouge, C., Berger, G., et al. 2013. Sulphide mineral reactions in clay-rich rock induced by high hydrogen pressure. Application to disturbed or natural settings up to 250°C and 30bar. *Chem. Geol.* **351**: 217-228. https://doi.org/10.1016/j.chemgeo.2013.05.025

Ugarte, E.R., and Salehi, S. 2021. A Review on Well Integrity Issues for Underground Hydrogen Storage. *ASME. J. Energy Resour. Technol.* **144**(4): 042001. https://doi.org/10.1115/1.4052626

Udegbunam,O., Yaman, I., Aktan, H., et al. 1999. Developing a rapid measure of concrete permeability for use in QA/QC specifications. Paper presented at the Transportation Research Board, 78th Annual Meeting, Washington D.C., 10 – 14 January.

US Energy Information Administration, Annual Energy Outlook 2022 (AEO2022)

van Bruegel, K. 1991. Simulation of Hydration and Formation of Structure in Hardening Cement-Based Materials. Meinema, Delft: University of Delft.

Vrålstad, T., Saasen, A., Fjær, E. et al. 2018. Plug & abandonment of offshore wells: Ensuring long-term well integrity and cost-efficiency. *J. of Petroleum Sci. and Eng.* **173**: 478-491. https://doi.org/10.1016/j.petrol.2018.10.049.

Wang, Z., Roberts, R.R., Naterer, G.F., and Gabriel, K.S. 2012. Comparison of Thermochemical, Electrolytic, Photoelectrolytic and Photochemical Solar-to-Hydrogen Production Technologies. *Int. J. Hydrogen Energy*, **37**(21): 16287–16301. https://doi.org/10.1016/j.ijhydene.2012.03.057.

Wu, L., Yi, L., Taoutaou, S., et al. 2014. Well Integrity in Underground Gas Storage Wells in China Using a Novel Cementing Technology. Paper presented at the Abu Dhabi International Petroleum Exhibition and Conference, Abu Dhabi, UAE, November https://doi.org/10.2118/171938-MS

Xu, H., Zhang, H., Xie, R., et al. 2016. Characterization of Rock Mechanical Properties Using Lab Tests and Numerical Interpretation Model of Well Logs. *Mathematical Problems in Engineering* **2016**: 1-13. https://doi.org/10.1155/2016/5967159

Yu, P., Kirkpatrick, J., Poe, B., et al. 2004. Structure of Calcium Silicate Hydrate (C-S-H): Near-, Mid-, and Far-Infrared Spectroscopy. *Journal of American Ceramic Society* **82**(3): 742-748. https://doi.org/10.1111/j.1151-2916.1999.tb01826.x

Zhang, W. 2016. Evaluation of Susceptibility to Hydrogen Embrittlement—A Rising Step Load Testing Method. *Materials Sciences and Applications* **7**: 389-395. https://doi.org/10.4236/msa.2016.78035.

Zhong, A., Johnson, M., Kohn, G., and Saleh, M. 2015. Performance Evaluation of a Large Bore Expandable Liner Hanger for Field Operations in the Gulf of Mexico. Paper presented at the *Offshore Technology Conference*, Houston, TX, USA. https://doi.org/10.4043/25995-MS

Zivar, D., Kumar, S., and Foroozesh, J. 2020. Underground hydrogen storage: A comprehensive review. *Int. J. Hydrog. Energy*. **46**(45): 23436-23462. https://doi.org/10.1016/j.ijhydene.2020.08.138.